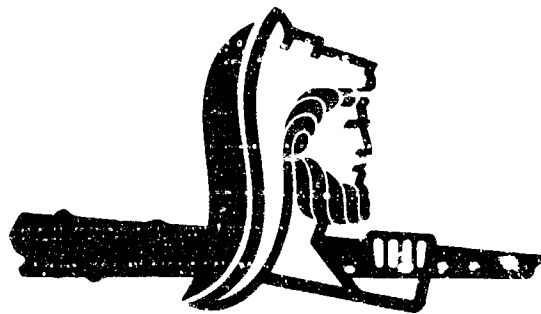


# UNCLASSIFIED

AD NUMBER
AD484720
NEW LIMITATION CHANGE
TO Approved for public release, distribution unlimited
FROM Distribution authorized to U.S. Gov't. agencies and their contractors; Administrative/Operational Use; JUN 1966. Other requests shall be referred to Ballistic Systems Division, Norton AFB, CA.
AUTHORITY
SAMSO USAF ltr, 28 Feb 1972

THIS PAGE IS UNCLASSIFIED

484720



**HERCULES**

CHEMICAL PROPULSION DIVISION  
**HERCULES POWDER COMPANY**  
INCORPORATED  
BACCHUS WORKS    MAGNA, UTAH



## HERCULES POWDER COMPANY

INCORPORATED

AIR FORCE PLANT 81

P O BOX 450 · MAGNA, UTAH

20 June 1966

IN REPLY

REFER TO 127/10/9-498

Headquarters  
Ballistic Systems Division  
Air Force Systems Command  
Norton Air Force Base  
San Bernardino, California

Attention: BSRPQ-3 - Capt. W. R. Cosgrove

Subject: Final Report Investigation and Recovery Program for Nozzle Port  
Flange Snap Ring Groove Cracking Problem of the Minuteman Stage III  
Motor, Report No. MTO-752-50

Reference: Contract AF 04(694)-127, CCN 261

Gentlemen:

In accordance with Contract AF 04(694)-127, one copy of the subject report is submitted.

Very truly yours,

  
W. PLUNKETT, MANAGER  
MINUTEMAN PROGRAM

MWP:RTRasmussen:vib

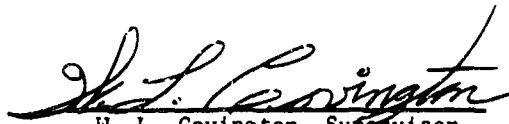
Enclosure: Report No. MTO-752-50

FINAL REPORT  
INVESTIGATION AND RECOVERY PROGRAM  
FOR  
NOZZLE PORT FLANGE SNAP RING GROOVE CRACKING PROBLEM  
OF THE  
MINUTEMAN STAGE III MOTOR

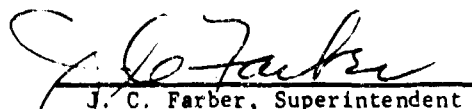
WEAPON SYSTEM 133A

MTO-752-50

Prepared by:

  
W. L. Covington, Supervisor  
Sustaining Engineering

Approved by:

  
J. C. Farber, Superintendent  
Sustaining Engineering

## FOREWORD

This report describes the work accomplished by Hercules Incorporated in isolating, evaluating, and correcting conditions that resulted in cracks within the snap-ring groove of the nozzle-port flange of the Minuteman third stage motor. The investigation and recovery program was conducted at Hercules/Bacchus Works and at the Goodyear Tire and Rubber Company.

Authority for the preparation of this report was obtained under Contract Change Notification (CCN) 261 to Contract AF 04(694)-127.

## ABSTRACT

In October 1967, cracking in the inner base corner of the machined snap-ring groove of nozzle-port flange number 3 was discovered on post-hydrotest inspection of case S/N HP00406. The insulator for this case was manufactured by Goodyear Tire and Rubber Company and serialized GY00505. Subsequent inspection of all cases and insulators in process proved the phenomenon was peculiar only to insulators manufactured by Goodyear.

Hercules Incorporated immediately initiated an investigational program described in document MTO-752-24, Investigation and Recovery Program for Nozzle-Port Flange Snap-Ring Groove Cracking Problem. This program plan was submitted to and approved by AFBSD/TRW. The program was conducted under Contract Change Notices 261 and 273 to Contract AF 04(694)-127.

The results of the study provided the following significant findings:

1. A complete documentation review of all manufacturing processes from the forging of the aluminum 2014-T652 billet through the final nozzle-port machining operation showed that:
  - a. No failure correlation to specific forging heat lots existed.
  - b. Aluminum alloy met material property specifications.
  - c. All nozzle-port flanges met drawing requirements.
2. Metallurgical analyses of the hand-forged aluminum billets gave evidence of poor flow-line orientation throughout the billets that would accentuate failure conditions under improper loads.
3. A significant contour mismatch of 0.046 in. was measured between the flange and the aft-dome mold.
4. Internal mold pressures resulting from a fully loaded aft-dome mold were of sufficient magnitude to crack improperly supported nozzle-port flanges.
5. Vendor attempts to reduce flange cracking during aft-dome molding by controlling the volume of rubber put into the mold were ineffective because of volumetric-tolerance buildups of the component parts within the mold cavity.

Two aft domes were studied during the molding operation. Results of these studies demonstrated that a fully-loaded mold, with existing flange support, would consistently crack all flanges. The following modifications were then made to the mold, molding process, and forging to eliminate the cracking:

1. The mold cooling plug was changed to properly locate the nozzle-port flange relative to the mold.

2. Rubber volume control was established to fill the mold to capacity.
3. Both snap-ring groove radii were increased.
  - a. Forward radius from 0.005 maximum to  $0.040 \pm 0.010$  in.
  - b. Aft radius from 0.005 maximum to  $0.025 \pm 0.005$  in.
4. The hand-forged aluminum flange was replaced with a die-forged aluminum flange containing improved flow-line characteristics.
5. The brittle, anodized surface within the snap-ring groove was changed to a chemical conversion coating.

After three test-dome moldings demonstrated the effectiveness of these modifications in eliminating the flange cracking, a qualification program of seven additional aft-dome moldings was performed. Three of the seven aft domes were molded and the nozzle-port flanges found free of cracks by metallurgical analysis. The remaining four domes were molded into insulators S/N GY00557X, GY00549RX, GY00545RX, and GY00558X; wound into cases RH00298, RH00297, RH00299, and RH00300; and processed through the hydrotest operation at Hercules Plant 2. All of these units were successfully processed. Metallurgical examination of the post-hydrotest nozzle-port flanges proved soundness of their structure. As a result of this qualification program, production of internal insulators was resumed at Goodyear.

During the Goodyear aft-dome mold evaluation, a program was established to determine the status of the Minuteman field force. Examination of all Quality Assurance static-fired hardware for both Wing I and Wing II provided data that 32 firings of motors with cracked nozzle-port flanges had been conducted with no evidence of motor performance degradation. Based on the statistical analysis of the failure rates of nozzle-port flanges in motors, it was estimated that 18 flight-test motors with cracked nozzle-port flanges had been flown with no evidence of failure or degradation attributable to the cracked nozzle-port flange.

In addition, a case (S/N HP00406) with one cracked nozzle-port flange, was hydroburst to determine the effect of a cracked flange on the case burst pressure. This case burst at 706 psi, well in excess of the 615 psi average case hydroburst pressure of that production period.

As a result of the examination of post-fired hardware and case testing, the reliability study concluded that the cracking of nozzle-port flanges in Goodyear insulators does not impair the reliability of the third-stage motor in the operational inventory. For this reason, no replacement of any unit found to have a cracked flange was recommended by Hercules.

For additional comprehension of the flange cracking phenomena, Allied Research Associates, Concord, Massachusetts, was subcontracted to apply photo-elastic stress analysis techniques to the aft-dome problem. These techniques, combined with metallurgical analyses, provided additional evidence that flange failure was caused by the excessive loads in the molding process.

Since the completion of the qualification program at Goodyear, production of acceptable insulators has demonstrated that the nozzle-port flange cracking problem has been eliminated by the modifications introduced as a result of this study.

As of 10 May 1966, the nozzle-port flanges of 92 consecutive cases passed inspection establishing a 97.5 percent reliability demonstration at the 90 percent confidence level.



# TABLE OF CONTENTS

<u>Section</u>	<u>Title</u>	<u>Page</u>
	FOREWORD . . . . .	ii
	ABSTRACT . . . . .	iii
	LIST OF FIGURES . . . . .	vii
	LIST OF TABLES . . . . .	ix
I	INTRODUCTION . . . . .	1-1
II	INVESTIGATIVE EFFORTS	
	A. Process Analysis . . . . .	2-1
	B. Case Tooling Evaluation . . . . .	2-2
	C. Nozzle Port Flange Loading Studies . . . . .	2-2
	D. Metallurgical Analysis . . . . .	2-38
	E. Conclusions . . . . .	2-55
	F. Recommendations . . . . .	2-56
III	FLANGE MODIFICATION TESTING . . . . .	3-1
IV	GOODYEAR MOLD MODIFICATIONS . . . . .	4-1
V	GOODYEAR REQUALIFICATION AND VERIFICATION . . . . .	5-1
VI	RELIABILITY ANALYSIS . . . . .	6-1
VII	OVERALL CONCLUSIONS . . . . .	7-1

# LIST OF FIGURES

<u>Number</u>	<u>Title</u>	<u>Page</u>
1	Flange Cross Section . . . . .	1-3
2	Flange Cracking Zone . . . . .	1-3
3	Strain Gage Location, Firing Pressure Effects Test . . . . .	2-4
4	Strain Gage Data, Gages 6B Minus 6A and 7B Minus 7A . . . . .	2-7
5	Strain Gage Data, Gages 5, 8, and 10 . . . . .	2-8
6	Strain Gage Data, Gages 1, 3, and 4 . . . . .	2-9
7	Case Stresses, Gages 8 and 10 . . . . .	2-10
8	Case Stresses, Gages 1, 3, 4, and 5 . . . . .	2-11
9	Strain Gage Location, Hydroproof Effect Test . . . . .	2-12
10	Hydroproof Effect Test Configuration . . . . .	2-13
11	Original Hydroproof Closure Installation . . . . .	2-17
12	Operational Nozzle Flange Installation . . . . .	2-18
13	Hydrotest Closure Comparison . . . . .	2-20
14	Strain Gage Location, Modified Closure Test . . . . .	2-21
15	Strain Gage Location, Molding Effect Test . . . . .	2-25
16	Molding Effect Test Configuration . . . . .	2-33
17	Cooling Plug with Shims . . . . .	2-35
18	Segment Bending Configuration, Clamped Condition . . . . .	2-35
19	Segment Bending Configuration, Unclamped Condition . . . . .	2-36
20	Leaf Type Deflectometer . . . . .	2-37
21	Unfractured Adapter . . . . .	2-41
22	Typical Failure Specimen . . . . .	2-41

# LIST OF FIGURES (CONT)

<u>Number</u>	<u>Title</u>	<u>Page</u>
23	Flange Failure Sample . . . . .	2-42
24	Fracture Regions . . . . .	2-43
25	Crack Orientation . . . . .	2-44
26	Photomicrograph of Cracked Flange . . . . .	2-45
27	Grain Flow Lines in Kaiser Hand-Forged Billet . . . . .	2-46
28	Fracture Surface . . . . .	2-47
29	Typical Corrosion Fracture . . . . .	2-49
30	Fracture Surface Transition Zone . . . . .	2-50
31	Typical Tensile Fracture . . . . .	2-51
32	Metallurgical Structure of Flange . . . . .	2-53
33	Typical Forging Flow Lines . . . . .	3-3
34	Strain Gage Location on Nozzle-Port Flange . .	4-3
35	Flange-to-Mold Contour with Modified Tooling . . . . .	4-8
36	Aft-Dome Mold Nozzle Port Subassembly . . . .	4-9
37	Shimming Support . . . . .	4-10
38	Geometry of Flange . . . . .	6-5
39	Strain Gage Location on Aft Domes of Motors 5R0, 5T0, and 5T3 . . . . .	6-6

# LIST OF TABLES

<u>Number</u>	<u>Title</u>	<u>Page</u>
I	Goodyear Mold Comparison . . . . .	1-2
II	Strain Gage Data . . . . .	2-5
III	Hydroproof Effect Test Data . . . . .	2-14
IV	Hydroproof Matrix . . . . .	2-22
V	Molding Effect Test Matrix . . . . .	2-26
VI	Molding Effect Test Data . . . . .	2-30
VII	Data From Segment Bending Test Clamped Condition . . . . .	2-39
VIII	Data From Segment Bending Test Unclamped Condition . . . . .	2-39
IX	Billet Chemical and Physical Test Data . . . . .	3-2
X	Flange Chemical and Physical Test Data . . . . .	3-5
XI	Thermal Strain Gage Data . . . . .	4-4
XII	Specific Gravity Versus Mold Load . . . . .	4-7
XIII	Metallurgical Evaluation of Nozzle Port Flanges . . . . .	5-2
XIV	Firing Effects Data . . . . .	6-3
XV	Aft Dome Case Strain . . . . .	6-7
XVI	Fired Motors with Known Cracked Flange (s) . . . .	6-10

## SECTION I

### INTRODUCTION

On 23 October 1964, a post-hydrotest visual examination of Minuteman Case HP00406 revealed a crack in the aluminum flange snap-ring groove of port number 3. The crack occurred in the forward radius area of the flange snap-ring groove at 180 degrees from the keyway. The nozzle port-flange was hand forged 2014 T652 aluminum alloy produced by Kaiser Aluminum Company and utilized in an insulator aft-dome molding at Goodyear Tire and Rubber Company.

The nozzle-port cracking problem had been encountered previously during the Wing I and II R&D phases of the Minuteman Program at a nominal five percent loss rate. Since the loss rate was within expected production loss rates, and a no change policy was in effect at that time, no changes to the aft dome were made. However, a dye-penetrant inspection instituted after molding of the aft domes assured that no cracked parts were being permitted to enter the fabrication system.

In May 1964, Goodyear changed from the -243 R&D aft-dome mold (USAF-243-318-3) to the -690 production aft-dome mold (USAF-690-5003-13). The mold nomenclature, i.e., -243 and -690, represent the contract numbers under which they were purchased. This change was necessary when the -243 mold became worn and continued use would have resulted in the production of unacceptable parts. The main differences in these molds are shown in Table I.

An informal First Article Acceptance (FAA) of an aft dome produced by the -690 mold was performed to assure that the dome molding parameters such as time, temperatures, and pressures, would remain the same. As further proof, the chemical, physical, and dimensional characteristics of the aft dome produced on the -690 mold were found to be the same as those produced by the -243 mold. Based on the data from this FAA, Goodyear was permitted to replace the -243 "pot heater" mold with the -690 "steam jacketed" mold.

With the discovery of cracked flanges entering the fabrication system, Hercules in October 1964 initiated a dye-penetrant inspection of all units in the various stages of fabrication at the Bacchus and Clearfield plants. The investigation showed that the nozzle port cracking problem was of serious proportions, eventually reaching 65 percent of all units made from the combination of Kaiser hand-forged flanges and the -690 aft-dome mold at Goodyear. Production at Goodyear was stopped when the severity of the problem was defined.

Each instance of flange cracking was found to be in the forward radius area of the snap-ring groove at the keyway and/or 180 degrees from the keyway as shown in Figures 1 and 2. These cracks were found to be a maximum of ten inches in circumferential length.

TABLE I  
GOODYEAR MOLD COMPARISON

Item	-243 Mold	-690 Mold
Method of Heating	Steam heated autoclave (pot heater)	Steam jacketed mold
Method of Pressure	Steam pressure and ram in autoclave	Ram press
Movement of Work Points in the Mold	The work point was moved approximately 0.100 in. fwd away from the aft center port	The work point was moved approximately 0.090 in. aft toward the aft center port
Position of Greatest Flange Gap Between Mold and Flange Contour	There was an average gap of 0.030 between the mold and the edge of the flange toward the aft center port	There was an average gap of 0.036 between the mold and the edge of the flange away from the aft center port
Contours	The contours were approximately the same for both molds	
Cracking Problem	Both molds produced aft domes with cracked flanges	

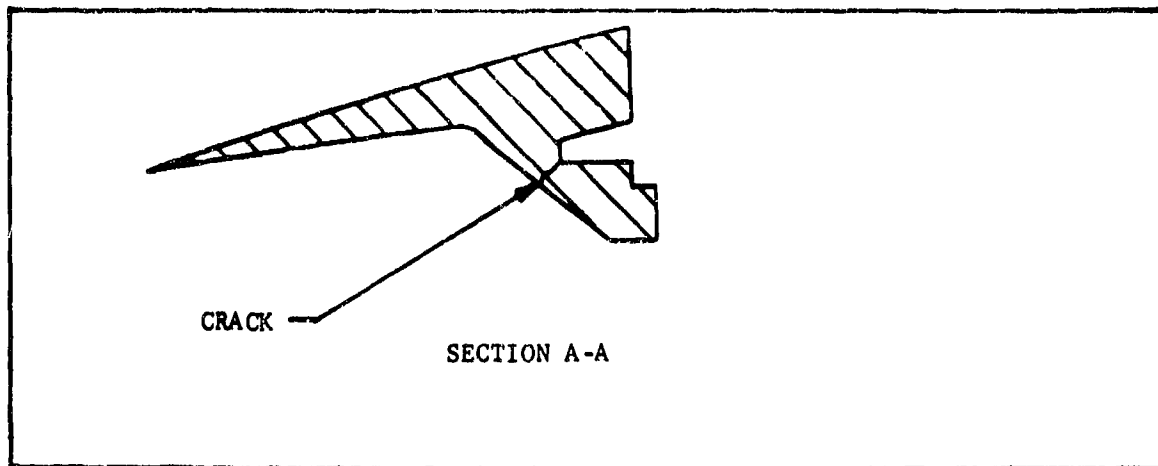


Figure 1. Flange Cross Section

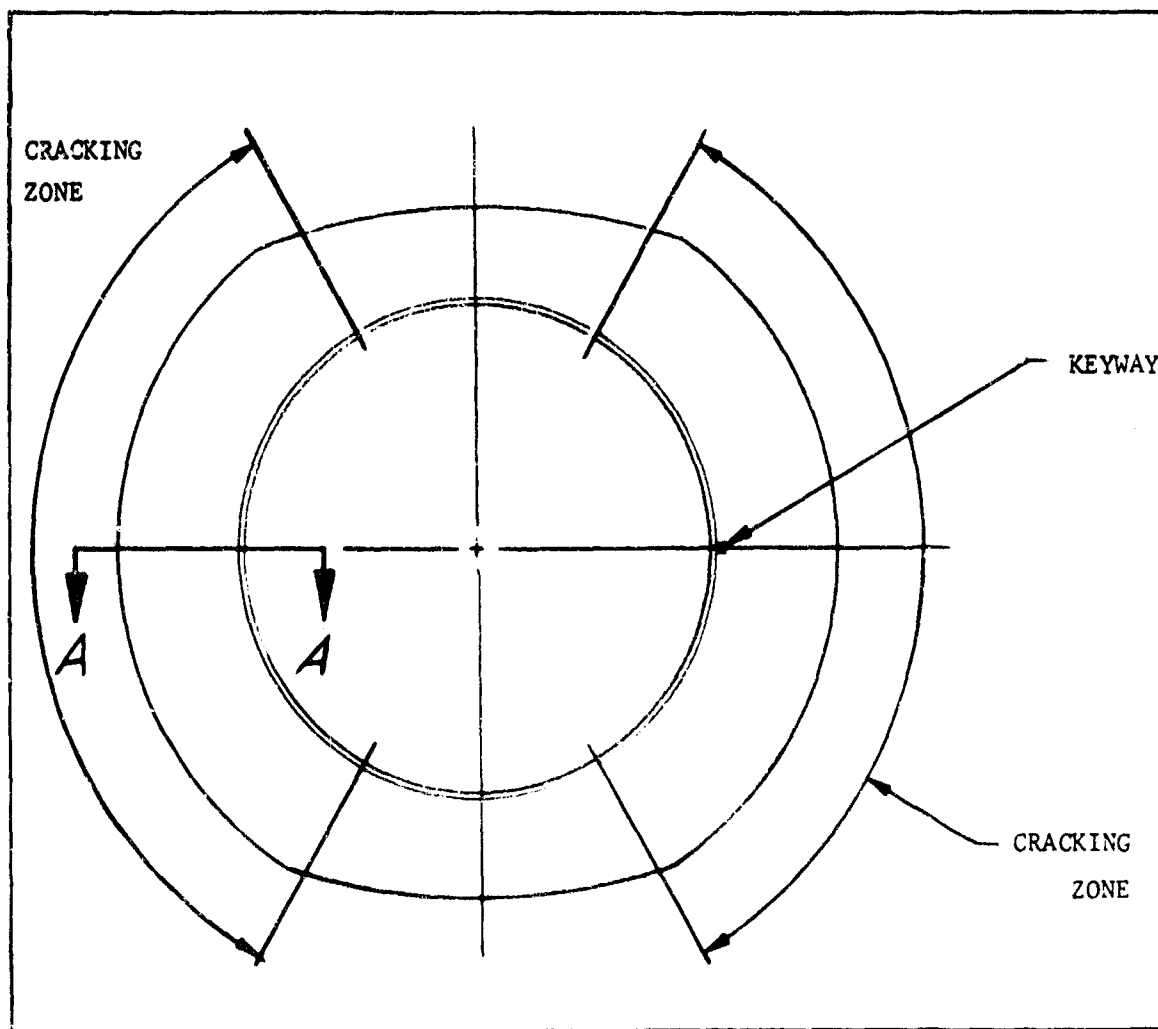


Figure 2. Flange Cracking Zone

A Program Plan entitled Investigation and Recovery Program for Nozzle Port Flange Snap Ring Groove Cracking Problem (MTO-752-24) was submitted to BSD/TRW for approval on 9 November 1964 and amended on 16 November 1964. The approval was received by HPC on 11 December 1964 by TWX BSRPK-3/12198 from BSD/TRW.

Hercules immediately launched a multipronged investigative effort. Documentation was reviewed which traced the aluminum from machined flange to forging to heat lot; metallurgical and dimensional analyses were performed; tooling was evaluated; and, the nozzle-port flange was tested under every condition it sees during its life cycle.



## SECTION II

### INVESTIGATIVE EFFORTS

The Hercules investigative effort covered the following areas:

- A. Process Analyses
- B. Case Tooling Evaluation
- C. Nozzle-Port Flange Loading Studies
- D. Metallurgical Analysis

This section discusses these areas in the above order with the resulting conclusions and recommendations.

#### A. PROCESS ANALYSES

In a documentation review, every cracked flange was traced to its heat lot. These data showed that the cracked flanges came from many forging heat lots. Since the Certificates of Analysis from the forging heat lots involved in flange cracking were in conformance with the prescribed specification QQ-A-367, the flange-cracking problem could not be correlated to a particular heat lot or a specification discrepancy.

A review of the aft-dome fabrication process was undertaken beginning with the nozzle-port flange machining operation at Admiral Machine Company. Special attention was given to the clamping and holding fixtures used in the machining operation. The results of this review indicated that the cracking problem could not be correlated to the machining process.

The manufacturing process Standard Operating Procedure (SOP) review performed at Goodyear showed that the SOP had been followed with the exception of Goodyear "heat soaking" the rubber for thirty minutes prior to applying the ram pressure in the dome molding operation. Since this is a standard practice in the rubber industry, this practice was incorporated into the SOP as an "as built" condition. The SOP review was negative in defining the cracking problem.

A dimensional analysis of all parts and tooling pertaining to the aft dome fabrication was performed. The analysis consisted of measuring the nozzle port flanges and the process tooling to determine their interaction. The investigation included an evaluation of the contour mismatch between the nozzle port flange and the aft-dome mold and showed a maximum gap of 0.046 in. at the outer perimeter of the flange on the side most distant from the center port, varying to contact for the inboard edge of the nozzle-port flange face on all four ports.

A study of the nozzle port cooling-plug diameters, with respect to the mating nozzle-port flange interface diameters, was made. At the flange O-ring diameter and the cooling plug interface, it was possible to have an interference fit of 0.009 to 0.025 in. at the keyway location and 180 degrees from the keyway extending approximately one inch on either side of the keyway on the nozzle port flange O-ring (10.300 in.) diameter. This restraint in the O-ring diameter was a normal part of the process imposed by Goodyear to prevent ovality of the flange during the aft-dome molding process. This was caused by the fit and loading conditions in the molding process coupled with the nonuniform cross-sectional configuration of the flange.

In summary then, the dimensional analysis showed a mismatch between the nozzle port flange and the aft-dome mold of 0.046 in. Also, a possible interference fit between flange O-ring diameter and the cooling plug of 0.025 in.

In addition to the foregoing dimensional analysis, a determination of the rubber volume of the mold cavity was made. Goodyear had attempted in the past to prevent nozzle-port flange cracking by controlling the weight of rubber put in the mold. However, the above determination showed that the tolerance stackups of the hardware in the mold coupled with permitted rubber density variations allowed a 73 cubic-inch range in volume of rubber in the mold. Therefore, the Goodyear method of controlling flange loads by controlling the weight of the rubber added to the mold was considered not feasible.

#### B. CASE TOOLING EVALUATION

After discovery of the cracked nozzle-port flange in port number 3 of case HP00406, all available motors, cases, insulators, and hardware were dye penetrant inspected for cracked flanges. Results of this inspection showed that many of the cases embodying Goodyear insulators, which had been hydro-proofed, had cracked nozzle-port flanges.

These findings prompted Hercules to review and monitor the Clearfield case winding and Arrowsmith Plastic Tooling operation for environments or operations that could contribute to the flange cracking problem.

The review of the Clearfield case winding and Arrowsmith Plastic Tooling operations did not show any noticeable environments or operations that would contribute significantly to the flange cracking problem.

#### C. NOZZLE PORT FLANGE LOADING STUDIES

Hercules initiated a program to investigate the effect of cracked nozzle-port flanges on the structural integrity of the case; the effect of motor firing pressures on crack propagation; and the effect of hydrotesting pressures on crack propagation.

Before the initiation of these tests, all hydroproof tooling was physically and dimensionally inspected and found to be worn but still within

drawing specifications. However, to minimize tooling variables, new closures and snap rings were used for these tests.

#### 1. Structural Integrity Test

Case S/N HP00406, with one cracked nozzle port-flange, was selected as a representative sample of available cases containing cracked flanges for hydroburst testing. Visual and dye-penetrant inspection of the case had revealed a crack in the forward radius area of the flange snap-ring groove, extending approximately 75 degrees on either side of the keyway in nozzle port number 3.

The case was instrumented with the normal operational test matrix per Drawing 12S00402. In addition, hi-speed movies of the cracked flange area were taken during the hydroburst operation.

A pressure of 706 psig was required to burst the case. Failure occurred in the cylindrical section near the forward tangent line, an area that could not have been affected by the cracked nozzle port flange. By comparing the 706 psig burst pressure with the 615 psig average burst pressure for 20 consecutive lot acceptance hydrobursts (10 prior to and 10 subsequent to this test) it can be concluded that the structural integrity of a case is not impaired by a cracked nozzle port-flange.

Examination of the hydroburst data traces and the hi-speed movie showed no evidence of unusual case deflection.

#### 2. Evaluation of Firing Pressure Effects

This evaluation was initiated to determine if case pressurization during motor firing produces sufficient forces to crack a Goodyear nozzle-port flange.

In addition to the firing pressure information, it was also desirable to obtain information on the forces acting on a flange at hydroproof pressures.

For these purposes, nozzle port number 1 of case S/N HP00450 was instrumented with strain gages as shown in Figure 3. This case had been rejected for operational use because of cracked nozzle-port flanges in ports number 2 and 4. Dye-penetrant and radiographic inspection indicated there were no cracks in the flanges of nozzle ports number 1 or 3.

In order to accommodate installation of the strain gages, 3/4 in. dia. holes were drilled from the interior through the insulator and phenolic at 90 degrees and 180 degrees, clockwise, from the keyway. Strain gages number 3 and 8 were then bonded to the aluminum flange through these access holes. Likewise, at the same degree locations, 3/4 in. holes were drilled from the exterior through the Spiralloy to accommodate strain gages number 1, 4, and 5. The snap-ring groove was drilled out so gages number 9 and 10 could be placed across the area at the base of the ring groove. Four electronic deflection indicators (number 6A, 6B, 7A, and 7B) were substituted for strain gages number 6 and 7.

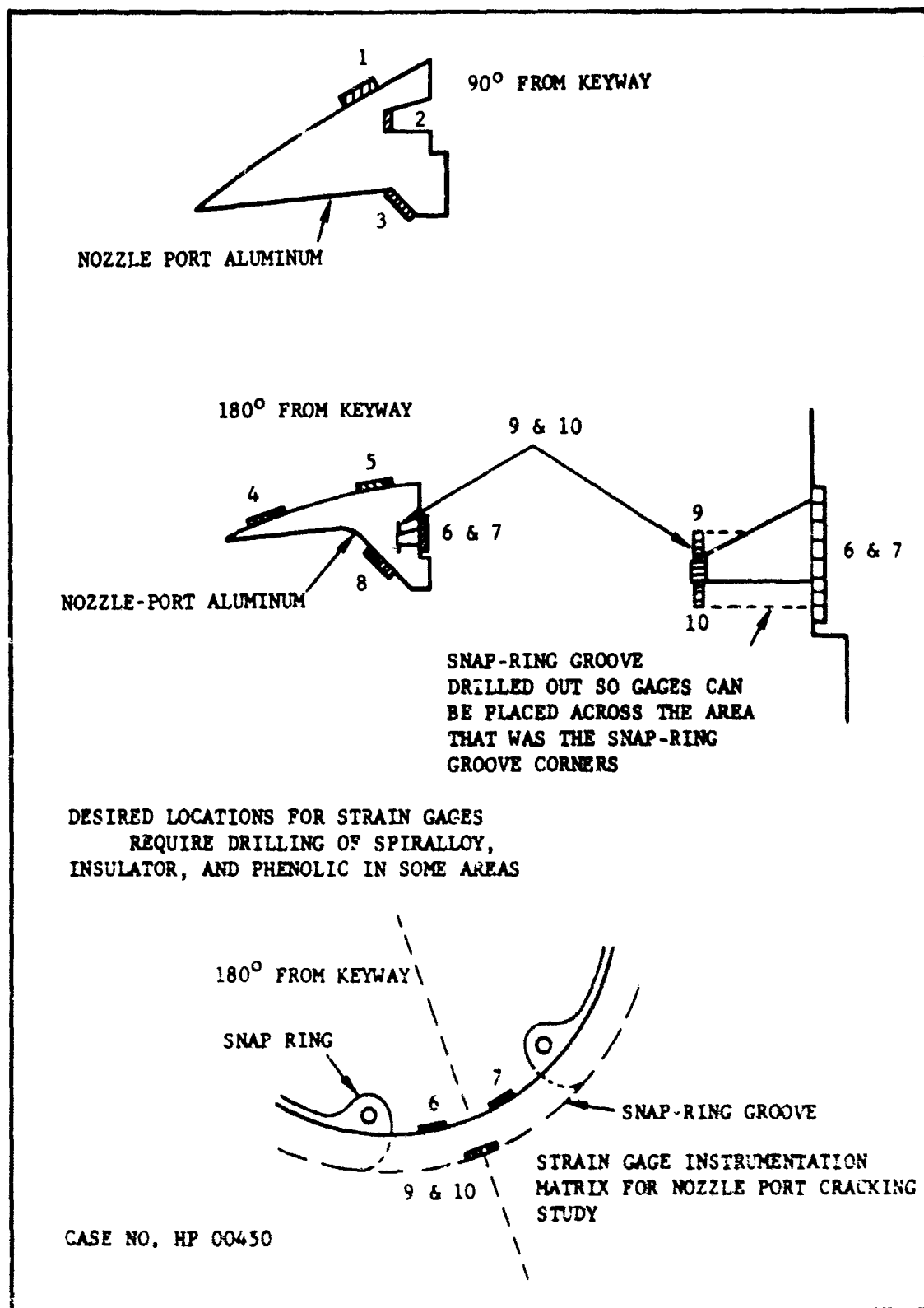


Figure 3. Strain Gage Location,  
Firing Pressure Effects Test

TABLE II

STRAIN GAGE DATA  
HYDROBURSTING OF CASE S/N HP00450

Time Sec.	Pressure Psig	Gage 1 Micro Inches	Gage 3 Micro Inches	Gage 4 Micro Inches	Gage 5 Micro Inches	Gage 8 Micro Inches	Gage 10 Micro Inches	Gage 6A Inches (.000)	Gage 6B Inches (.000)	Gage 6A Inches (.000)	Gage 7A Inches (.000)	Gage 7B Inches (.000)	7B-7A Inches (.000)
1	-	-	-	-	-	-	-	-	-	-	-	-	-
2	-	-	-	-	-	-	-	-	-	-	-	-	-
3	-	-	-	-	-	-	-	-	-	-	-	-	-
4	-	-	-	-	-	-	-	-	-	-	-	-	-
5	-	-	-	-	-	-	-	-	-	-	-	-	-
6	-	-	-	-	-	-	-	-	-	-	-	-	-
7	-	-	-	-	-	-	-	2	2	2	1	5	4
8	25	-	-12	+16	+16	+60	-20	17	20	38	15	25	10
9	45	-40	+8	36	22	+30	0	38	42	40	37	47	10
10	50	48	8	44	25	0	+30	40	50	40	42	52	10
11	75	60	20	56	24	-10	70	65	72	65	63	80	17
12	95	80	40	76	28	130	240	92	92	100	82	100	18
13	107	92	48	88	36	200	300	92	105	110	92	110	18
14	115	96	52	112	48	300	350	100	110	100	100	115	15
15	122	104	56	124	56	400	410	107	120	105	105	122	17
16	135	108	60	148	72	540	410	117	130	117	117	135	18
17	150	120	68	172	88	700	500	128	140	127	127	147	20
18	167	132	76	200	116	900	630	142	158	140	140	162	22
19	185	144	80	236	136	1100	730	158	175	157	157	180	23
20	200	156	84	264	160	1300	850	170	188	170	170	192	22
21	217	160	84	296	192	1500	980	185	202	185	210	210	25
22	235	172	84	324	216	1650	1080	200	217	200	222	222	22
23	250	172	84	356	252	1760	1150	213	232	212	212	240	28
24	267	172	84	380	280	1890	1250	225	245	225	225	250	25
25	283	172	75	416	316	2000	1350	240	260	240	240	267	27
26	300	172	78	440	352	2100	1440	250	272	250	250	280	30
27	302	172	78	452	372	2170	1460	255	280	255	253	282	29
28	302	176	76	456	384	2170	1470	255	280	255	253	282	29
29	302	176	76	460	392	2180	1460	255	280	255	253	282	29
30	302	180	76	460	396	2190	1460	255	280	255	253	282	29
31	302	180	76	460	400	2190	1460	255	280	255	253	282	29
32	302	180	76	468	404	2190	1460	255	280	255	253	282	29
33	302	180	78	460	408	2190	1450	255	280	255	253	282	29
34	302	180	78	464	412	2190	1450	255	280	255	253	282	29
35	302	184	78	464	412	2190	1450	255	280	255	253	282	29
36	302	184	80	468	416	2190	1450	255	280	255	253	282	29
37	305	184	80	472	424	2190	1450	258	281	258	253	282	29
38	310	184	80	480	432	2210	1500	260	285	260	260	285	25
39	320	176	76	508	456	2290	1560	270	292	270	270	290	28
40	335	172	72	536	488	2400	1660	282	310	282	282	315	33
Max	355	172	70	560	516	2500	1750	-	322	-	-	-	-

@ 40.8 Sec.

Gages number 2 and 9 failed prior to test and were deleted from data requirements by the test conductor.

After completion of the above instrumentation, the case was pressurized to  $300 \pm 5$  psig at a rate of 15 psig/sec. The 300 psig was held for 10 seconds after which an attempt was made to increase the pressure to  $420 \pm 5$  psig; however, at 414 psig the case failed in the area that had been weakened by the installation of gages number 4 and 5. (The strain gage data indicated that the case actually started to yield at approximately 355 psig. Gage readings above this pressure were so erratic that they served no purpose and are not included in this report.)

Table II shows the strain gage readings during the test cycle, whereas, Figures 4, 5, and 6 show the same data in graphic form. Using the modulus of  $10.6 \times 10^6$  psi, these strains were converted to stress and plotted in Figures 7 and 8.

An evaluation of these data shows that the maximum stresses were at the base of the snap-ring groove (gage number 10) and on the back side of the flange, opposite the snap-ring groove (gage number 8). At the 355 psig internal pressure, the measured tension strain was 0.00175 in./in. and the compression strain was 0.00250 in./in., or 18,550 psi and 26,500 psi stress, respectively. The 355 psig pressure is in excess of maximum firing requirements per Model Specification S-133-1003-0-1 for Rocket Motor M57-A1, dated 17 April 1963.

Since all cracked flanges failed in tension, the tensile stress at the root of the snap-ring groove was considered to be the parameter of most concern for motor firing loads. By comparing the 18,550 psi stress produced at 355 psig internal pressure with the 50,000 psi minimum force required to crack a flange during the simulated hydroproof testing described below, it was concluded that firing pressures would not produce sufficient stresses to crack a nozzle port flange that had withstood hydroproofing loads.

### 3. Evaluation of Hydroproofing Effects

All flanges used in the hydroproof effects tests were instrumented with strain gages as shown in Figure 9. The fixture used in these tests is shown in Figure 10. The objectives of these tests were to establish baseline performance levels of hand forged nozzle port flanges manufactured at Goodyear; determine if the insulator manufacturing or case winding processes reduce the capability of a flange to withstand hydroproof pressures; and, determine the effects hydroproofing has on a nozzle-port flange.

In comparing the baseline performance and capabilities of new flanges with flanges from various stages of the insulator and case manufacturing processes, no significant differences could be noted.

The simulated hydroproof tests (Table III) produced excellent data on the effects of the configuration variables. Following is a discussion of the major findings.

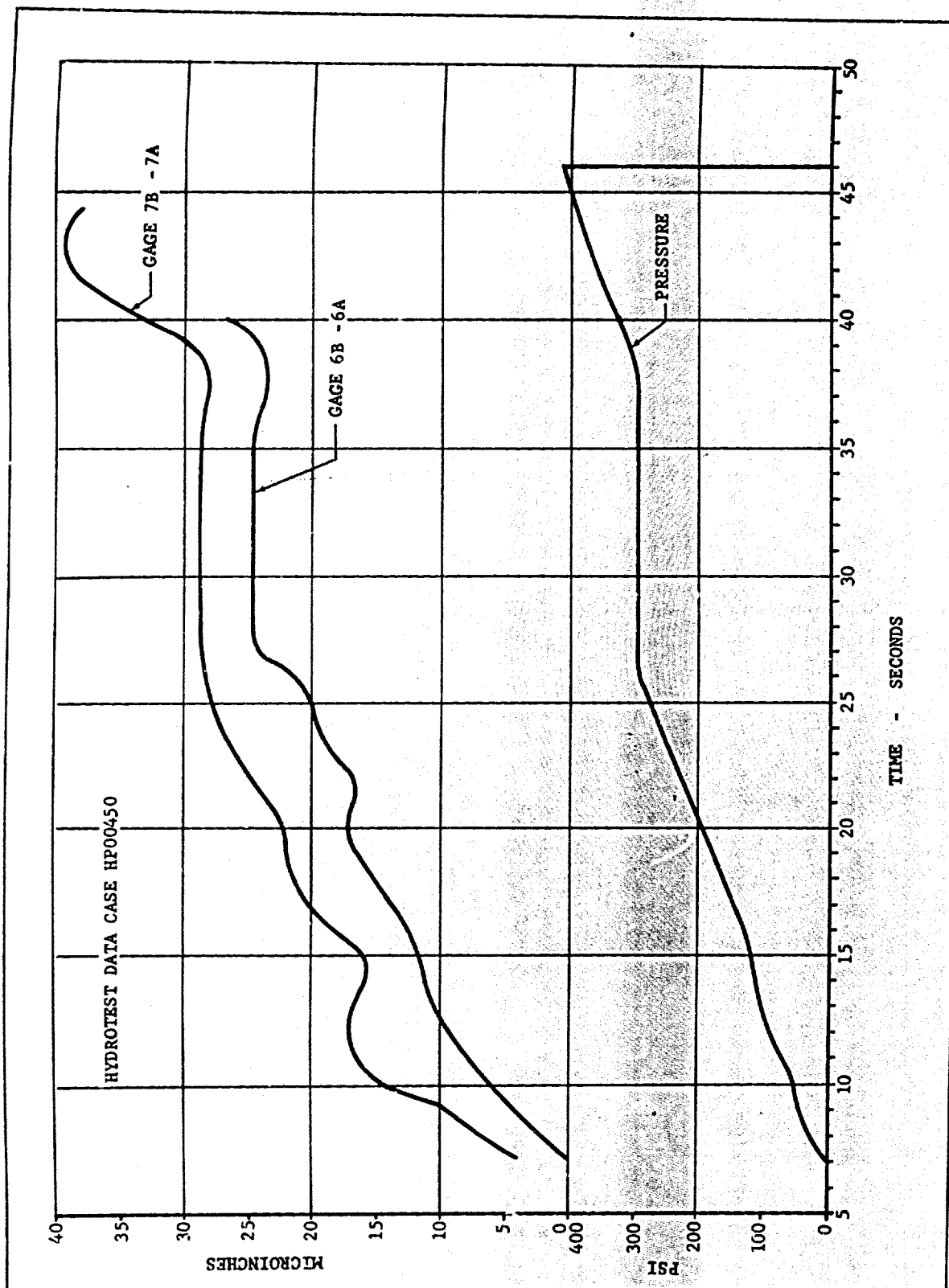


Figure 4. Strain Gage Data, Gages 6B Minus 6A and 7B Minus 7A

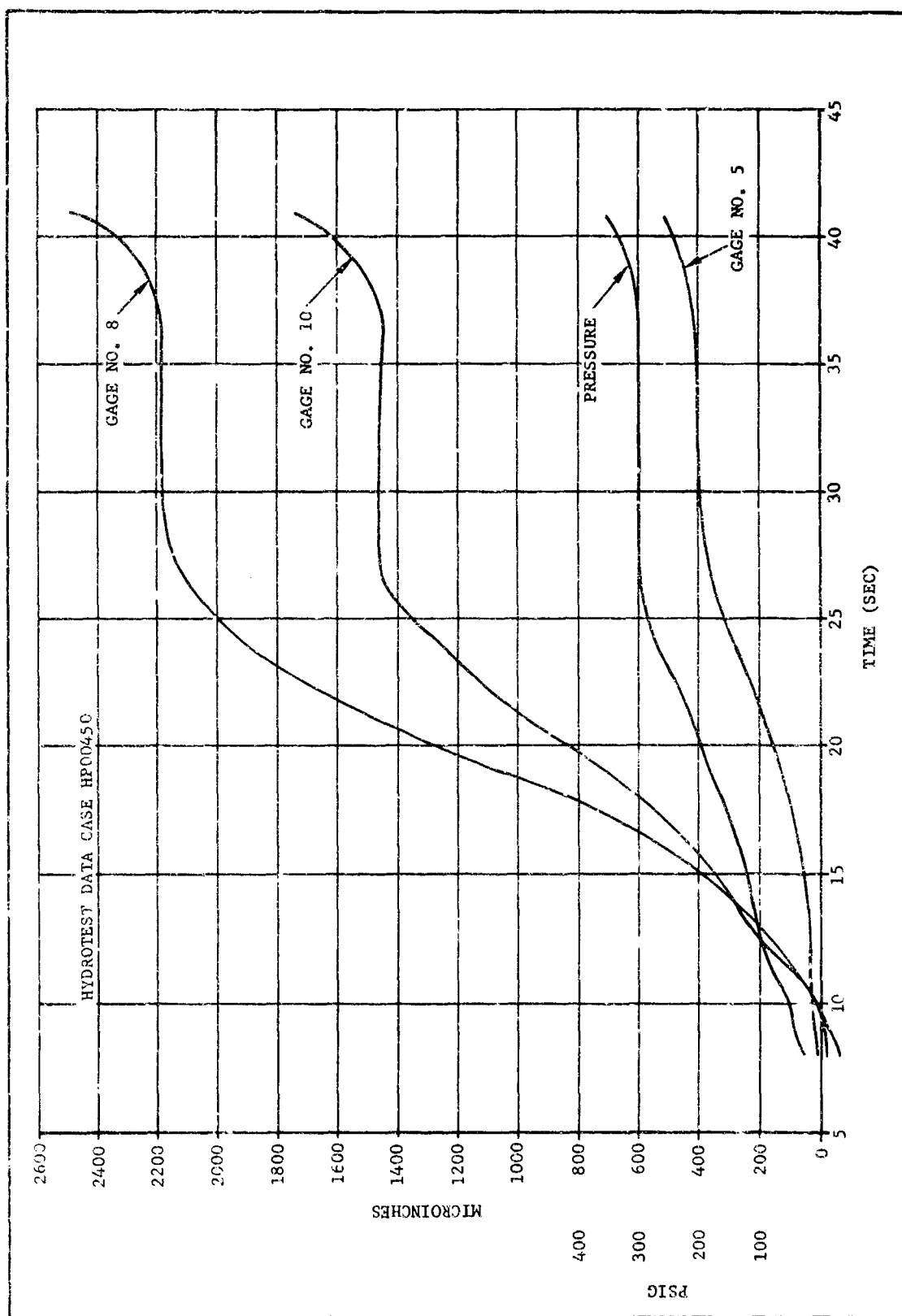


Figure 5. Strain Gage Data, Gages 5, 8, and 10



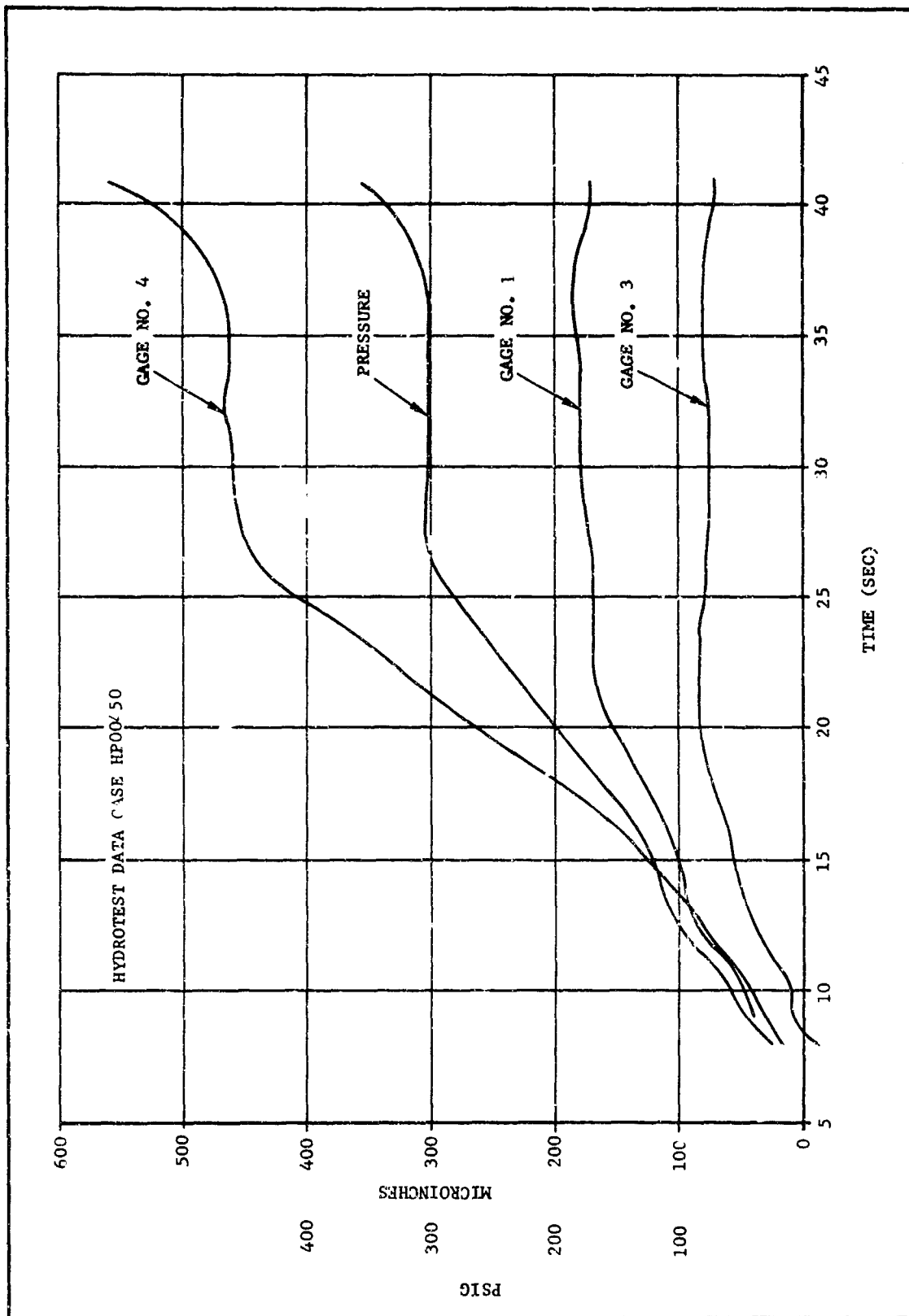


Figure 6. Strain Gage Data, Gages 1, 3, and 4

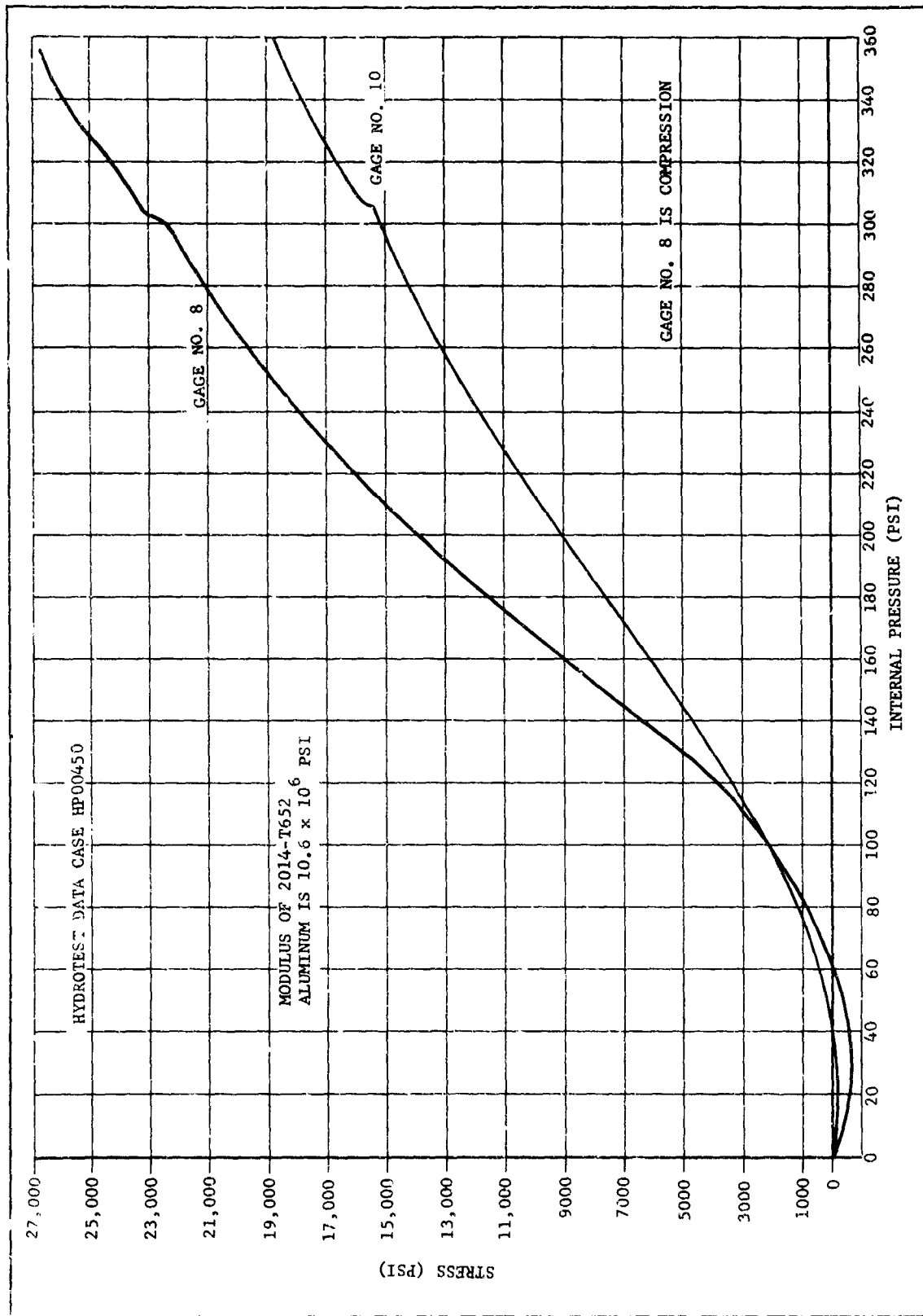


Figure 7. Case Stresses, Gages 8 and 10

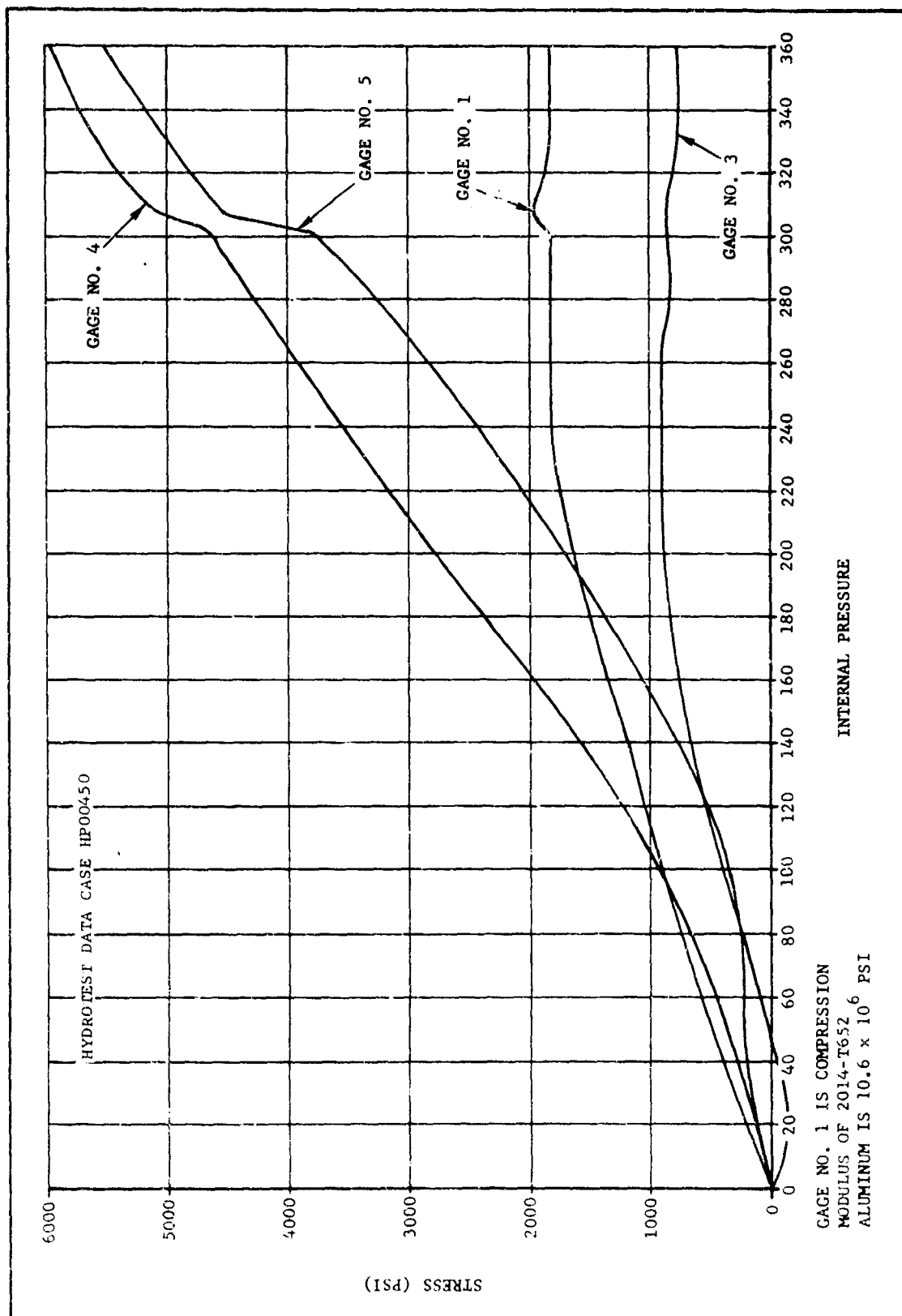


Figure 8. Case Stresses, Gages 1, 3, 4, and 5

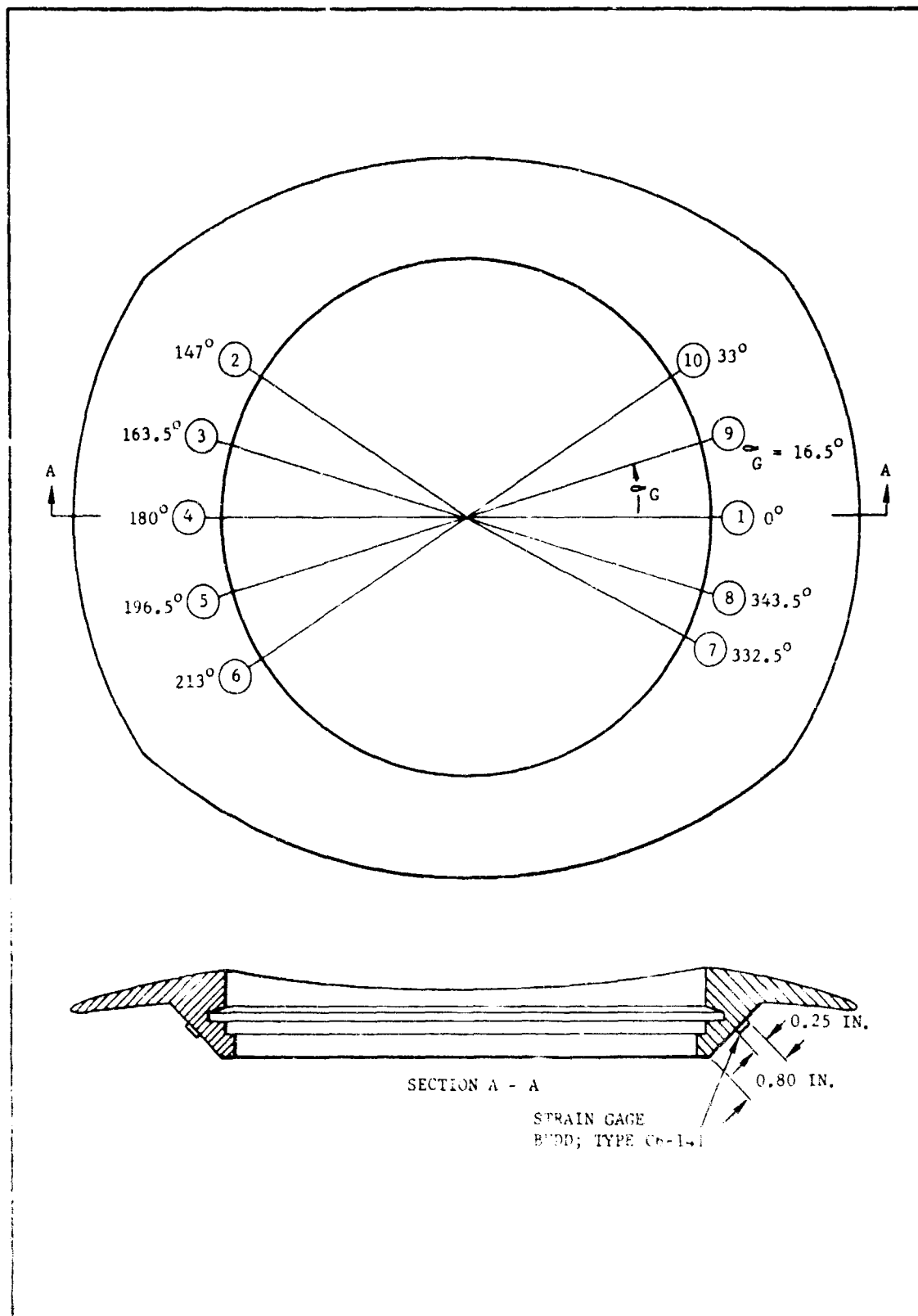


Figure 9. Strain Gage Location, Hydrocool Effect Test

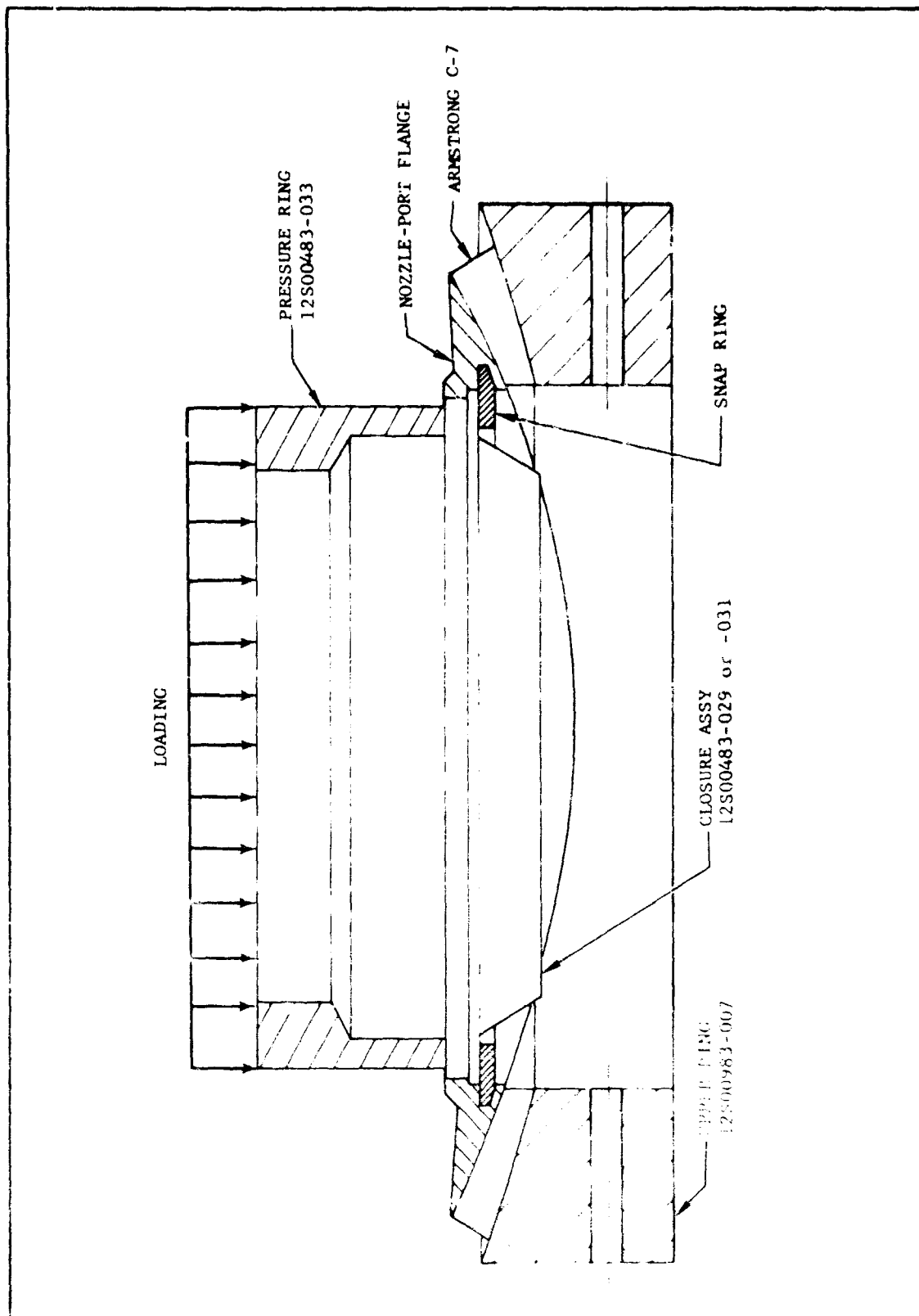


Figure 10. Hydroproof Effect Test Configuration

TABLE III

## HYDROPROOF EFFECT TEST DATA

Test No.	Test Run No.	Flange Serial No.	Primary Test Variable	Inspection Data				Load Rate	Load Max	Test Run Description
				Groove Dia	Groove Height	Groove Angle	Corner Radius			
1	1	GY-01972	Baseline Strain	11.146	0.145	15° 5'	--	50 K/M	50K	Determine if cycling degrades strength
	2	"	"	"	"	"	"	"	"	"
	3	"	"	"	"	"	"	"	"	"
	4	"	"	"	"	"	"	"	"	"
	5	"	"	"	"	"	"	"	"	"
	6	"	Gap in support	"	"	"	"	"	"	.006 gap in support 50° to 13°, 230° to 310°
	7	"	"	"	"	"	"	"	"	Same as Run No. 6 - check repeatability
	8	"	"	"	"	"	"	"	"	.012 gap in support 50° to 130°, 230° to 310°
	9	"	"	"	"	"	"	"	"	Same as Run No. 8 - check repeatability
	10	"	Baseline strain	"	"	"	"	"	"	Recheck baseline: .179 snap ring centered 196.50 M = .185, h = .150
	11	"	Snap ring position	"	"	"	"	"	"	Snap ring gap centered at 180°
	12	"	Closure lip thickness	"	"	"	"	"	"	Same as Run No. 10 except h = .175, t = .179
	13	"	"	"	"	"	"	"	"	Same as Run No. 12 except h = .150
	14	"	"	"	"	"	"	"	"	Same as Run No. 13 - strain gage zero shift
	15	"	"	"	"	"	"	"	"	Same as Run No. 13 - recalibrated gages still slight zero shift
	16	"	Maximum strain	"	"	"	"	"	70K	Same configuration as Run No. 13
2	Test Not Conducted									
3	59	US-21352	Strain distribution	11.142	0.147	16° 30'	.010 to .020	"	32.8K	h = .175, m = .120, t = .175
	60	"	Closure lip thickness	"	"	"	"	"	"	Same as Run No. 59 except h = .150
	61	"	Gap in support	"	"	"	"	"	"	Same as Run No. 60 except .010 gap 303° to 330°, 147° to 213°
	62	"	"	"	"	"	"	"	"	Same as Run No. 61 except gap .020
	63	"	Maximum strain	"	"	"	"	"	100K	Same as Run No. 60 - flange did not fail
4	20	GY-02615	Strain distribution	"	0.140	15° 1'	0.010	"	50K	h = .150, M = .185, t = .191 snap ring gap 196.50 strain gage drifted
	21	"	"	"	"	"	"	"	"	Recheck Run No. 20 gage still drifted
	22	"	Maximum strain	"	"	"	"	"	78.5K	Same configuration as Run 20
5	33	GY-02600	Strain distribution	11.145	0.140	15° 10'	0.010	"	50K	Snap ring gap centered at 196.5°, h = .150, m = .185, t = .188
	34	"	Snap ring position	"	"	"	"	"	"	Same as Run No. 33 except snap ring at 16.5°
	35	"	"	"	"	"	"	"	"	Same as Run No. 33 except snap ring at 180°
	36	"	Maximum strain	"	"	"	"	"	99.2K	Same as Run No. 33

1) Chemical analyses accomplished

2) No evidence of stress corrosion cracks indicated by metallurgical tests

TABLE III (Cont)

## HYDROPROOF EFFECT TEST DATA

Test No.	Test Run No.	Flange Serial No.	Primary Test Variable	Groove Dia	Inspection Data Groove Height    Groove Angle    Corner Radius	Load Rate	Load Max	Test Run Description
6	42	GY-02641	Strain distribution	11.147	0.140    15° 0'    0.010	50 K/M	32.8K	h = .175, t = .185, t = .190 32.8K steam-jets 425 Psi hydroproof
	43	"	Closure lip thickness	"	"    "    "	"	"	Same Conf. Run No. 42 except h = .150
	44	"	Maximum strain	"	"    "    "	"	49.85 K	Same Conf. as Run No. 43
7	48	GY-01940	Strain distribution	--	--    --    --	"	32.8K	h = .150, m = .185, t = .190
	49	"	Maximum strain	--	--    --    --	"	50K	Same Conf. as 48 except m = .120, t = .175
	50	"	"	--	--    --    --	--	50K	Same Conf. as 49 except no failure
8	51	"	"	--	--    --    --	--	55K	Same Conf. as 49 except no failure
	45	GY-02644	Strain distribution	11.141	0.140    15° 1'    0.010	"	32.8K	h = .150, m = .185, t = .190
	46	"	"	--	--    --    --	"	"	Same as Run No. 45 except m = .120, t = .175
9	47	"	Maximum strain	--	--    --    --	"	55K	Same as Conf. 49, Run No. 46
	17	GY-00024	Strain distribution	11.142	--    15° 10'    0.073 Full	"	50K	h = .150, m = .185, t = .188 snap ring at 196.5 <sup>0</sup>
	18	"	Snap ring position	--	--    --    --	"	"	Same as Run 17 except snap ring at 180°
10	19	"	Maximum strain	--	--    --    --	"	85K	Same as Run 17 - No failure or permanent set

1) Chemical analyses accomplished

2) No evidence of stress corrosion cracks indicated by metallurgical tests

a. Snap-Ring Position

Although the procedure for installing the nozzle closure required the opening of the snap ring to be opposite the keyway, it did not require it to be symmetrically opposite the keyway. Therefore, it was postulated that the positioning of the opening could have an effect on the resultant stresses at the base of the snap-ring groove during hydroproofing. To establish the effects of the snap-ring position, a series of simulated hydroproof tests were conducted with the center of the snap ring opening positioned at 16.5 degrees, 180 degrees, and 196.5 degrees clockwise from the flange keyway.

As expected, the lowest strains occurred between the free ends of the snap ring. However, the strains measured at the ends of the snap ring were not significantly different than those measured 180 degrees from the opening. Based on these data, it was concluded that snap-ring position has no detrimental effect on the flange during hydroproof.

b. Hydroproof Closure Lip Thickness

During inspection of the hydroproof closures used for production case testing, it was discovered that the nominal thickness of the closure lip was 0.150 in. This dimension was 0.025 in. thinner than the nominal thickness of the lip on an operational nozzle. Figures 11 and 12 show that the snap ring does not seat as deeply into the snap-ring groove with the operational nozzle as it does with the hydroproof closure.

Simulated hydroproof tests were performed to determine the effect of the hydroproof closure lip thickness on flange stresses. The resulting data showed a marked increase in strain attributable to the 0.025 in. thinner test closure lip thickness. In the area where the flange is cracking, strains increased from approximately 0.0003 in./in. for the 0.175 in. closure, to 0.0007 in./in. for the 0.150 in. closure.

These findings were confirmed by photoelastic investigations of the hydroproof closure lip thickness. These investigations were performed with an accurate twotimes full-size model of the cross section at the keyway of both a hand and a die-forged nozzle port flange. The tests were performed with the snap ring located all the way into the groove and then spaced at 0.075 and 0.150 in. from the back of the groove.

The stress patterns show that the maximum stress condition for both the hand- and die-forged flanges occurred when the snap ring was fully seated in the snap ring groove; also, the maximum stress was substantially the same for both hand- and die-forged flanges.<sup>1</sup>

---

<sup>1</sup>Becker, Hamilton and Kyle, Photoelastic Investigation of the Stage III Minuteman Nozzle Port Flange, Documents No. ARA 289-1, ARA 289-2, and ARA 289-3



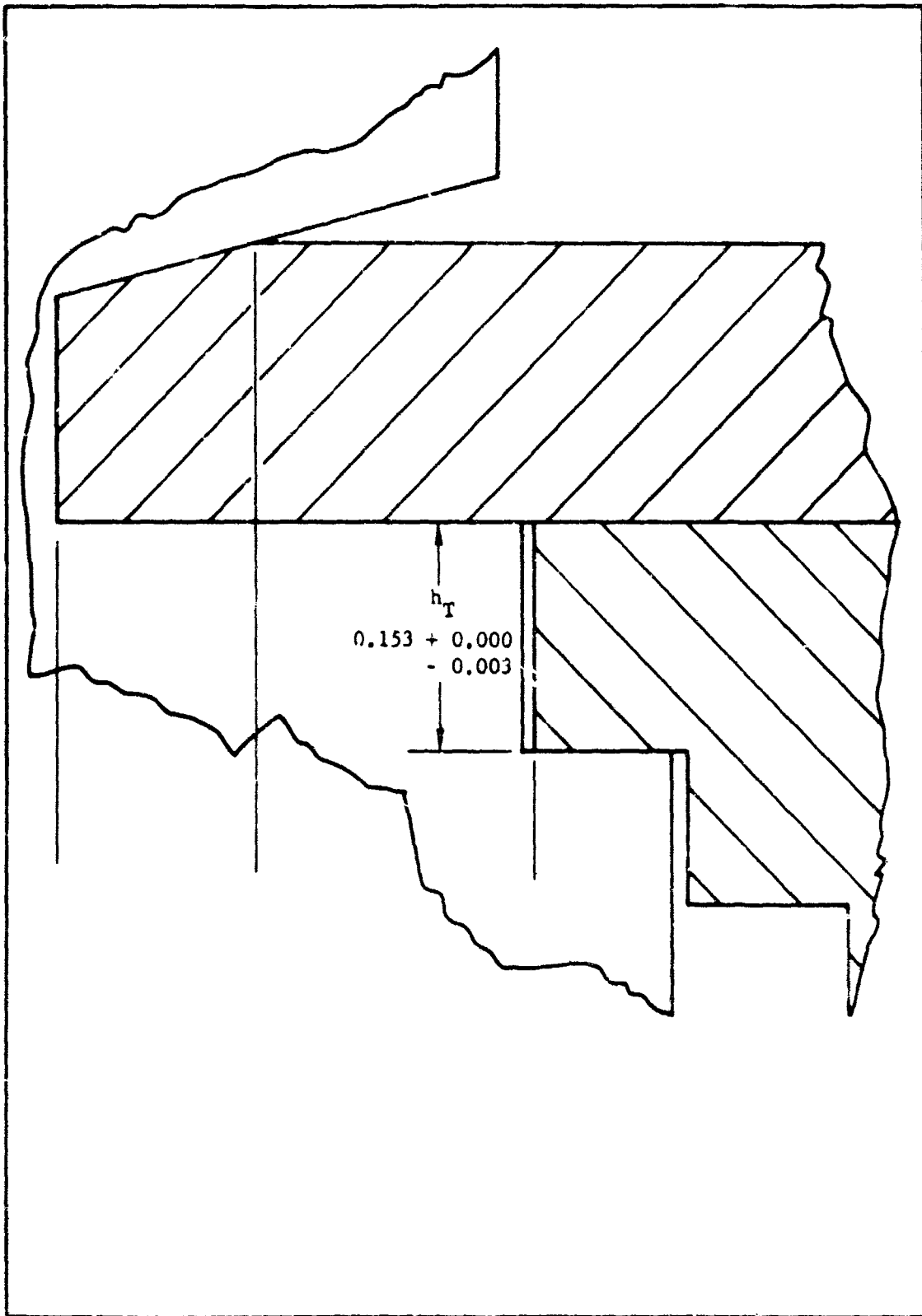


Figure 11. Original Hydroproof Closure Installation

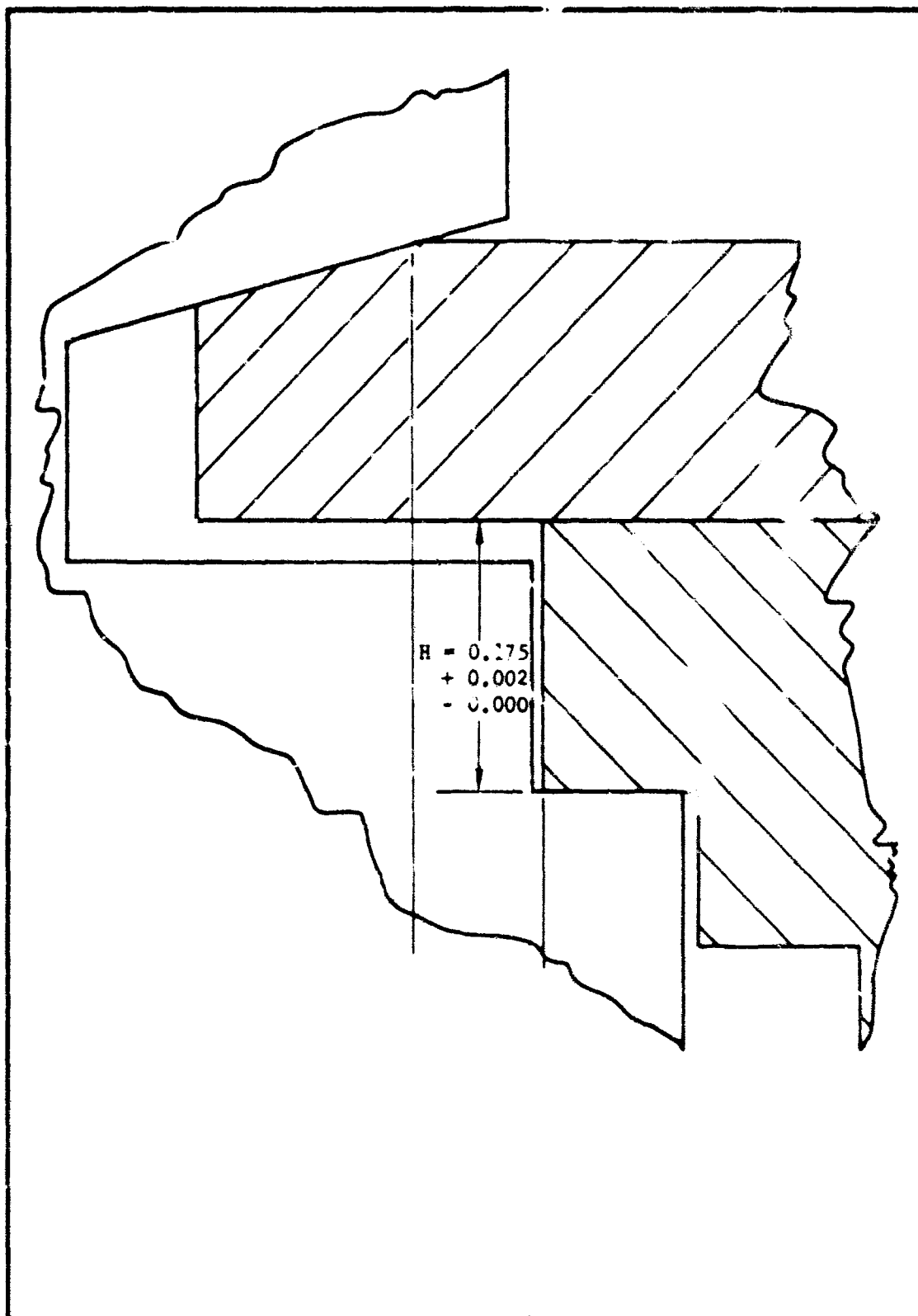


Figure 12 Operational Nozzle Flange Installation

#### 4. Modified Hydroproof Closure

Tests indicated that at any given pressure, hydroproof closures produced higher stresses in a nozzle port flange than the flight hardware. Therefore, a program plan (MTO-162-236) was submitted to AFBSD/TRW to evaluate the differences between the strains generated by existing hydroproof closures and closures simulating nozzle blast tube lip thickness.

The original hydroproof nozzle port closures have a lip thickness dimension of 0.150 to 0.153 in., whereas, the corresponding dimension for the operational nozzle hardware is 0.175 to 0.180 in. Simulated hydroproof loading tests showed that a change in closure-lip thickness had a marked effect on the stresses in the snap ring groove area of a nozzle port flange. The purpose of these tests was, therefore, to evaluate and compare the stresses on a nozzle-port flange during actual hydroproofing with the standard hydroproof closures and with closures modified to correspond to the operational nozzle hardware dimensions. (See Figure 13.)

From the available cases rejected for operational use because of cracked nozzle port flanges discovered after hydroproofing, four cases, S/N HP00408, HP00442, HP00433, and HP00436, were selected for these tests. Dye-penetrant inspection of the flanges indicated one cracked flange per case.

Two ports on each case, determined by dye-penetrant inspection to contain uncracked nozzle-port flanges, were instrumented as shown in Figure 14. Per BSD approval, TWX number BSRKP-3/20811 dated 18 January 1965, additional hydroproof cycles were added to the program plan to test the effect of the turnbuckle assembly, P/N 7480, on flange stresses.

After instrumentation, the cases were put through normal hydroproof cycles per HPC-133-08-2-1. The configuration for each test run is shown in Table IV.

In tests number I and II, the modified closures were used for the first two hydroproof cycles of each test. The recorded strains showed excellent repeatability and all gages returned to zero, indicating no yielding of the flange. The standard closures were then installed for the subsequent test runs.

After run number 3, all strain gages in port number 1, test number I and port number 4, test number II did not return to zero thus indicating yielding of the flange in some area. Dye-penetrant inspection of nozzle port flanges in these two ports revealed typical snap-ring groove cracks.

On tests number III and IV, the closure sequence was reversed using the standard closure for the first cycle. Inspection of the instrumented flanges after the first run showed that on test number III both flanges were cracked, and on test number IV one flange had cracked during the hydroproof cycle. Two subsequent runs with modified closures on test number IV, however, did not crack the nozzle-port flange that survived the standard closure run.

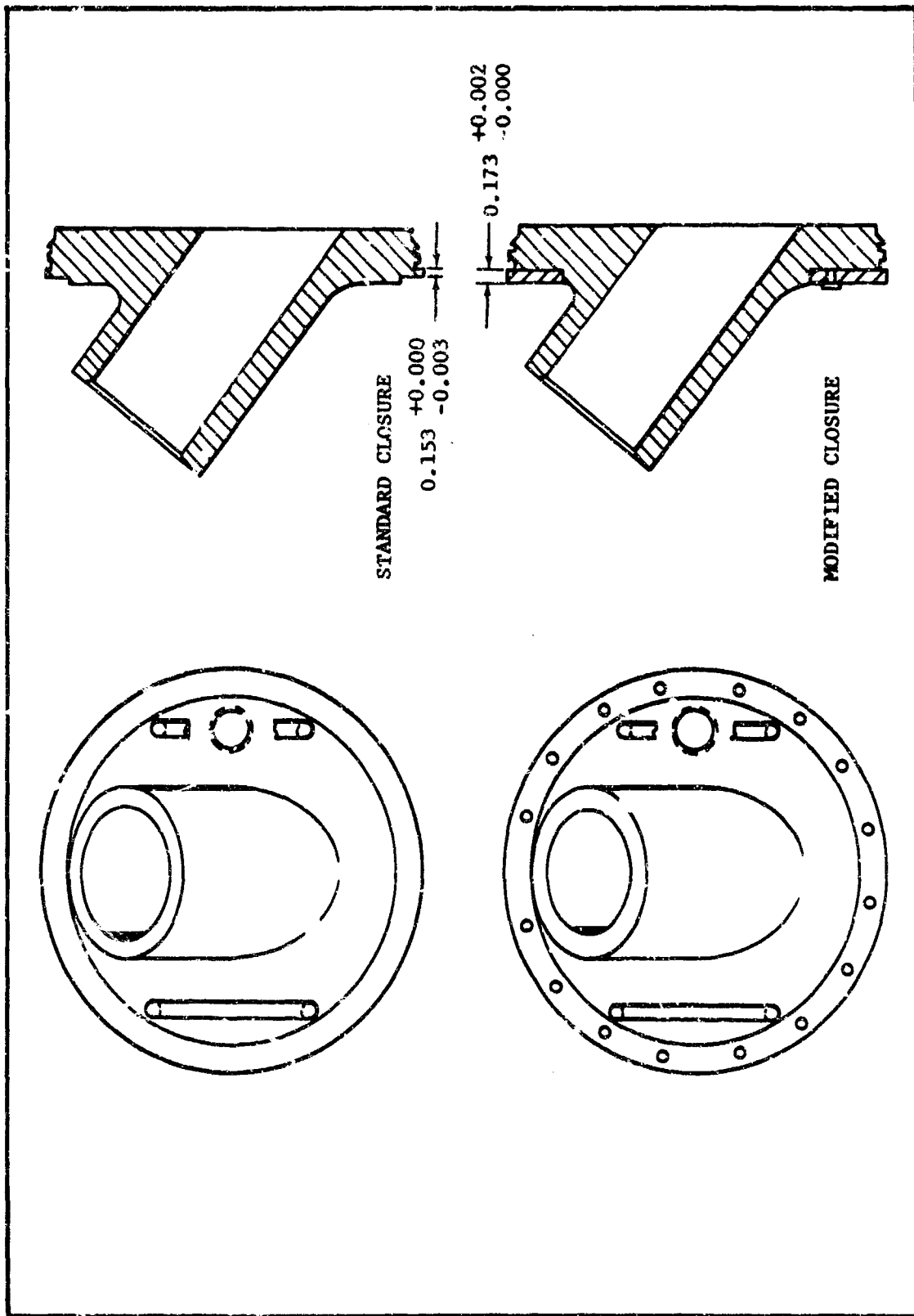


Figure 13. Hydrotest Closure Comparison

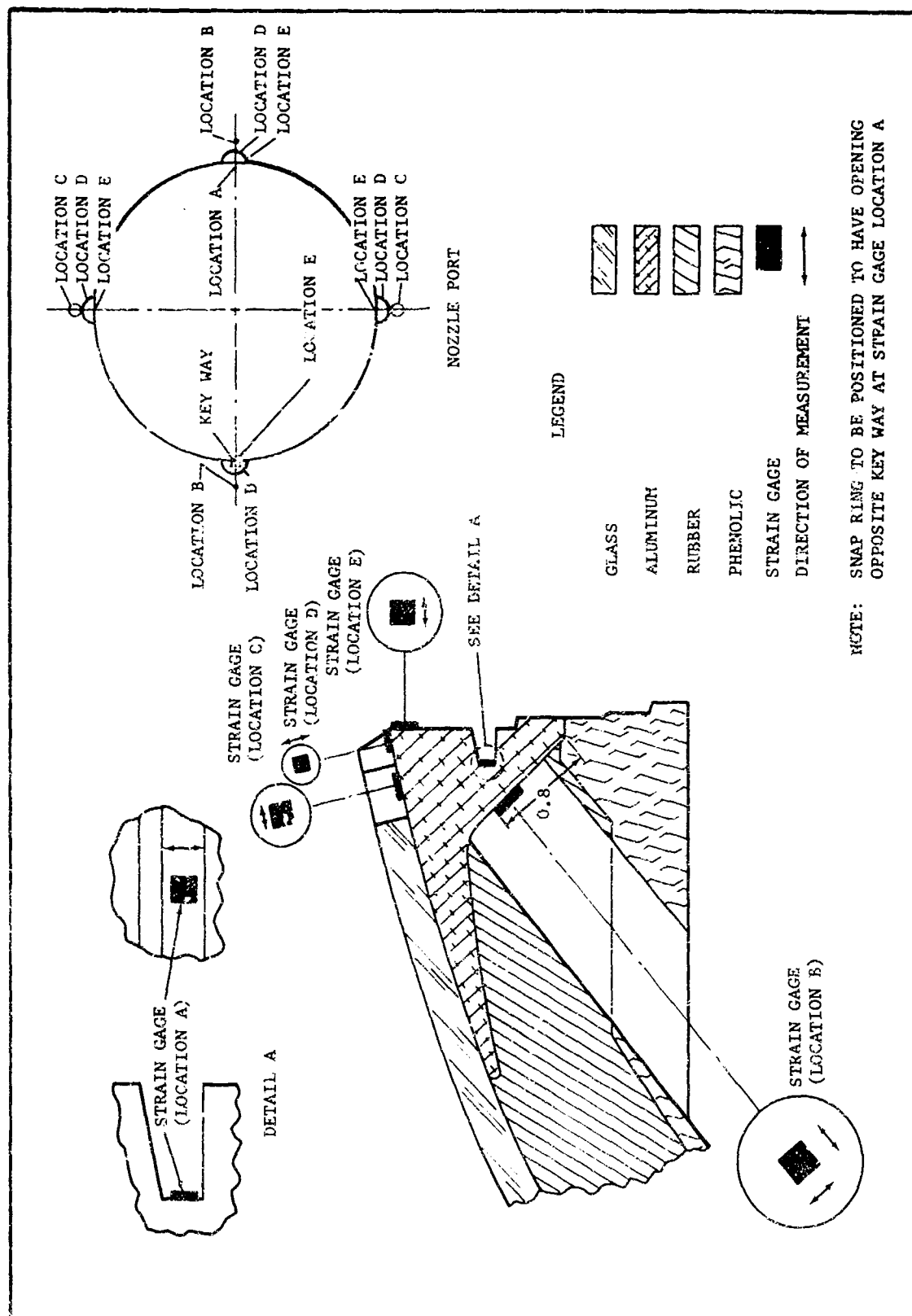


Figure 14. Strain Gage Location, Modified Closure Test

TABLE IV  
HYDROPROOF MATRIX

Case No.	Test No.	Run No.	Configuration			
			Standard Closures	Standard W/Turnbuckles	Modified Closures	Modified Closures W/Turnbuckles
HP00408	I	1			X	
		2			X	
		3	X			
		4		X		
HP00442	II	1			X	
		2				X
		3	X			
HP00433	III	1	X			
		2		X		
		3			X	
HP00436	IV	1	X			
		2			X	
		3				X

From these findings alone, it could be concluded that standard closures produce the more severe stresses on nozzle-port flanges during hydroproofing.

The strain gage data also show that flange stresses associated with the standard closure were substantially higher than those associated with the modified closure. Gage "A", located at the base of the snap ring groove and gage "B", located on the back side of the flange behind the snap-ring groove, are the most significant indicators of the resultant strains. Comparison of the strain data from these two gages shows that when standard closures were used, the recorded strains averaged 30 to 40 percent higher than the recorded strains for the modified closures. By averaging the measured strains for the four tests and converting the strain to stress, using the modulus of elasticity of  $10.6 \times 10^6$  psi in tension, the average stress at the base of the snap ring groove during hydroproofing at 425 psi was 36,000 psi with the standard closure and 24,600 psi with the modified closure. Maximum measured strain with a standard closure, however, was 0.0048 in./in. or approximately 52,000 psi stress.

By comparing this maximum calculated stress with the results of the simulated hydroproof tests, where failures were observed as low as 50,000 psi, it can be concluded that under certain conditions hydroproof pressures produce adequate stresses to cause flange cracking; these conditions being a hand-forged flange, minimum radius in the corners of the snap-ring groove, and full penetration of the snap ring into the snap-ring groove during hydroproofing.

Maximum measured strain with a modified closure was only 0.0031 in./in. or approximately 33,000 psi stress. Therefore, the data obtained in these tests indicate that the stresses induced during hydroproofing with modified closures would be only 66 percent of the magnitude required to crack a sound nozzle-port flange.

Metallurgical examination of the cracked flanges from the four test cases revealed two types of failure, i.e., one flange showed typical overstressed tensile fracture only, whereas, the other four flanges showed both stress-corrosion, cracking and overstressed tensile cracking. These findings indicated that stress corrosion resulted from stresses induced prior to hydroproofing, thus impairing the structural integrity of the flange.

The use of the turnbuckles, P/N 7480, had little effect on the measured strain when used with either the standard or modified closure. It appears, however, that there was a slight increase in the flange strains in the groove area between the free ends of the snap ring when turnbuckles were used with the modified closures.

Following completion of the hydroproof closure test evaluation, Hercules proceeded to qualify the modified closures for production use in accordance with BSD's TWX number BSRKP-3/20839, March 1965. In compliance with the above referenced TWX, use of the modified closures on U. S. Rubber

insulated cases was qualified on case S/N HP00553, "Hydroburst QA for HP Sublot 18B". (See Hercules message reference number 544/2/6-311 dated 17 April 1965.)

Qualification testing of the modified closure for use on Goodyear insulated cases was performed on case S/N HP00456, "Hydroburst QA for HP Sublot 22B". A summary of the data from this hydroburst test was transmitted to BSD (Hercules message reference number 544/2/6-412 dated 14 September 1965) requesting concurrence and release of the modified closures for hydroproofing Goodyear insulated cases. Final approval of this request was granted in BSD's TWX number BSRPQ-21969, September 1965.

#### 5. Flange Loads in Mold Investigation

The objectives of this investigation were to establish the ultimate physical capability of the Goodyear 01A00480 nozzle-port flange and to isolate conditions which were resulting in overstressing, degradation, or failure of the flanges. Flanges obtained from various manufacturing steps were utilized in the testing and analysis to determine the effect of forces acting on the nozzle-port flange during aft-dome molding.

Each flange used in the tests was instrumented with strain gages as shown in Figure 15. The purpose of this instrumentation was to establish and isolate induced stresses produced by the dome molding operation. The test fixture, shown in Figure 16, was designed to simulate actual forces imposed on a flange during the molding operation.

In order to establish baseline strain data, one new hand-forged Goodyear flange was subjected to a 40,000 pound load test. Flanges from various stages of the insulator and case manufacturing processes (Tables V and VI) were then subjected to the same load test for comparative purposes. The results showed unexpectedly wide variations in strains.

An analysis of the test fixture revealed the Devcon support ring (Figure 16) had been molded to the contour of the Goodyear control flange (S/N GY01929), and the resulting mismatch between the ring and the other test flanges caused areas of high localized stress.

A rerun of the 40,000 pound comparative load tests, using a Devcon support ring formed to each flange contour, showed the maximum strain averaged for both sides of the flange to be nearly equal for all flanges, indicating no measurable strength degradation of the flanges tested in this series.

Further analysis of the mismatch of contours between the support ring and flange indicated that similar localized stress areas would be produced during actual insulator dome molding if there was a mismatch between flange and mold contours.



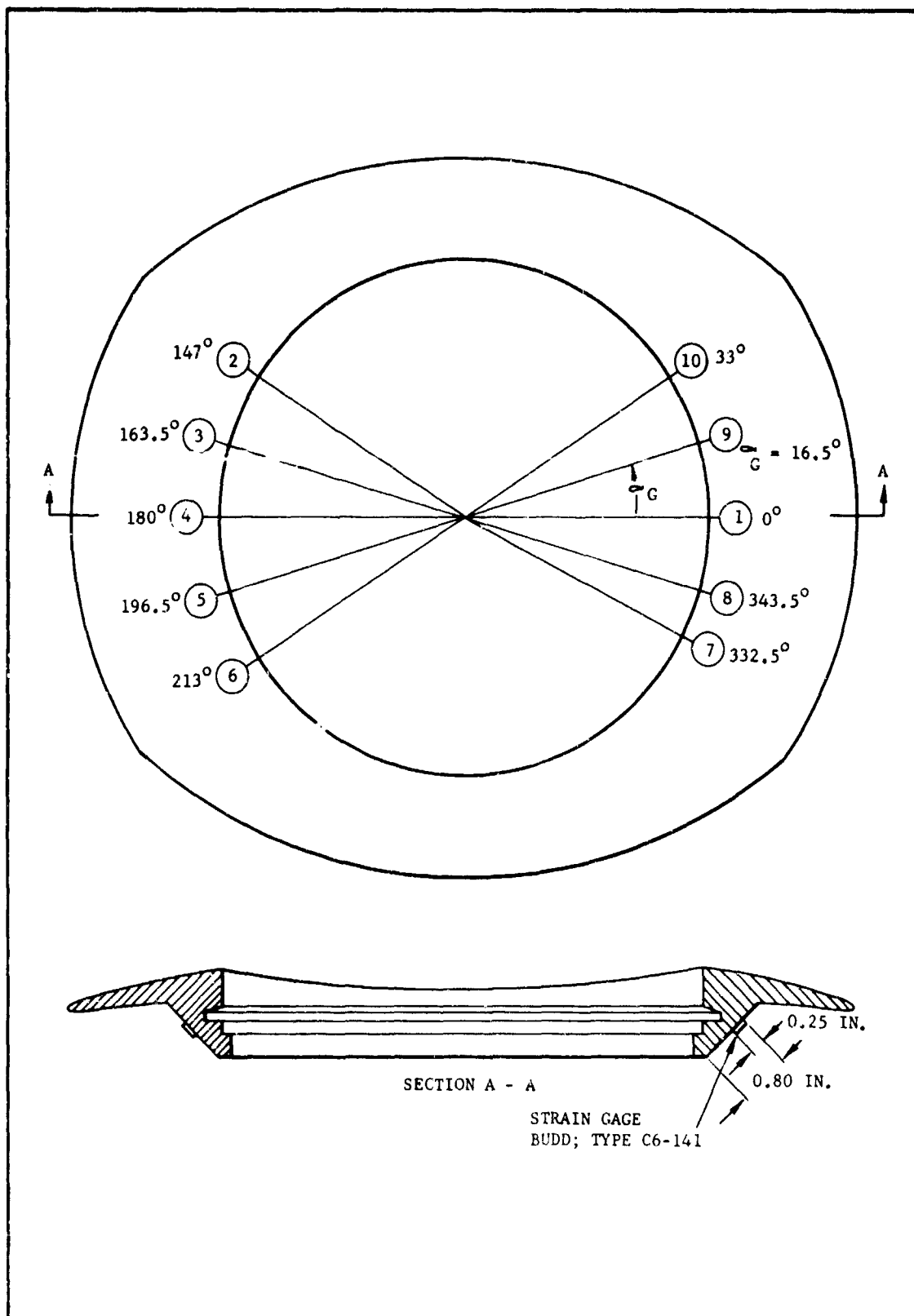


Figure 15. Strain Gage Location, Molding Effect Test

TABLE V  
MOLDING EFFECT TEST MATRIX

Test No.	Type of Test	Test Run No.	Material	Test Objective	Test Conditions
1	Molding effect	40	Goodyear flange, OIA00480-003 configuration S/N GY01929 new hand forged	Establish base line performance level	1 load cycle to failure
2	Molding effect	64 thru 66	Goodyear flange, S/N GY01912, new die forged	Determine difference in ultimate strength capability for resistance to simulated molding forces	2 cycles 0 to 40,000 lbs, 1 cycle to failure
3	Molding effect	52 thru 58	U. S. Rubber flange, S/N US21559, new die forged	Same as Test No. 2	3 cycles 0 to 20,000 lbs 3 cycles 0 to 40,000 lbs 1 cycle to failure
4	Molding effect	23	Goodyear flange, S/N GY02624, Good flange from rejected insulator	Determine if molding process degrades ultimate strength capability	1 cycle to failure
5	Molding effect	37	Goodyear flange, S/N GY02601, Good flange from rejected case	Determine if combination of molding case winding and hydroproof testing degrades the ultimate strength capabilities	1 cycle to failure
6	Molding effect	67 thru 69	Goodyear flange, S/N GY00026, S-20 configuration <sup>1</sup>	Same as Test No. 2	2 cycles 0 to 40,000 lbs 1 cycle to failure
<sup>1</sup> The R&D S-20 configuration flange has more base metal in the area where cracking occurs than the operational flange.					

TABLE V (Cont)  
MOLDING EFFECT TEST MATRIX

Test No.	Type of Test	Test Run No.	Material	Test Objective	Test Conditions
7	Molding effect	41	Goodyear flange, S/N GY00024, S-20 configuration. Reused from hydroproof effect Test No. 9	Same as Test No. 2	1 cycle to failure
8	Molding effect	70 thru 72	Goodyear flange, S/N GY01940, new hand forged reused from hydroproof Test No. 7	Determine if gap in support area degrades the ultimate strength capabilities	2 cycles 0 to 40,000 lbs 1 cycle to failure
9	Molding effect	73 thru 75	Goodyear flange, S/N GY02050, new hand forged	Determine if gap in support area without simulated molding degrades the ultimate strength capabilities	2 cycles 0 to 40,000 lbs 1 cycle to failure
1	Hydroproof effect	1 thru 16	Goodyear flange, S/N GY01912, new hand forged	Establish base line performance level	15 cycles from 0 to 50,000 1 cycle to failure
2	Hydroproof effect		Goodyear flange from die forging	Determine difference in ultimate strength capabilities to simulate hydroproof testing forces	
3	Hydroproof effect	59 thru 63	U. S. Rubber flange, S/N US21582, new die forged	Same as Test No. 2	4 cycles 0 to 50,000 lbs 1 cycle to failure
4	Hydroproof effect	20 thru 22	Goodyear flange, S/N GY02015, good flange from rejected insulator	Determine if molding process degrades ultimate strength capabilities	2 cycles 0 to 50,000 lbs 1 cycle to failure

TABLE V (Cont)

## MOLDING EFFECT TEST MATRIX

Test No.	Type of Test	Test Run No.	Material	Test Objective	Test Conditions
5	Hydroproof effect	33 thru 36	Goodyear flange, S/N GY02600, Good flange from rejected hydroproof case	Determine if combination of molding, case winding and hydroproof testing degrades the ultimate strength capabilities	3 cycles 0 to 50,000 lbs 1 cycle to failure
6	Hydroproof effect	42 thru 44	Goodyear flange, S/N GY02641, Good flange from rejected insulator	Determine effect on ultimate strength by increasing hydrotest closure flange thickness from 0.150 to 0.175 in.	2 cycles 0 to 32,000 lbs 1 cycle to failure
7	Hydroproof effect	48 thru 51	Goodyear flange, S/N GY01940, new hand forged	Determine the effect of snap ring positioning on strain distribution	1 cycle 0 to 32,000 lbs 2 cycles 0 to 50,000 lbs 1 cycle to failure
8	Hydroproof effect	45 thru 47	Goodyear flange, S/N GY02644, Good flange from rejected insulator	Determine the effect of snap ring bevel on strain distribution	2 cycles 0 to 50,000 lbs 1 cycle to failure
1	Segment Bending	24 thru 26	Goodyear flange, S/N GY01971, new hand forged, 3 segments	Establish base line performance for standard segment	1. Unclamped-load to failure 2. Clamped-load to failure 3. Clamped-load to failure
2	Segment Bending	27 thru 29	Goodyear flange, S/N GY02630, good flange from rejected insulator (3 segments)	Determine if molding affects segment properties	Same as Test No. 1
3	Segment Bending	Not Tested	Goodyear flange, good flange from rejected case	Determine if properties are affected by the combination of molding, winding and hydroproof testing	Same as Test No. 1

TABLE V (Cont)  
MOLDING EFFECT TEST MATRIX

Test No.	Type of Test	Test Run No.	Material	Test Objective	Test Conditions
4	Segment Bending	38 thru 39	Goodyear flange, S/N GY00013, S-20 configuration (2 segments)	Determine the segment properties for S-20 configuration flange	1. Unclamped-load failure 2. Clamped-load failure
5	Segment Bending	30 thru 32	U. S. Rubber flange, S/N US00259, from rejected case (3 segments)	Determine the segment properties for U. S. Rubber flange	Same as Test No. 1

TABLE VI

## MOLDING EFFECT TEST DATA

Test Run No.	Flange Serial No.	Primary Test Variable	Ins. Data Corner Radius	Loading Rate	Maximum Test Load	Test Run Description	Metallurgical Test
40	GY01929	Max. Strain	0.003 - 0.005	50 K/M	62 K	Clamped closure	Chem. analysis acc., no evidence of stress corrosion cracking (SCC)
64	GY01912	Gap in Support	0.007	50 K/M	40 K	0.010 in. gap in support 147° to 213° and 303° to 33°	Chem. analysis acc., no evidence of SCC
65	GY01912	Gap in Support	0.007	50 K/M	40 K	Same as Test Run 64 except 0.020 in. gap	
66	GY01912	Max. Strain	0.007	50 K/M	57.2 K	Same as Test Run 64, no gap	
52	US21559	Clamping Effect	0.020	50 K/M	20 K	Test closure not clamped	Chem. analysis acc., no evidence of SCC
53	US21559	Gap in Support	0.020	50 K/M	20 K	Same as Test Run 52, except 0.010 gap 303° to 33°, 147° to 213°	
54	US21559	Gap in Support	0.020	50 K/M	20 K	Same as Test Run 53 except 0.020 gap	
55	US21559	Effect of Spreader	0.020	50 K/M	40 K	Test closure clamped, dia. spread 0.012 0° to 180°	
56	US21559	Gap in Support	0.020	50 K/M	40 K	Same as Test Run 53 except closure clamped	

TABLE VI (Cont)

## MOLDING EFFECT TEST DATA

Test Run No.	Flange Serial No.	Primary Test Variable	Ins. Data Corner Radius	Loading Rate	Maximum Test Load	Test Run Description	Metallurgical Test
57	US21559	Gap in Support	0.020	50 K/M	40 K	Same as Test Run 54 except closure clamped	
58	US21559	Max. Strain	0.020	50 K/M	82.3 K	Test closure clamped, no gap	
23	GY02624	Max. Strain	0.010	50 K/M	56.4 K	Test closure clamped	Chem. analysis acc., no evidence of SCC
37	GY02601	Max. Strain	0.010	50 K/M	62.6 K	Test closure clamped	Chem. analysis acc., no evidence of SCC
67	GY00026	Gap in Support	0.072 Full	50 K/M	40 K	Same as Test No. 2, Run No. 64	Chem. analysis acc., no evidence of SCC
68	GY00026	Gap in Support	0.072 Full	50 K/M	40 K	Same as Test No. 2, Run No. 65	
69	GY00026	Max. Strain	0.072 Full	50 K/M	75.8 K	Same as Test No. 2, Run No. 66	
41	GY00024	Max. Strain	0.073 Full	50 K/M	78 K	Did not break, rapid yielding at 78,000 lb	Chem. analysis acc., no evidence of SCC
70	GY01940	Gap in Support	NA	50 K/M	40 K	Same as Test No. 2, Run No. 64	Chem. analysis acc., cracking occurred before mechanical failure
71	GY01940	Gap in Support		50 K/M	40 K	Same as Test No. 2, Run No. 64	

TABLE VI (Cont)

## MOLDING EFFECT TEST DATA

Test Run No.	Flange Serial No.	Primary Test Variable	Ins. Data Corner Radius	Loading Rate	Maximum Test Load	Test Run Description	Metallurgical Test
72	GY01940	Max. Strain	NA	50 K/M	69 K	Same as Test No. 2, Run No. 66	Chem. analysis acc., cracking occurred before mechanical failure
73	GY02050	Gap in Support	NA	50 K/M	20 K	Test closure not clamped, 0.010 gap in support	Chem. analysis acc., no evidence of SCC
74	GY02050	Gap in Support		50 K/M	20 K	Test closure not clamped, 0.020 gap in support	
75	GY02050	Max. Strain		50 K/M	32.5 K	Test closure not clamped, no gap	



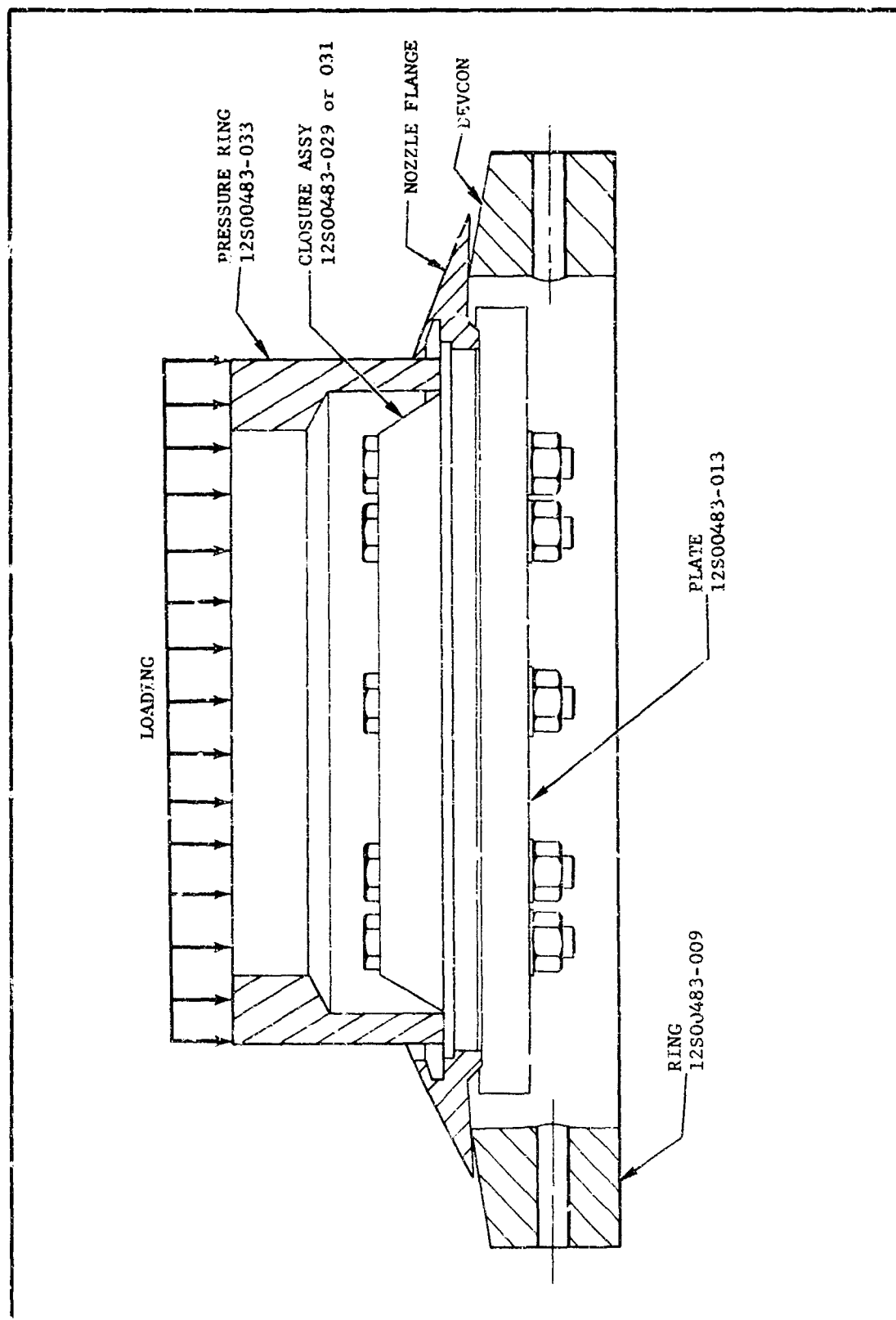


Figure 16. Molding Effect Test Configuration

Additional testing of this mismatch, or gap effect, showed a marked increase in strain as the gap increases. For example, on a new hand forged flange, S/N GY01940, the strain increased approximately 0.002 in/in. for each 0.010 in. increase in gap between the flange and support ring contours.

Failure load tests of various flanges are shown in Table VI. The failure of S/N GY01929 at a strain gage reading of just over 0.002 in/in. is very revealing when compared with the 0.0016 in/in. failure strain of S/N GY02601. Inspection data revealed a significant difference in the snap-ring groove corner radius of the two flanges. From these observations, it was concluded that a change in corner radius from 0.004 in. to 0.010 in. results in a 25 percent increase in a flange's ability to withstand mold load forces.

The effect of the Goodyear cooling-plug spread shims also warranted investigation as part of the simulated molding tests. During dome insulator molding and subsequent cooldown, Goodyear uses flange inserts (called cooling plugs) to maintain flange concentricity. The cooling plugs have spreader shims at the keyway and 180 degree area (Figure 17) that could result in an interference fit of up to 0.025 in. Therefore, tests designed to simulate the cooling-plug conditions were run and the data showed the only effect was local prestressing adjacent to the contact area during plug insertion. Once the prestress forces were exceeded by the simulated mold load forces, the cooling-plug effect was no longer measurable.

#### 6. Flange Segment Bending Studies

Half-inch wide segments from a new Goodyear hand-forged flange, S/N GY01971, a Goodyear hand-forged flange, S/N GY02630, obtained from a rejected insulator, and a new U. S. Rubber die-forged flange, S/N US00258, were tested. (A used Goodyear flange from a hydroproofed case was not available for these tests, so the U. S. Rubber flange was used for comparative purposes.) Prior to any segment testing, each specimen was dye-penetrant inspected, metallurgically polished, etched, and examined to determine if the grain structure of the material from the used flanges would reveal any indication of prestressing resulting from dome molding, case winding, and/or hydroproofing.

After completion of the metallurgical examination, each segment was loaded to failure in accordance with the clamped test configuration (simulating dome molding) shown in Figure 18. In addition, half-inch wide segments from the flanges used in the tests above, were loaded to failure in accordance with the test configuration shown in Figure 19. This test configuration gave comparative data of unclamped flange segments subjected to the same loads.

##### a. Clamped Configuration (Simulated Dome Molding)

A total of six (6) tests were conducted in this series of tests. Each segment was instrumented with a Budd Type C6-141 strain gage in the area shown as S.6 in Figure 18. Two leaf-type deflectometers (Figure 20) were used to measure the deflection resulting from the load, 4F, applied at a constant rate of 5000 lb/minute.

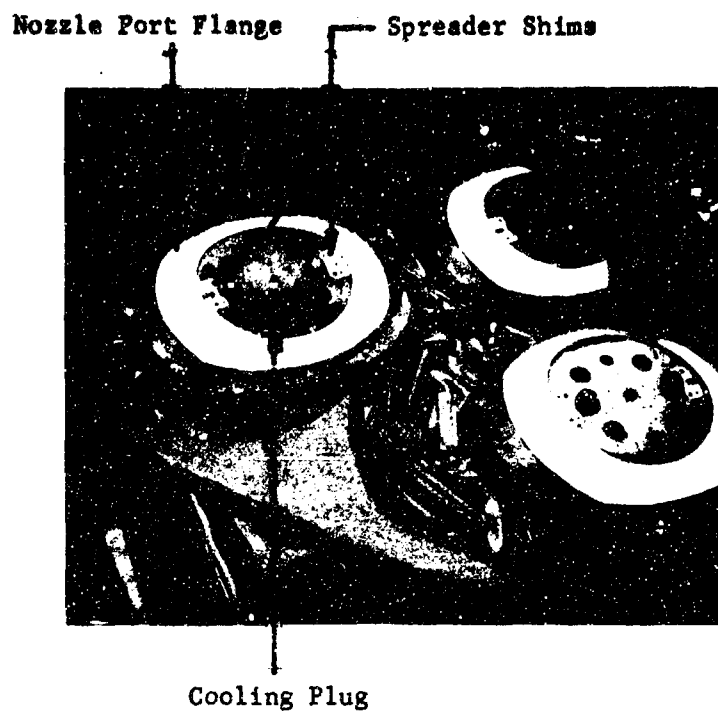


Figure 17. Cooling Plug with Shims

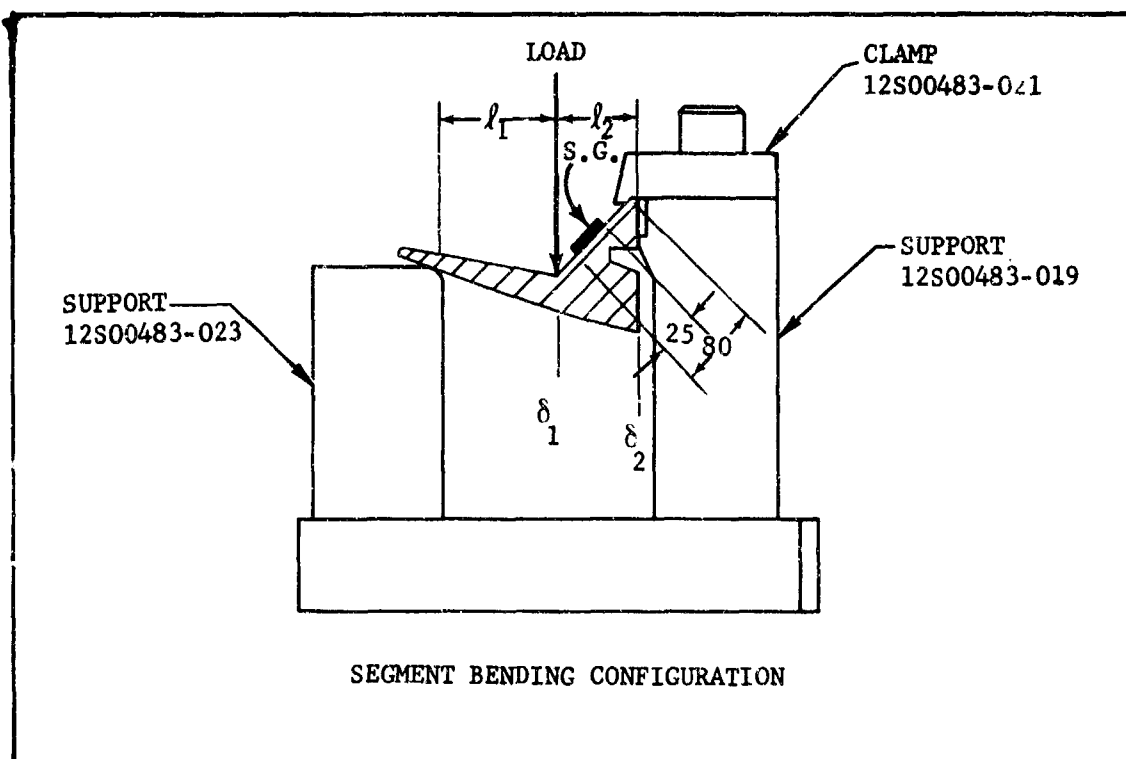
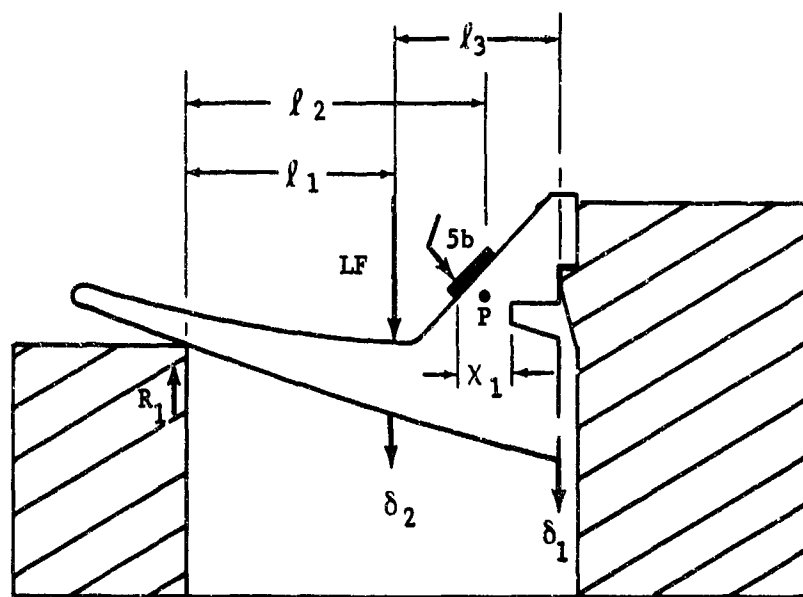


Figure 18. Segment Bending Configuration, Clamped Condition



(UNCLAMPED CONDITION)

Figure 19. Segment Bending Configuration, Unclamped Condition

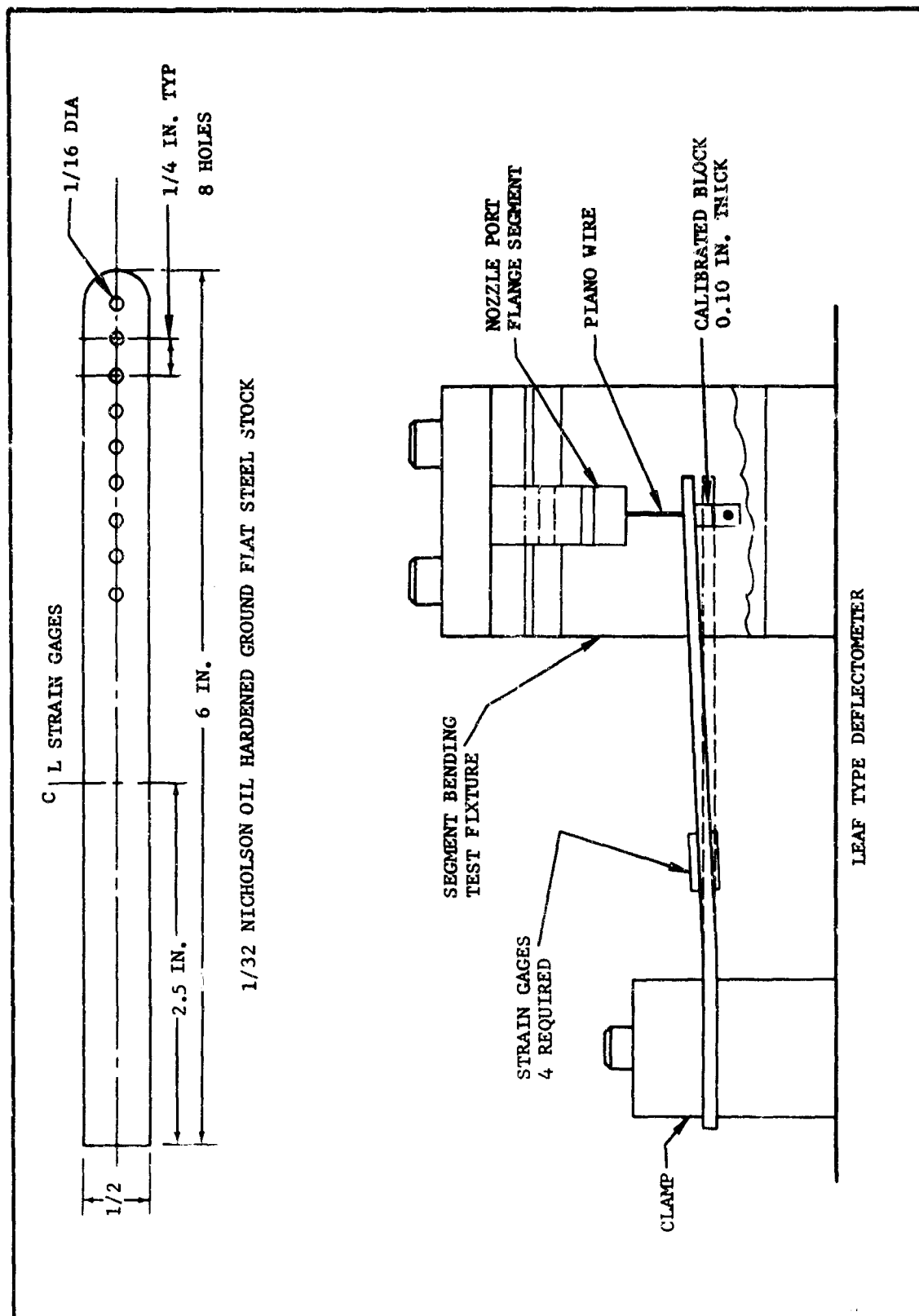


Figure 20. Leaf Type Deflectometer

Table VII contains the load test data and shows the comparative strength of segments from a new Goodyear hand-forged flange, S/N GY01971, a Goodyear hand-forged flange, S/N GY02630, obtained from a rejected insulator, and a new U. S. Rubber die-forged flange, S/N US00258.

Analysis of the comparative data indicates that the specimen used for test run number 28 had been overstressed during the molding operation at Goodyear. Although the dye-penetrant inspection did not indicate any cracks in the flange prior to testing, metallurgical examination of the failed test specimen showed the dye had penetrated two minute cracks having dimensions approximately 0.080 in. to 0.100 in. long by 0.050 in. deep. Another specimen from the same flange did not show any evidence of cracking and the failure load was comparable to those measured on the new Goodyear flange.

Both segments taken from U. S. Rubber die forged-flanges exhibited significantly greater strength. Furthermore, the plane of failure of the Goodyear segments was typical of the failures observed in all cracked nozzle port flanges; the segments from the U. S. Rubber flanges failed in a plane parallel to the load.

#### b. Segment Tests - Unclamped Condition

Half-inch wide segments from the same flanges used in the preceding tests were tested using the configuration shown in Figure 19. The only difference from the tests described above was the removal of the clamping fixture in order to test the beam strength of the segments.

Results of these tests, Table VIII, show that the beam strength of a new Goodyear hand-forged flange is approximately equal to the strength of a U. S. Rubber flange. Metallurgical examination of the failed Goodyear segment obtained from a rejected insulator indicated the presence of a minute crack prior to testing. Using the failure stress load of the new (unmolded) Goodyear flange as base line, the strength of the flange, apparently overstressed during dome molding, was reduced approximately 35 percent.

#### D. METALLURGICAL ANALYSIS

Studies were initiated to establish physical properties, metallurgical structures, and mode of failure of the cracked flanges. Comparative studies of the physical and metallurgical properties of flanges fabricated from hand-forged and die-forged billets were also conducted to determine if the use of die forgings would help alleviate the flange cracking problem.

##### 1. Chemical and Physical Analyses

Chemical and physical properties were obtained from representative samples of Kaiser flanges and forgings. All physical properties of the representative samples tested were as specified for aluminum alloy 2014-T652 in QQ-A-367, and none of the specimens tested had physical properties less than specified minimum requirements. Except for six minor variations in silicon content, all chemical tests met QQ-A-367 requirements. As X-ray fluoroscopy

TABLE VII

DATA FROM SEGMENT BENDING TESTS  
CLAMPED CONDITION

Run No.	Flange		Measurements at Failure				Stress (Calc.) psi	Stress Concentration Factor $\delta_{Max}/\delta$
	S/N	Section Length (in.)	LF (lb)	$\delta_1$ (in.)	$\delta_2$ (in.)	S.G. (in./in.)		
24	GY01971	0.468	1370	0.008	0.028	N/A	7,730	8.0
25	GY01971	0.4785	1870	0.010	0.037	0.0062	10,620	5.8
28	GY02630	0.490	1140	0.007	0.022	0.0040	6,230	9.9
29	GY02630	0.496	1400	0.006	0.021	0.0051	8,190	7.6
31	US00258	0.489	2590	0.006	0.104	0.0035	11,670	--
32	US00258	0.4325	2110	0.007	0.100	0.0050	11,000	--

TABLE VIII

DATA FROM SEGMENT BENDING TESTS  
UNCLAMPED CONDITION

Test Run No.	Flange		Measurements at Failure				Stress (Calc.) psi
		Section Length (in.)	LF (lb)	$\delta_1$ (in.)	$\delta_2$ (in.)	S.G. (in./in.)	
26	GY01971	0.468	1150	0.011	0.022	0.0059	106,700
27	GY02630	0.487	810	0.0045	0.018	0.0043	70,100
30	US00258	0.5595	1695	0.0055	0.041	0.0068	104,700

was used for most of the chemical analysis, the excess silicon found in the above samples was probably caused by minute quantities of grinding media left on the surface of the samples during sample preparation.

## 2. Metallurgical Analyses

### a. Hand Forgings - Macro and Microstructures

Micro examinations show the failures were always associated with the forward 0.005 in. maximum snap-ring groove radius. The fractures appeared to have initiated at the keyway or 180 degrees from the keyway and usually extended from three to five inches circumferentially on both sides of the initiation point. (See Figures 21, 22, 23, 24, 25, and 26.)

In the early stages of the program, studies were made to establish the metallurgical structures of the flanges of typical hand forgings (Figure 27). For control purposes, specimens were prepared from heat treated hand forgings processed through but not beyond the flange machining operation.

Figure 28 shows the typical macrostructure of a control flange sectioned through the zone where cracking normally occurs. The elongated grain structure, varying in size across the section, is typical of the hand forging process used in the production of these flanges. A comparison of the macro and microstructures of cracked flanges, from various stages in the manufacturing process, with those of the control flanges did not reveal any significant difference.

Further metallographic studies showed that the Minuteman third-stage nozzle-port flanges made from Kaiser hand forgings when machined result in a poor configuration for resistance to stresses applied normal to the snap-ring groove surfaces because of the grain flow. This flow is parallel to the upper and lower surfaces of the snap-ring groove. Furthermore, the transverse (weakest) direction is normal to the direction of the grain flow. During dome molding and case hydroproofing, the direction of maximum stress applied to the snap-ring groove is also normal to the direction of the grain flow. This results in the maximum applied external stresses paralleling the direction in which the part is weakest. In this type of flange, the elongated grains developed by the hand forging process terminate in the bottom of the snap-ring groove. With this condition, a maximum number of grains are exposed endwise in the area of the forging where internal tensile stress is at its greatest. (See Figure 26.)

In any biscuit forging, such as those used in the nozzle-port flange, the forging is under internal compressive stress inwardly from the edges to about 10 percent of the width of the cross section. The remaining area of the cross section is under internal tensile stress with a maximum value at the center of the forging. The snap-ring groove in Kaiser's hand forgings are machined into the center of the billet; this exposes the region of highest internal tensile stress to whatever external environment is present. In summary, the snap-ring groove area in a Kaiser hand forging is the region of greatest contained internal tensile stresses and is weakest in the direction of highest external stresses.





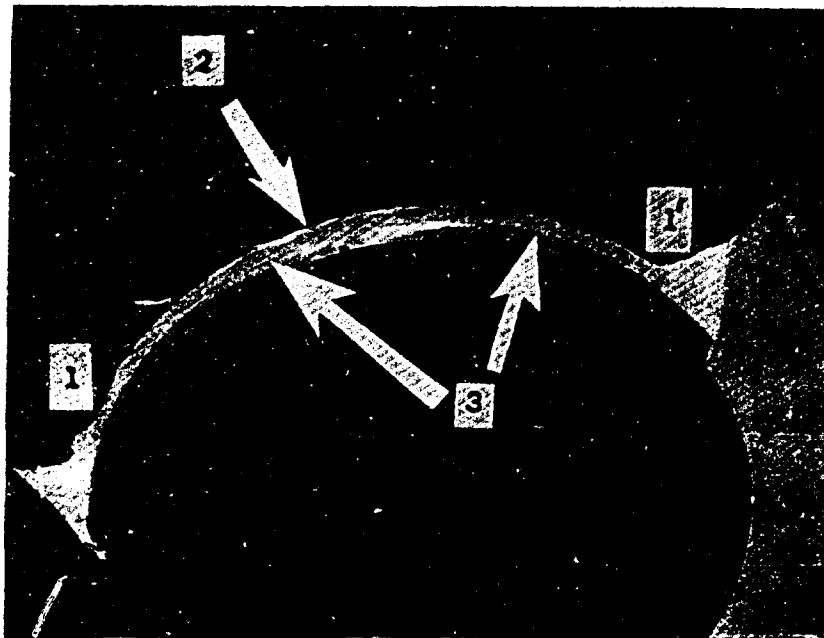
No failure occurred in adapter GY 027828  
removed from insulator RP-13, Port No. 4

Figure 21. Unfractured Adapter (1/5 actual size)



Polished, etched cross section of specimen  
taken 180° from adapter keyway. Arrow points  
to point of origin of fracture.

Figure 22. Typical Failure Specimen (Adapter GY 02643, 1-1/5 actual size)



Shown (approximately 1/5 actual size) is adapter GY 02508 from Case HP 00429, Nozzle Port 3. The original failure extended from (1) to (1') on the figure. The bright edge indicated by arrow (2) is where shear failure occurred when the fracture was mechanically exposed for surface examination. Arrows (3) point to small shiny, irregular areas extending into the failure surface from the inside edge of the snap-ring groove. These are indications of stress corrosion cracking. The fracture originated in these areas.

Figure 23. Flange-Failure Sample

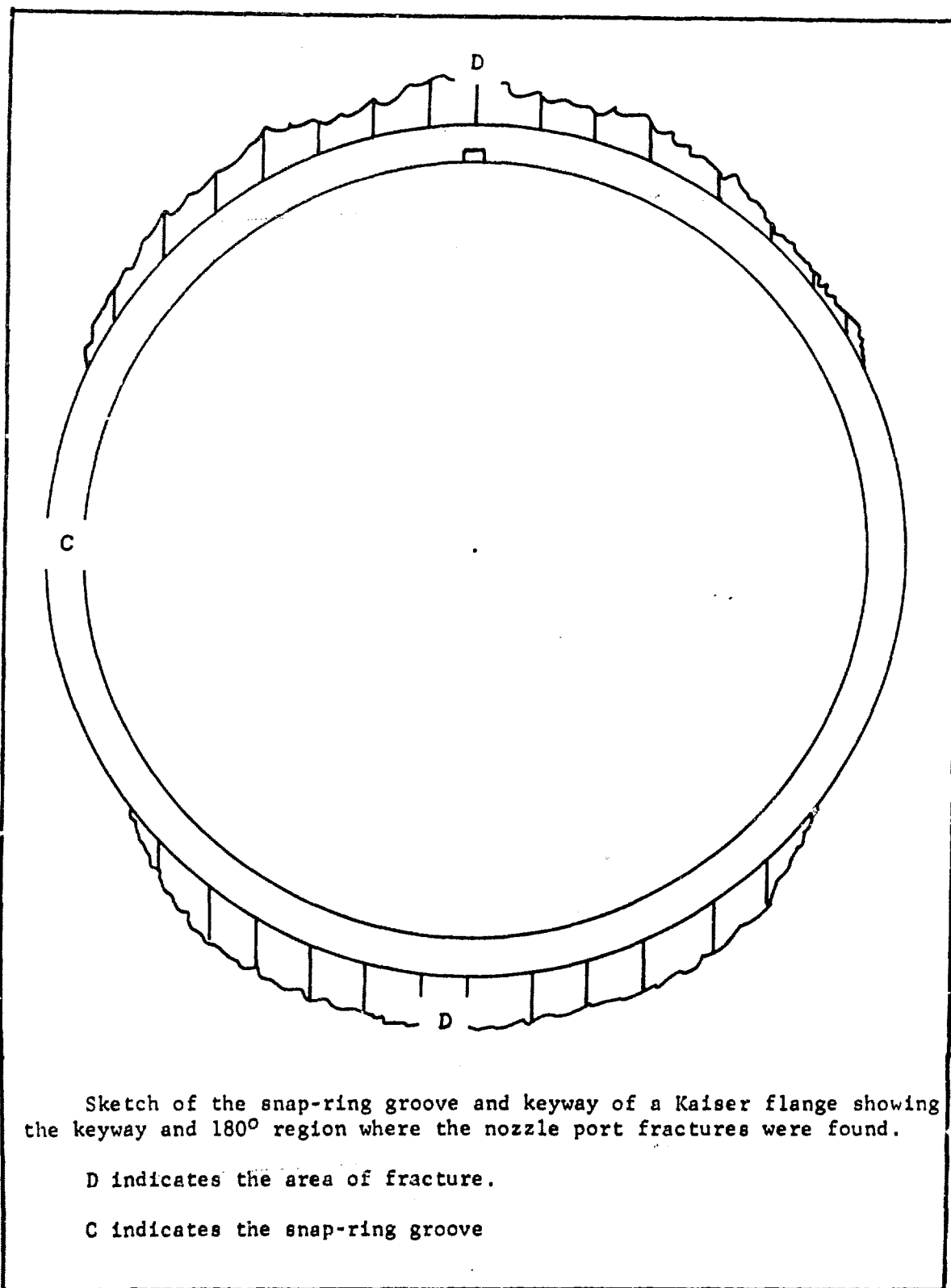
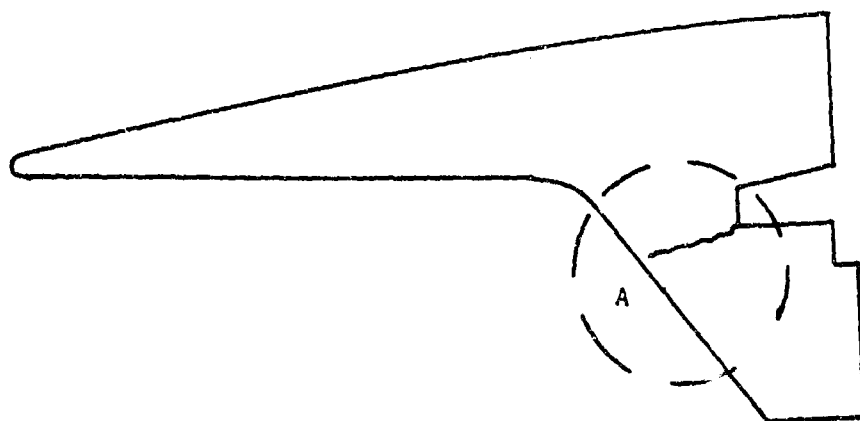
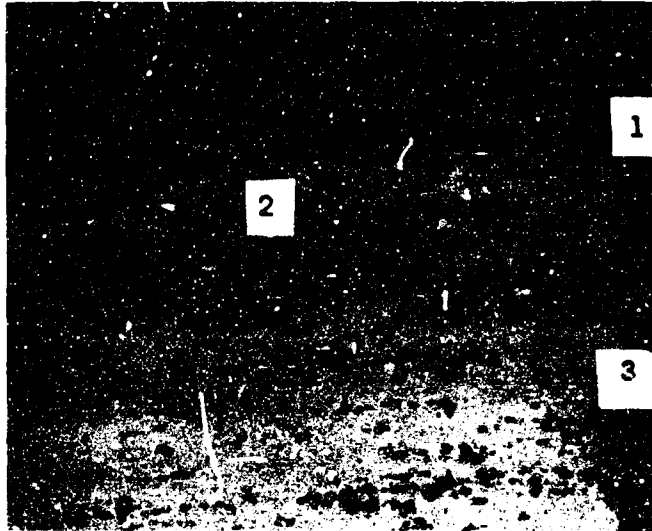


Figure 24. Fracture Regions



Sketch showing general orientation and length of crack  
in Kaiser hand-forged flanges. Crack extends to approx-  
imately  $3/32$  in. of the outboard edge of the flange  
(area A on sketch).

Figure 25. Crack Orientation

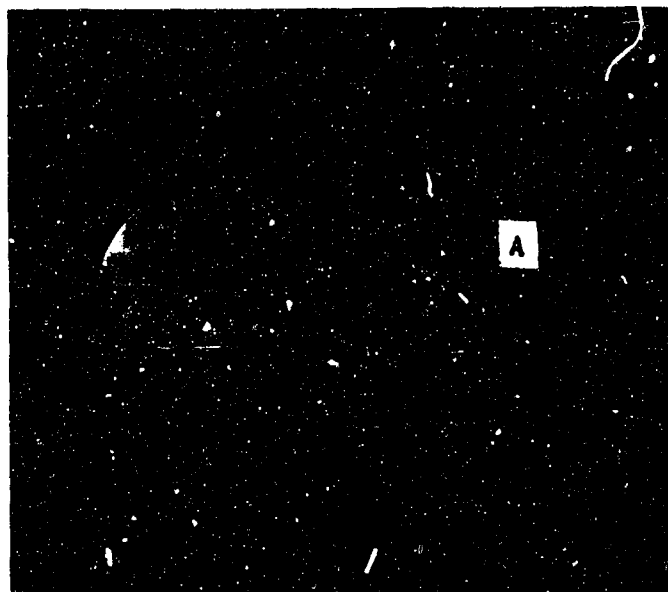


This is a photomicrograph (133X magnification) of a polished, etched, cross section taken from cracked adapter GY 02586. Removed from case HP 00446 Nozzle Port 3. Hand forging from the Kaiser Aluminum Company.

Legend

- 1- Inboard, interior radius of the snap-ring groove
- 2- Large grain which has failed intergranularly
- 3- Snap-ring groove area. Note how grain flow terminates at a 90° angle to the bottom surface of snap-ring groove

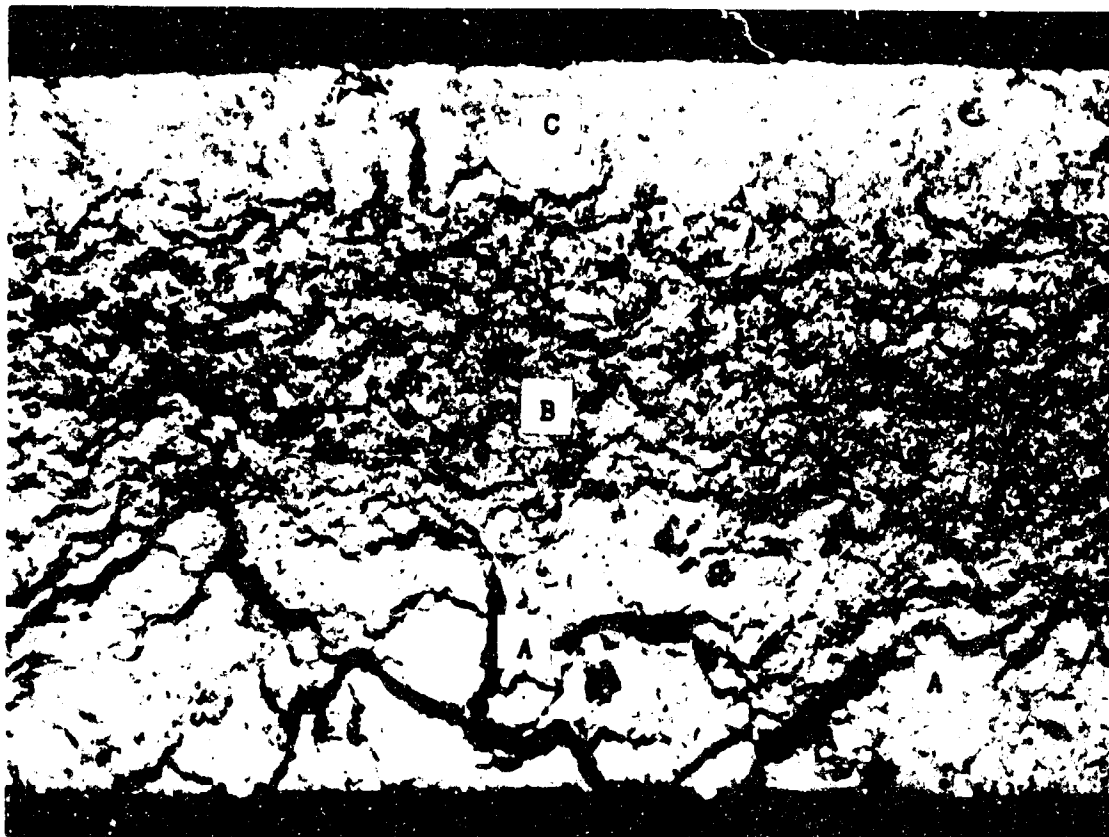
Figure 26. Photomicrograph of Cracked Flange



Reduced to 2/3 Actual Size

This photomicrograph shows the typical grain flow configuration of a Kaiser hand-forged billet. The grain size is quite large in some regions of this forging (Note Point A).

Figure 27. Grain Flow Lines in Kaiser Hand-Forged Billet



Mag. 16 Diameters

Section of fracture surface taken from cracked aluminum alloy (2014-T652) adapter GY 02508. The adapter was installed in Case HP 00429, Nozzle Port 3.

Region (A) shows a structure typical of a stress corrosion cracking fracture surface.

Region (B) shows a structure typical of an overstressed tensile fracture surface.

Region (C) is an area of shear failure created when the fracture was mechanically opened for surface examination.

The part is a hand forging manufactured by Kaiser Aluminum Company.

Figure 28. Fracture Surface

b. Crack Path and Characteristics

On the majority of specimens prepared to determine and establish identifying characteristics of the cracks developed in the flanges, the following fracture surface characteristics were observed:

- (1) A shiny, flaky area was usually visible, without magnification, at the point of crack initiation.
- (2) Using a stereomicroscope at low magnification (10 to 20 power), the fracture surface at point of initiation had a woody appearance. This woody appearance was present on some specimens even though the shiny, flaky structure was not visible. (See Figure 28.)
- (3) Examination of the fracture surface with a light metallograph at 1500-2000 magnification, using an oil immersion lens and focusing up and down over the fracture surface, a planar crystalline structure was observed. It was also observed that the crystal planes usually intersected one another at approximately 120 degree angles.

Because of the difficulty encountered in making detailed studies and the impossibility of making photomicrographs by this method, Hercules obtained the services of an Electron Microscope at Hill Air Force Base. Figures 29 and 30 show typical planar crystalline surfaces with grain intersections at approximately 120 degree angles. Some corrosion products could also be seen on the planar surfaces as well as the intergranular crack path.

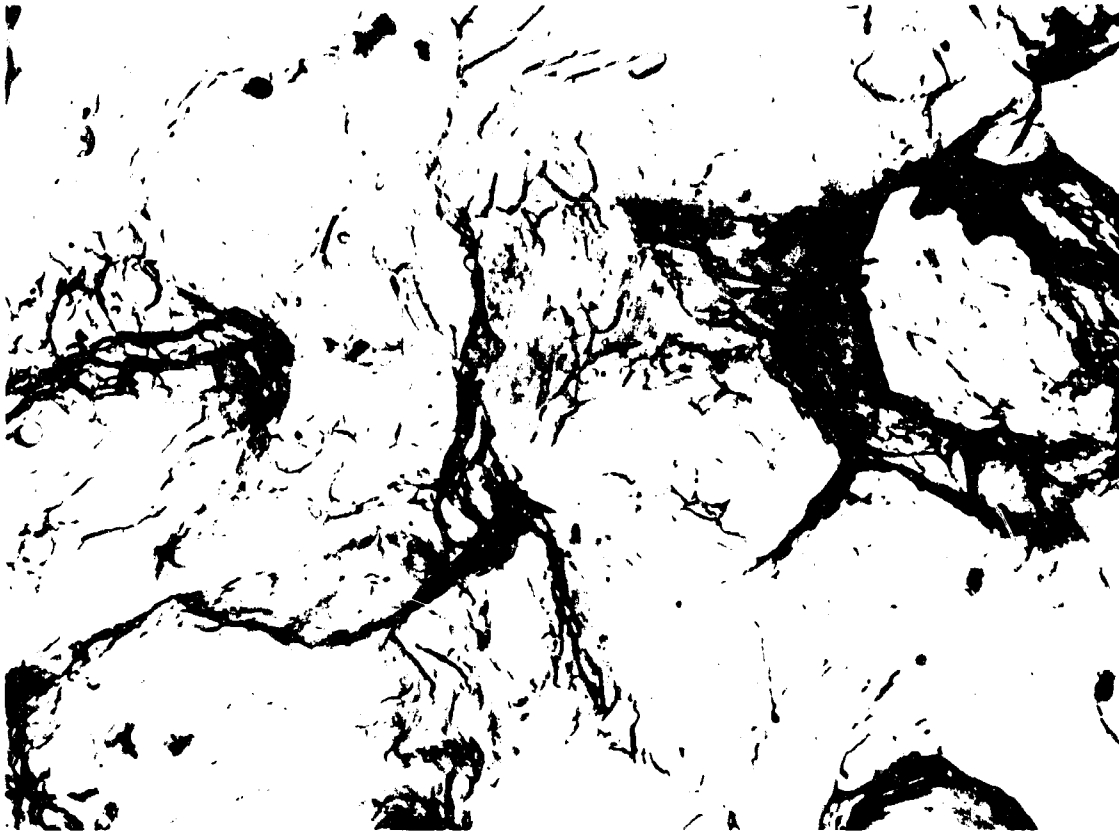
The establishment of the above listed characteristics as typical of stress corrosion fractures is rather recent and is best illustrated and described in the Electron Fractography Handbook ML-TR-64-416, 1965 Edition.

Beyond the initial stage of fracture, the surface characteristics of the cracks were typical of an overstressed tensile failure with a transition zone between the stress corrosion fracture area and the tensile overstress fracture area. (See Figures 28, 30, and 31.)

On those specimens that did not evidence stress corrosion characteristics at the point of initiation, the entire fracture surface exhibited typical ductile tensile failure characteristics.

Classification of the two types of failure (stress corrosion at initiation point then ductile tensile failure or ductile tensile failure only) revealed that all specimens taken from cracked flanges discovered at post-hydroproof exhibited stress corrosion characteristics, and specimens taken from cracked flanges discovered after dome molding or after case hydroburst exhibited either type of failure.



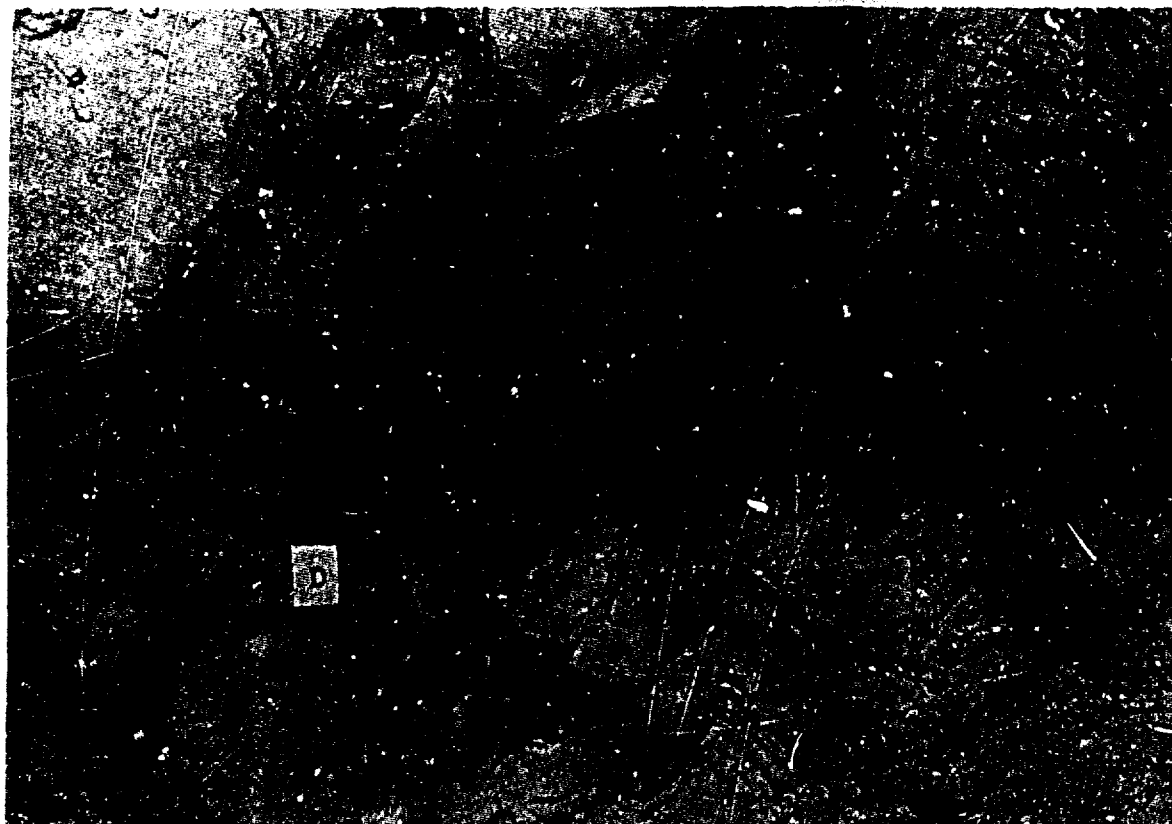


Mag. 3000X

This is a classical example of stress corrosion cracking on the fracture surface of aluminum alloys. Note flat planar structure with grain intersections approximating  $120^\circ$ .

This photomicrograph was taken with the electron microscope at Hill Air Force Base.

Figure 29. Typical Corrosion Fracture



Mag. 4200X

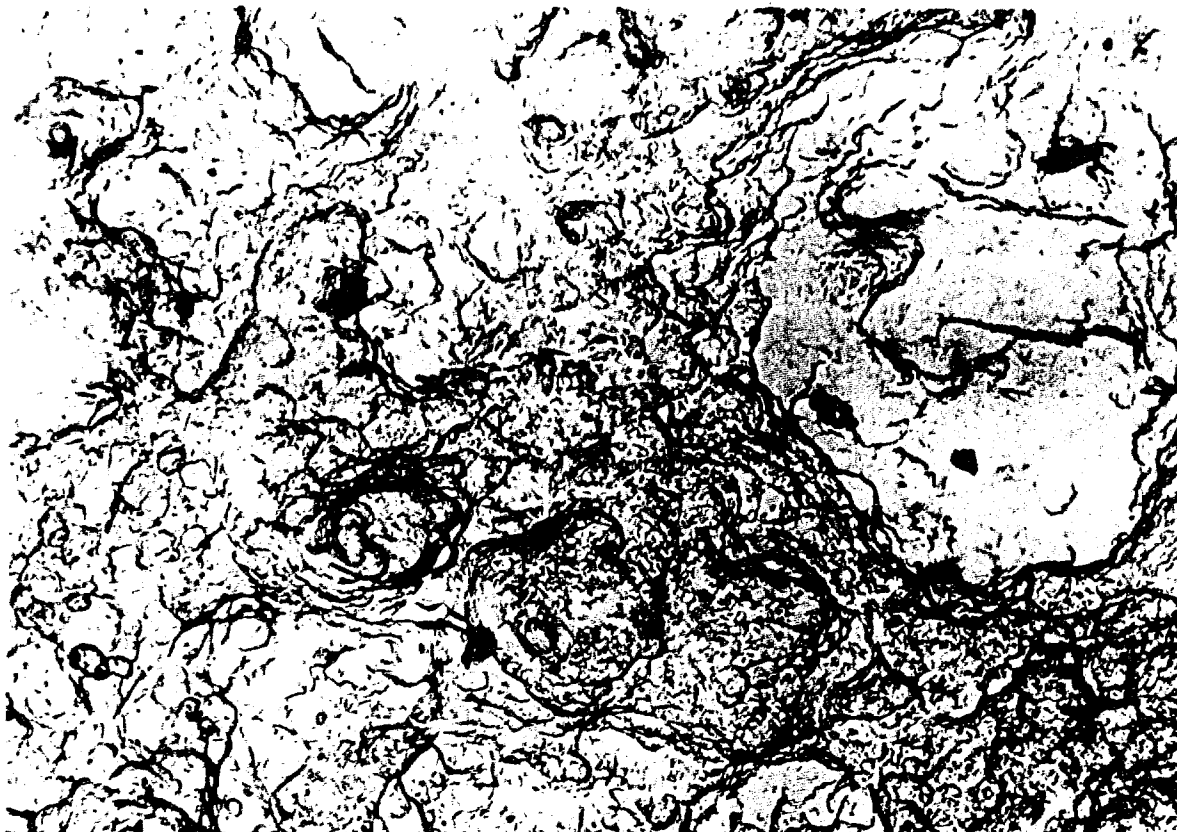
Flange GY 02643 Removed from Goodyear Insulator Serial No. 573

This electron microscope photomicrograph shows a transition zone between a stress corrosion crack fracture area and a tensile overstress (dimpled) fracture area.

C is tensile overstress.

D is stress corrosion crack area. Note planar structure and  $120^\circ$  angles between crystal surfaces.

Figure 30. Fracture Surface Transition Zone



Mag. 3000X

This electron microscope photomicrograph shows the typical dimpled fracture surface of an overstress tensile failure.

As shown in Figure 29 stress corrosion cracking was present in other areas of the same flange.

Figure 31. Typical Tensile Fracture

c. Mode of Failure

From the above finding, it was concluded that the initiating cause of nozzle-port flange failures, observed after dome molding and after case hydroproofing, was overstressing of the flange during dome molding. The degree of stressing depended on variables within the molding process and resulted in tensile failure of the flanges during molding or stressing of the flange to the point where it became susceptible to stress corrosion.

(1) Residual Stress Determination

Several tests were run in an effort to establish a method of determining residual stress level existing in a flange at the various stages of production. At first, it appeared that the use of liquid mercury, in the presence of a saturated aqueous solution of mercuric chloride, could be used as an indicator of residual tensile stress levels in the area of the snap ring groove. Analyses of the tests showed that some of the specimens exhibited evidence of severe pitting only on the exposed surfaces while others exhibited severe pitting plus intergranular cracking caused by grain boundary penetration of the liquid mercury. From these results, it could be concluded that the mercuric chloride test did indicate the presence of a tensile stress if that stress had a value equal to or greater than a certain "threshold stress". However, the specific "threshold stress" value could not be established and mercuric chloride could not be used as a valid test for establishing stress levels.

As part of the photoelastic study, Allied Research Associates performed an independent metallurgical study of the nozzle port cracking problem and reported findings substantiating Hercules' findings described above.<sup>1</sup>

(2) Anodic Coating

As specified by drawing 01A00480, the entire bore surface of the nozzle port flange was hard anodized per Specification HPC-133-02-4-8, whereas all other surfaces are chemical conversion coated (alodined) in accordance with Specification HPC-133-02-4-1.

Microexamination of flanges in the snap-ring groove (bore) area revealed that the anodized layer often contained defects which could be associated with the overall cracking problem. Typical examples of such defects, which include cracking at corners of the anodized layer, thinning of anodized layer in the snap-ring groove radii and porosity within the anodized layer, are shown in Figure 32. Figure 32 also shows a typical anodized layer containing a crack which continues into the metal flange as well as several other surface cracks in the immediate vicinity.

---

<sup>1</sup>Becker, Hamilton and Kyle, Photoelastic Investigation of the Stage III Minuteman Nozzle Port Flange, Documents No. ARA 289-1, ARA 289-2, and ARA 289-3

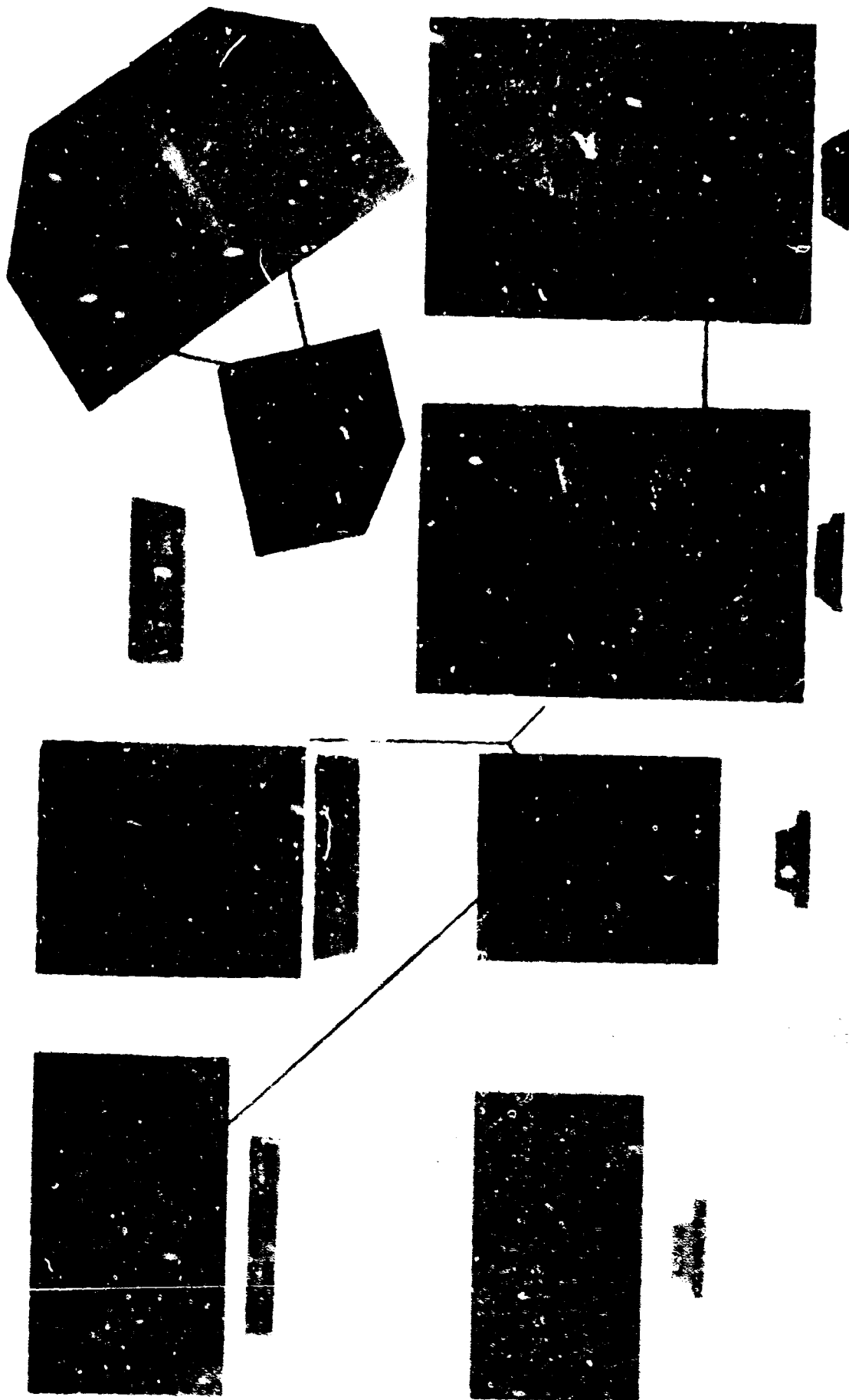


Figure 32. Metallurgical Structure of Flange

When related to the overall cracking problem, these defects in the surface coating would not only act as stress risers but they would also expose base metal that was susceptible to stress corrosion. Since part of the flange was already protected with a more ductile coating which did not exhibit the undesirable characteristics of the brittle anodized coating, it was recommended that the chemical conversion coating be used on the snap-ring groove area instead of the hard anodized coating. See ECP-WS-135B-HF-B116-1R1 and 2R1.

### (3) Die Forgings

Metallurgical examination of Kaiser's die forgings and Minuteman third stage nozzle-port flanges machined from Kaiser's die forgings revealed a structure quite different from that of a hand-forged component. Figure 33 shows typical macrostructures of a flange machined from a Kaiser die forging and a flange machined from a Kaiser hand forging. Both samples were sectioned through the zone where cracking normally occurred.

From the above referenced photomacrographs, it can be seen that the grain flow is nearly perpendicular to the upper and lower surfaces of the snap ring groove. Examination of the die-forged microstructure also showed that a minimum number of grains terminate in the bottom of the snap-ring groove.

A comparison of the metallurgical structures of typical flanges machined from Kaiser's forgings showed that the use of die forgings would minimize the undesirable characteristics of the hand forging previously discussed in Section 2.a.

### 3. Conclusions

The principal factor leading to cracking of a hand-forged nozzle-port flange was overstressing of the flange during aft dome molding. The degree of stressing depended on variables within the molding process and resulted in: (1) tensile failure of the flange during molding, or (2) stressing of the flange to the point where it became susceptible to stress corrosion, or (3) acceptable flanges.

Although the exact conditions (corrosion environments, stress levels, etc.) necessary to promote stress corrosion cracking were not identified in this study, it could be concluded that the initiating cause of flange cracking observed after hydroproofing was overstressing at the flange during dome molding, i.e., during dome molding the flange had been stressed to the point where it became susceptible to stress corrosion. Stress corrosion had then proceeded sufficiently to weaken the flange thus causing failure during hydroproofing.

To increase the flange's ability to withstand the stresses induced during dome molding, it was recommended that:

- a. Flanges used at Goodyear Tire and Rubber Company be machined from Kaiser's die forgings rather than hand forgings.
- b. A chemical conversion coating be used on the snap-ring groove area instead of the hard anodizing treatment.

#### E. CONCLUSIONS

The investigative efforts led to the following conclusions:

1. The flange-cracking problem could not be correlated to a particular flange heat lot or specific material discrepancy.
2. The flange-cracking problem could not be correlated to the nozzle port machining process.
3. Case winding and machining did not contribute to the nozzle-port cracking problem.
4. The Goodyear method of determining the amount of rubber to be inserted into the mold was inaccurate and allowed a volume deficiency of up to 73 cubic inches.
5. The dimensional analysis showed a possible contour mismatch between the nozzle-port flange and the aft-dome mold of up to 0.046 in.
6. Structural integrity of the case is not impaired by a cracked nozzle port flange.
7. Firing pressures do not produce sufficient stresses to crack a nozzle-port flange that has withstood hydroproofing.
8. The position of the snap ring can have a minor effect on the flange during hydroproof.
9. Standard hydroproof closures produce more severe stresses on nozzle port flanges than modified hydroproof closures.
10. A change in the snap-ring groove corner radius from 0.004 to 0.010 in. results in a 25 percent increase in ability of a flange to withstand mold load forces.
11. Flanges machined from die forgings are stronger than the hand-forged flanges in the snap-ring groove.
12. The alodine in the snap-ring groove improves the resistance of the groove to environmental exposures.

13. The principal factor leading to cracking of hand-forged nozzle port flanges was overstressing of the flange during aft-dome molding.
14. Variables within the accepted procedures for aft-dome molding at Goodyear produced three flange conditions:
  - a. Flange tensile failure during molding.
  - b. Stressing the flange to the point where it became susceptible to stress corrosion.
  - c. Acceptable flanges.

#### F. RECOMMENDATIONS

As a result of the foregoing conclusions drawn from the investigative efforts, the following actions were recommended:

1. Increase the radii of the nozzle-port flange snap-ring groove.
2. Replace hard anodizing treatment of the snap-ring groove area of the nozzle port flange with a chemical conversion coating.
3. Use of die forgings rather than hand forgings.
4. Correct molding conditions at Goodyear which cause overstressing of nozzle port flanges.



## SECTION III

### FLANGE MODIFICATION TESTING

Recommended modifications to the nozzle-port flange were incorporated into hardware and tested as described below.

#### A. PROPOSED MODIFICATIONS

All production Goodyear nozzle-port flanges were machined per drawing 01A00480 from 2014-T652 hand-forged aluminum-alloy billets. Results of the metallurgical and simulated molding tests showed that three modifications of the flange would be required to eliminate the cracking problem. These are: (1) use die forgings rather than hand forgings for making the aluminum flanges; (2) increase the radii in the corners of the snap-ring groove; and (3) use chemical conversion coating on the snap-ring groove surface instead of the hard anodizing treatment.

#### B. FOUR FLANGE TEST

Four die forgings were randomly selected from the stock on hand at Goodyear to determine whether the metallurgical flow line configuration within the die-forged flange was improved compared to the flow line configuration of the hand-forged flange and to assure compliance of the forgings to chemical and physical requirements. The forgings met both the chemical and physical specifications described in QQ-A-367 (Table IX). The flow-line characteristics of the forgings were oriented perpendicular rather than parallel to the top and bottom edge of the nozzle port flange snap-ring groove (cracking zone). Comparative flow-line orientation for flanges machined from the two types of forgings is shown in Figure 33. The reorientation of the flow lines as seen in the die forging definitely improves the capability of the flange to withstand loads imposed upon the snap-ring groove.

#### C. SIX FLANGE TEST

Six flanges, machined from die forgings, were tested to evaluate suggested design modifications. The six flanges were manufactured to the 01A00480 drawing configuration with the following modifications.

##### 1. Flange Radii

All six flanges were fabricated with an increased radius in the snap-ring groove. The forward radius was  $0.040 \pm 0.010$  in. and the aft radius was  $.025 \pm .005$  in.

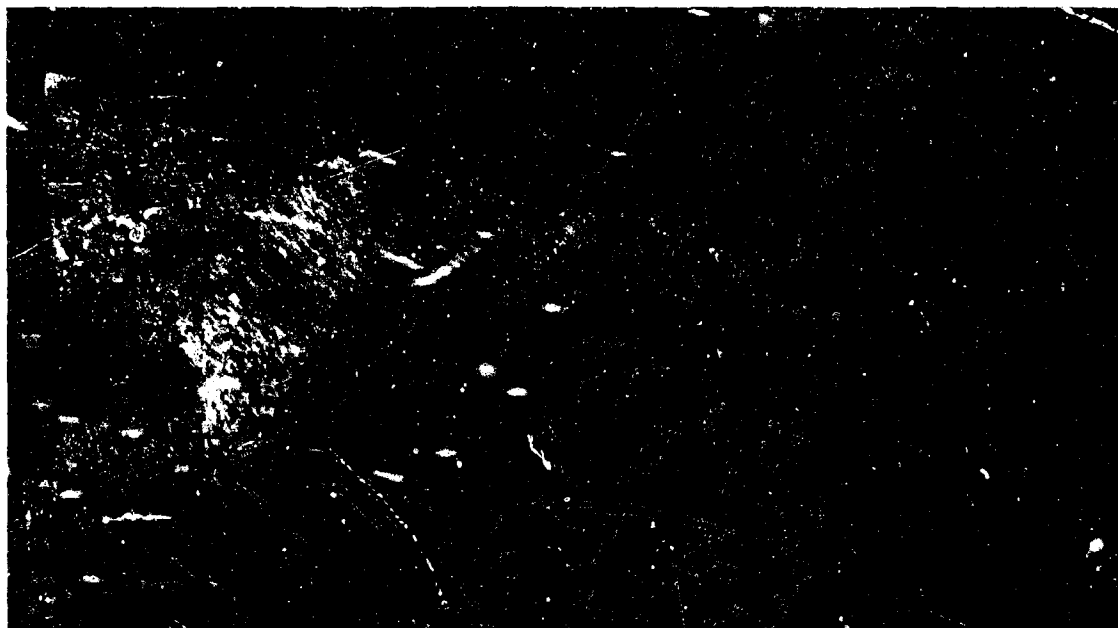
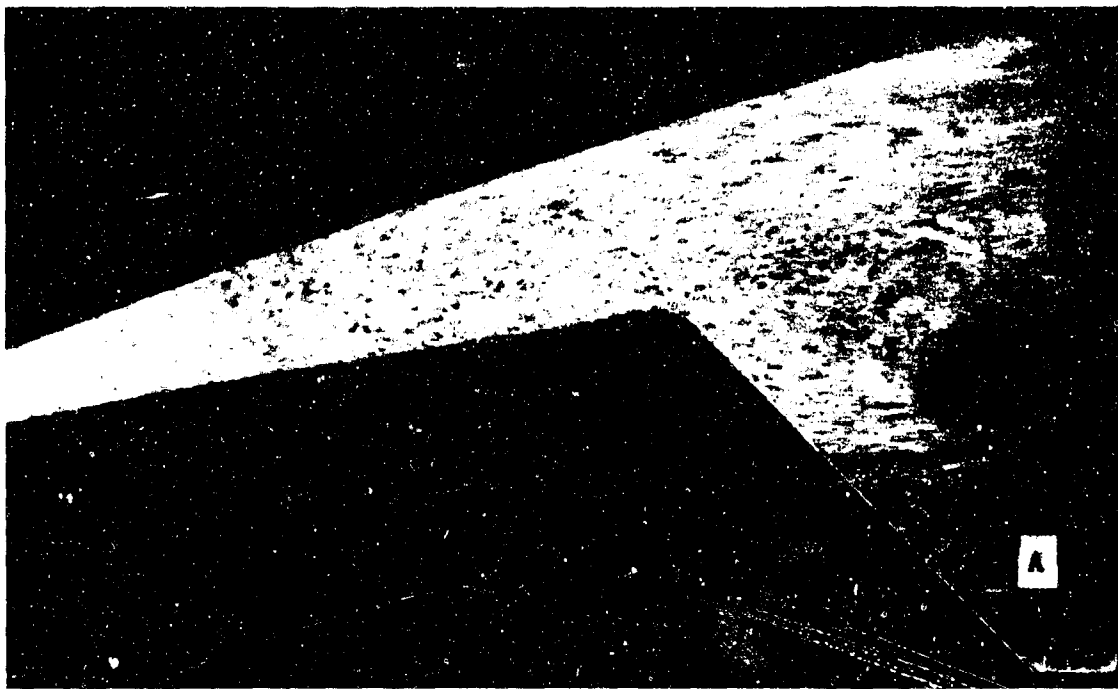
##### 2. Snap-Ring Groove Surface Preparation

The flanges were coated for protection as follows:

- a. Two flanges, SN GY02711 and GY02717, had hard anodize applied as specified in the drawing.

TABLE IX  
BILLET CHEMICAL AND PHYSICAL TESTING DATA

		Physical Results					Chemical Results (%)									
Billet GY P/N	Heat Lot	Tensile in KIP's			Rc Hardness		Mg	Si	Cu	Cr	Fe	Mn	Zn	Ti		
		High	Low	Ave.	High	Low									Ave.	
2F1-5-3C 986	GA4	71.0	66.0	68.9	83	83	.07	1.3	4.6	0.02	0.5	0.47	0.07	0.09		
2F1-5-3C 986	FA29	68.9	62.3	65.9	83	82	0.7	1.3	4.3	0.01	0.4	0.45	0.10	0.07		
2F1-5-3C 986	GA3	71.3	69.2	70.5	84	83	0.75	2.2	4.2	0.02	0.39	0.46	0.08	0.09		
2F1-5-3C 986	GA4	72.0	67.2	71.7	84	82	0.64	2.4	4.4	0.02	0.39	0.45	0.09	0.09		



Top photomicrograph shows typical grain flow lines of a Goodyear adapter machined from a Kaiser hand-forged billet (type in which fracture has occurred).

Bottom photomicrograph shows typical grain flow line configuration of an adapter machined from a Kaiser die forging.

Figure 33. Typical Forging Flow Lines

- b. Two flanges, S/N GY02744 and GY02745, had no coating applied.
- c. Two flanges, S/N GY02747 and GY02748, had hard anodize applied to all diameters except the snap-ring groove which was chemical conversion coated.

### 3. Flange Chemical and Physical Test Data

The chemical and physical results are listed in Table X and the typical flow line configuration is depicted in Figure 33. The results of these investigations were:

- a. All flanges met the chemical and physical properties as specified in QQ-A-367. (See Table X.)
- b. Mercuric chloride treatment of the flanges showed no evidence of residual stresses in the snap-ring groove.
- c. Metallurgical examinations showed the anodizing coat to be porous and brittle and therefore, susceptible to cracking. Such cracking creates stress risers and also allows exposure of the aluminum surface to environmental conditions conducive to corrosion.<sup>1</sup>
- d. The combined results of changing from hand to die forging and increasing the snap-ring groove radii from 0.005 in. maximum to 0.040 in. for the forward radius and 0.025 in. for the aft radius, increased the ultimate strength of the flange from 78,200 psi to 90,700 psi.<sup>1</sup>
- e. Macrographic study of flanges machined from die forgings indicated that the flow lines were oriented nearly perpendicular rather than parallel to the snap-ring groove as in hand forgings. (See Figure 33.) Perpendicular orientation of flow lines increases a flange's capability to withstand stresses applied normal to the snap-ring groove surfaces.

### 4. Flange Changes

At the conclusion of the evaluation, Engineering Change Proposals (ECP's) WS-133B-HP-B116-1R1 and 2R1 were prepared and submitted to Minuteman Configuration Control Board (CCB) for approval. Following is a description of the changes proposed:

---

<sup>1</sup>Becker, Hamilton and Kyle, "Photoelastic Investigation of the Stage III Minuteman Nozzle Port Flange", Documents No. ARA 289-1, ARA 289-2, and ARA 289-3

TABLE X

## FLANGE CHEMICAL AND PHYSICAL TEST DATA

Sample	Chemical Results (%)								Type of Protective Coating	Physical Results					
	Mg*	Si*	Cu*	Cr*	Fe*	Mn*	Zn*	Ti*		Tensile Tests Kip			Rp Hardness		
	0.2 0.8	0.5 1.2	3.9 5.0	0.1 Max.	1.0 Max.	0.4 1.2	0.25 Max.	0.15 Max.		High	Low	Avg	High	Low	Avg
GY02748	0.7	0.8	4.5	0.02	0.39	0.49	0.04	0.08	Anodized and Alodine	81.7	73.4	78.0	85	86.5	86
GY02745	0.7	0.9	4.5	0.02	0.39	0.51	0.04	0.08	Anodized	72.3	70.1	71.1	85	85.5	85.5
GY02717	0.7	0.8	4.2	0.02	0.36	0.47	0.03	0.07	Uncoated	67.2	65.3	66.3	85	85	85
GY02744	0.7	1.0	4.4	0.04	0.5	0.47	0.09	0.07	Anodized	74.5	73.8	74.1	85	82	85
GY02711	0.7	0.8	4.5	0.03	0.37	0.47	0.06	0.07	Uncoated	69.9	68.9	69.3	79	84	84
GY02747	0.7	0.9	4.3	0.02	0.37	0.49	0.03	0.07	Anodized and Alodine	70.6	67.7	69.5	80	85	83

\*Minimum and maximum limits for element.

- a. Incorporate a new forging drawing that specifies the usage of the die-forging process for the manufacture of nozzle port flanges to be used in insulators made at Goodyear Tire and Rubber Company.
- b. Increase the radii of the inside corners of the nozzle snap ring groove from 0.005 in. maximum forward and aft to  $0.040 \pm 0.010$  in. forward and  $0.025 \pm 0.005$  in. aft.
- c. Change from hard anodizing of the surfaces of the snap ring groove to chemical conversion coating.

Engineering Change Requests (ECR's) MM5438, MM5635, MM5685, and drawing 12A00511-001 formed the backup data for this portion of the ECP. Minuteman CCB issued a directive on 29 March 1965 approving these changes.

## SECTION IV

### GOODYEAR MOLD MODIFICATION

The following section describes the studies and testing performed to determine and implement changes necessary to correct the Goodyear -690 aft-dome mold.

#### A. FLANGE FAILURE DEMONSTRATION

Two aft domes (RP-1 and RP-2) were molded following Goodyear Standard Operating Procedure (SOP) but with conditions adjusted to intentionally cause flange failure and demonstrate cracking theories. Molding was accomplished under the following conditions:

1. Hand-forged flanges were randomly selected from existing stock at Goodyear.
2. The mold load was 16,940 grams, the maximum allowed by the SOP.
3. The -690 mold process tooling was used.
4. Both aft domes were molded at 500 ton ram force as allowed in the SOP.
5. The cooling plugs were selected for maximum interference between the plug and the flange O-ring diameter.
6. Both aft domes were molded at the nominal time and temperature as specified in the SOP.

Prior to molding, the contour mismatch (gap) between the flange and the mold measured from 0.000 to 0.046 in. and the interference fit between the cooling plugs and flanges measured from 0.016 to 0.019 in. at the O-ring diameter.

All four flanges in RP-1 cracked at the keyway and at a point 180 degrees from the keyway. The four flanges in RP-2 also cracked; however, flanges from ports number 2 and 3 cracked at 180 degrees from the keyway only. The flanges from ports number 1 and 4 cracked at the keyway as well as at 180 degrees from the keyway.

The failure demonstrations proved that a flange improperly supported within the mold will crack under loaded mold conditions and that the tooling, as it existed, did not adequately support the flanges.

Two subsequent tests on moldings RP-14 and RP-15 were performed to allow Allied Research Associates (ARA) to investigate the original and the modified fabrication processes at Goodyear. At ARA's request, RP-14 was a repeat of the failure demonstration moldings, RP-1 and RP-2, with the following modifications: (1) die-forged flanges of the 01A00480-007 configuration

were used in ports number 2 and 4; (2) hand-forged flanges of the 01A00480-002 configuration were used in ports number 1 and 3; (3) the flanges in ports number 3 and 4 were shimmed on the 10.530 diameter. (See discussion on RP-5.) Test of molding RP-15 will be discussed later in this report.

Dye-penetrant testing of the flanges after dome molding of RP-14 revealed two cracks in the snap-ring groove of port number 1; one of the other flanges had cracked. The flange in port number 1 was the only one that did not have some portion of the modifications referenced in section III.

The pressure gage revealed the general pressure in the flange area was 1560 psi. Photoelastic testing with a full-size epoxy model showed that the resultant stress at the base of the snap-ring groove, produced by the 1560 psi pressure, would be 73,400 psi, which is sufficient to cause flange failure.

The tests supported the cracking theories and verified the need for tooling modification.<sup>1</sup>

#### B. THERMAL STRESS ANALYSIS

An investigation was conducted to determine the stresses imposed on a flange by tooling installation and temperature cycling during a molding cycle. A hand-forged flange was instrumented with 12 strain gages as shown in Figure 34. The gages were placed on critical areas of the flange to show the strains induced during the mold preparations, curing, and cooling cycles. These data were tabulated as strain versus time and are listed in Table XI.

There were no indications of strains which would have produced high stress in the base of the snap-ring groove. The maximum stress recorded was on the strain gages mounted directly in back of the snap-ring groove (gages 4, 6, 9, and 12) and was only 7,700 psi. This occurred during the installation of the cooling plug and hardware assembly to the mold. This stress dropped as heat was applied and no further stresses in excess of 6,250 psi were recorded during the cycle.

The variation between gages number 4 and 12 indicate non-uniform torquing of the four bolts used to fasten the cooling plug and flange to the mold. Although the observed variation did not cause critical stresses in the flange, they did indicate a need for better control of the torquing operation.

#### C. NONADHESION TESTS WITH MODIFIED MOLD INSERTS

The failure demonstration moldings RP-1 and RP-2 were followed by two nonadhesion moldings.

---

<sup>1</sup>Becker, Hamilton and Kyle. "Photoelastic Investigation of the Stage III Minuteman Nozzle Port Flange", Documents No. ARA 289-1, ARA 289-2, and ARA 289-3



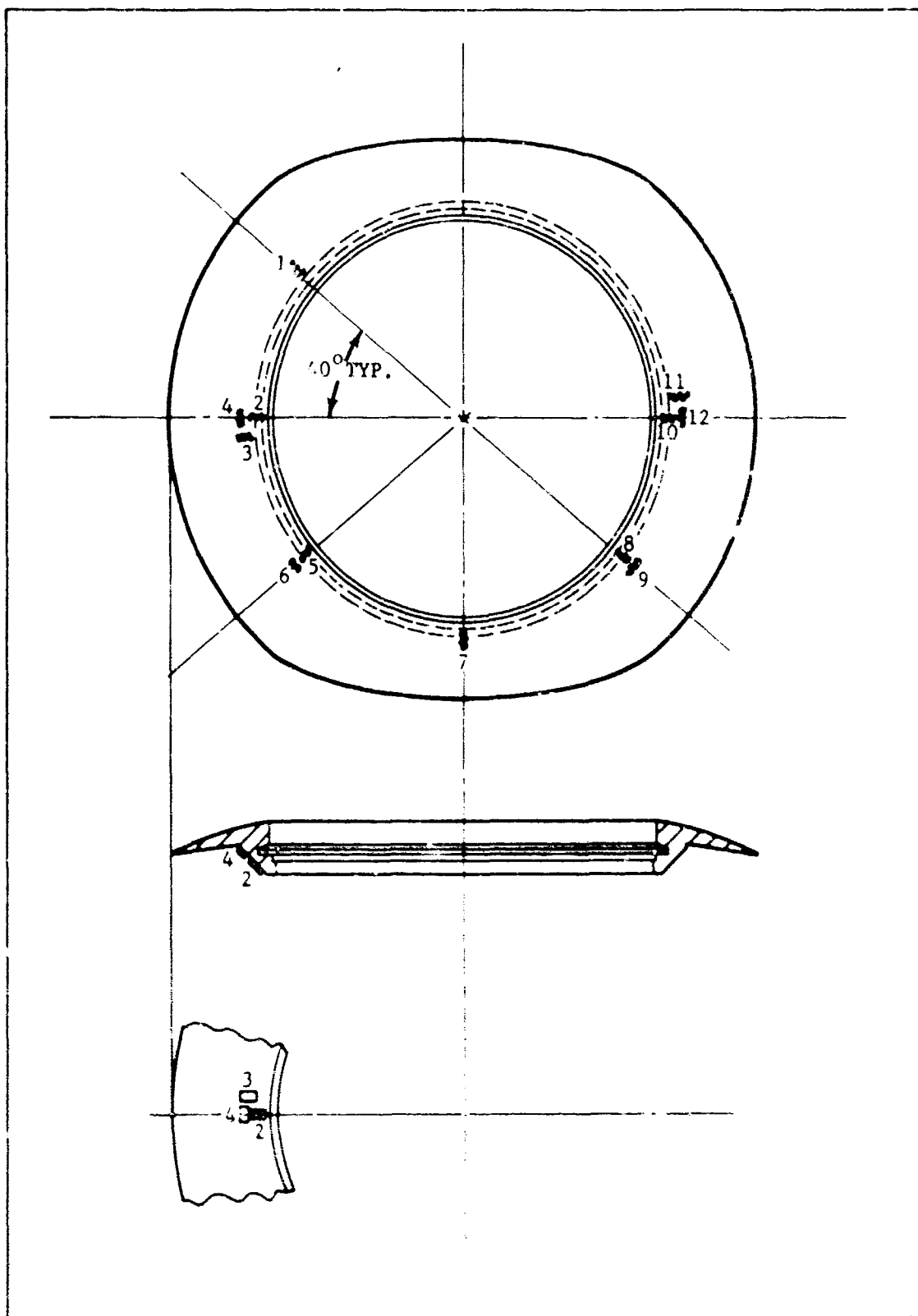


Figure 34. Strain Gage Location on Nozzle Port Flange

TABLE XI  
THERMAL STRAIN GAGE DATA

Event - Time	Strain Gage No.	Indicated Strain in Micro-Inches											
		1	2	3	4	5	6	7	8	9	10	11	12
Pre Test Zeroes	09:40	0	0	0	0	0	0	0	0	0	0	0	0
Plug Installed	09:43	205	211	126	-427	245	39	181	209	47	165	154	-574
6 Plug Belts	09:52	400	6	58	-317	567	-157	384	502	-94	0	171	-589
Installed													
4 Mold Belts	09:55	133	-161	78	418	142	625	218	-343	727	-181	317	524
Installer													
Start 250°F	10:00	50	-289	-147	340	87	408	239	-376	563	-255	309	424
	10:05	84	-272	-158	330	98	389	254	-368	540	-239	333	352
	10:10	122	-261	-158	317	109	354	261	-343	500	-222	341	330
	10:20	167	-239	-147	262	109	280	261	-319	407	-16	325	93
	10:40	211	-232	-95	211	131	221	268	-205	313	-16	325	43
	10:50	222	-222	-78	188	131	197	268	-243	266	-16	317	-115
	11:00	222	-222	-63	179	131	187	262	-293	266	-157	317	-158
	11:10	233	-211	-53	170	142	182	276	-284	266	-140	325	-151
End 230°F													
Start 310°F	11:14	239	-205	37	184	158	177	276	-279	242	-16	317	-101
	11:17	233	-211	-32	211	153	192	282	-284	258	-165	325	0
	11:20	205	-233	-47	239	131	226	276	-309	313	-198	333	22
	11:23	172	-261	-58	266	114	251	254	-326	336	-206	325	43
	11:25	161	-272	-58	285	104	271	247	-343	352	-222	325	86
	11:30	155	-300	-42	317	87	325	247	-385	422	-181	341	101
	11:35	161	-291	-16	317	93	339	247	-393	422	-222	358	63
	11:40	161	-300	26	321	98	359	247	-385	438	-206	366	108
	11:50	155	-283	100	308	98	379	305	-351	493	-165	415	136
	12:00	161	-283	178	271	93	389	305	-317	485	-107	423	93
	12:10	183	-250	237	271	114	394	348	-284	489	-58	431	65
	12:20	189	-233	274	248	109	394	353	-259	485	-17	455	50
	12:30	189	-222	300	243	109	394	363	-234	493	-8	463	43
	12:40	189	-200	221	239	98	413	370	-217	493	41	472	50
	12:50	189	-200	342	234	93	408	370	-217	500	58	472	43
	13:00	178	-200	352	225	82	408	363	-217	500	86	472	144
	13:10	167	-194	352	225	71	408	363	-209	500	49	480	86
	13:20	167	-184	358	220	60	408	363	-209	500	53	472	86
End 310°F	13:34	161	-183	363	211	49	413	348	-209	500	74	472	86

TABLE XI (Cont)  
THERMAL STRAIN GAGE DATA

Strain Gage No.		Indicated Strain in Micro-Inches											
Event - Time		1	2	3	4	5	6	7	8	9	10	11	12
End Steam Bleed 13:42	141	-183	373	373	207	49	418	355	-201	500	82	472	86
Start Cooling 13:44	161	-183	373	373	207	38	403	334	-201	485	107	472	13
Water	155	-183	373	373	193	44	394	341	-192	477	124	488	7
	183	-144	389	142	82	82	359	392	-125	422	190	504	72
	266	-83	426	83	136	169	320	464	-59	399	264	545	-115
	372	0	489	41	169	164	271	529	0	375	338	561	-165
	422	78	521	-64	164	202	202	522	67	336	380	553	-273
	438	128	537	-129	169	153	153	479	92	328	420	528	-337
	438	161	547	-193	147	108	108	435	92	321	420	504	-373
	438	183	547	-234	131	79	79	392	75	313	420	480	-381
	438	194	552	-257	125	98	98	363	8	305	420	455	-373
	427	211	552	-285	104	20	20	312	50	282	396	423	-388
	411	216	552	-294	87	0	0	290	42	282	396	407	-359
	405	216	547	-298	82	5	5	268	25	266	379	390	-359
	400	222	552	-298	76	15	15	247	17	266	371	374	-359
End Cooling Water													
All Solts Out 14:45	305	377	589	-312	278		0	297	560	156	404	252	-337
Plug Out 15:17	17	139	426	28	-136		-108	116	393	117	0	98	258
Zeroes 15:20	6	128	421	14	153		-118	109	385	78	0	65	223

NOTE - Plus (+) values represent tension, Minus (-) values represent compression

On both of these tests, the Standard Operating Procedures (SOP) were followed with the following conditions:

1. Random selected hand-forged flanges from existing stock at Goodyear were used.
2. The mold load was 16,300 grams.
3. Mold inserts were modified to improve the flange-to-mold match.
4. Both aft domes were molded at 500 ton ram force as allowed in the SOP.
5. The cooling plugs were selected for minimum interference between the plug and flange 10.300 in. O-ring diameter.
6. Both domes were molded at nominal time and temperature as specified in the SOP.

Before molding, the contour mismatch (gap) between the flange and mold measured from 0.000 in. to 0.015 in. maximum.

After molding, a dye-penetrant inspection revealed no cracks in any of the flanges from RP-3, but two of the flanges (ports 2 and 4) from RP-4 had cracks. Although the results of the two tests showed a marked improvement over RP-1 and RP-2, where all four flanges in each dome had cracked, they also showed that additional corrections to the tooling had to be made to prevent flange cracking during molding.

#### D. VOLUME CONTROL EVALUATION

The two aft domes RP-3 and RP-4 cited above were also used to determine the volume of rubber contained in the mold cavity and to establish a control to assure complete filling of the mold under all molding conditions. Both aft domes were nonadhesion moldings in which the hardware did not bond to the rubber. After the domes were molded, the hardware was removed and the rubber weighed. The specific gravity of the rubber was determined and used to calculate the volume of rubber in the mold cavity. The maximum rubber volume was 13,760 cc. In order to maintain a constant rubber volume, the weight of the mold load was changed with respect to the specific gravity of the rubber used. Table XII shows the relationship of the mold load to the specific gravity of the rubber in order to maintain the constant volume of 13,760 cc.

The mold load in subsequent moldings will be controlled by the specific gravity of the rubber. This rubber volume will, in all cases, assure complete filling of the mold and consistent molding pressures in every aft dome molding.

#### E. MODIFICATION OF MOLD INSERT TOOLING

In order to correct the flange-to-mold contour mismatch, four

TABLE XII

## SPECIFIC GRAVITY VERSUS MOLD LOAD

Specific Gravity	1.16 gms/cc	1.17 gms/cc	1.18 gms/cc	1.19 gms/cc
Mold Load	15,963 gms	16,100 gms	16,237 gms	16,374 gms

temporary mold inserts were fabricated. The configuration of these temporary inserts differed from the original design as follows:

1. The top sides of the inserts were tapered 0.026 in. across the diameter so that the inboard edges were 0.026 in. thicker than the outboard edges.
2. After tapering, 0.100 in. was removed from the bottom side of each insert.

## F. ADHESION TESTS RP-5, RP-6, AND RP-7

Although the modification of the mold inserts had reduced the contour mismatch (gap) between the flange and mold by approximately 0.030 in., analysis showed that this gap could not be eliminated on the existing mold.

1. RP-5

To minimize the effects of this contour mismatch, the following changes were incorporated and tested on RP-5 (Figures 35 and 36):

- a. A .081 in. shim was placed on each mold insert, thus leaving approximately 0.020 in. expansion gap between the mold insert and the cooling plug.
- b. After insertion of the cooling plug in each flange, gaps were shimmed between the flange and the cooling plugs on the 10.530 in. diameter. (See Figure 37.) Shimming supports the flange against the cooling plug during molding and reduces the stress in the corner of the snap ring groove.
- c. The four one-inch bolts were torqued to 400 in.-lbs to fully seat the flange in the mold, then loosened and retorqued to 150 in.-lbs.
- d. After assembling the flanges in the mold, each 3/8 in. bolt was loosened approximately one-half turn to allow the cooling plug to move with the flange, thereby eliminating stress on the step from the 10.300 in. to the 10.500 in. diameter of the flange.

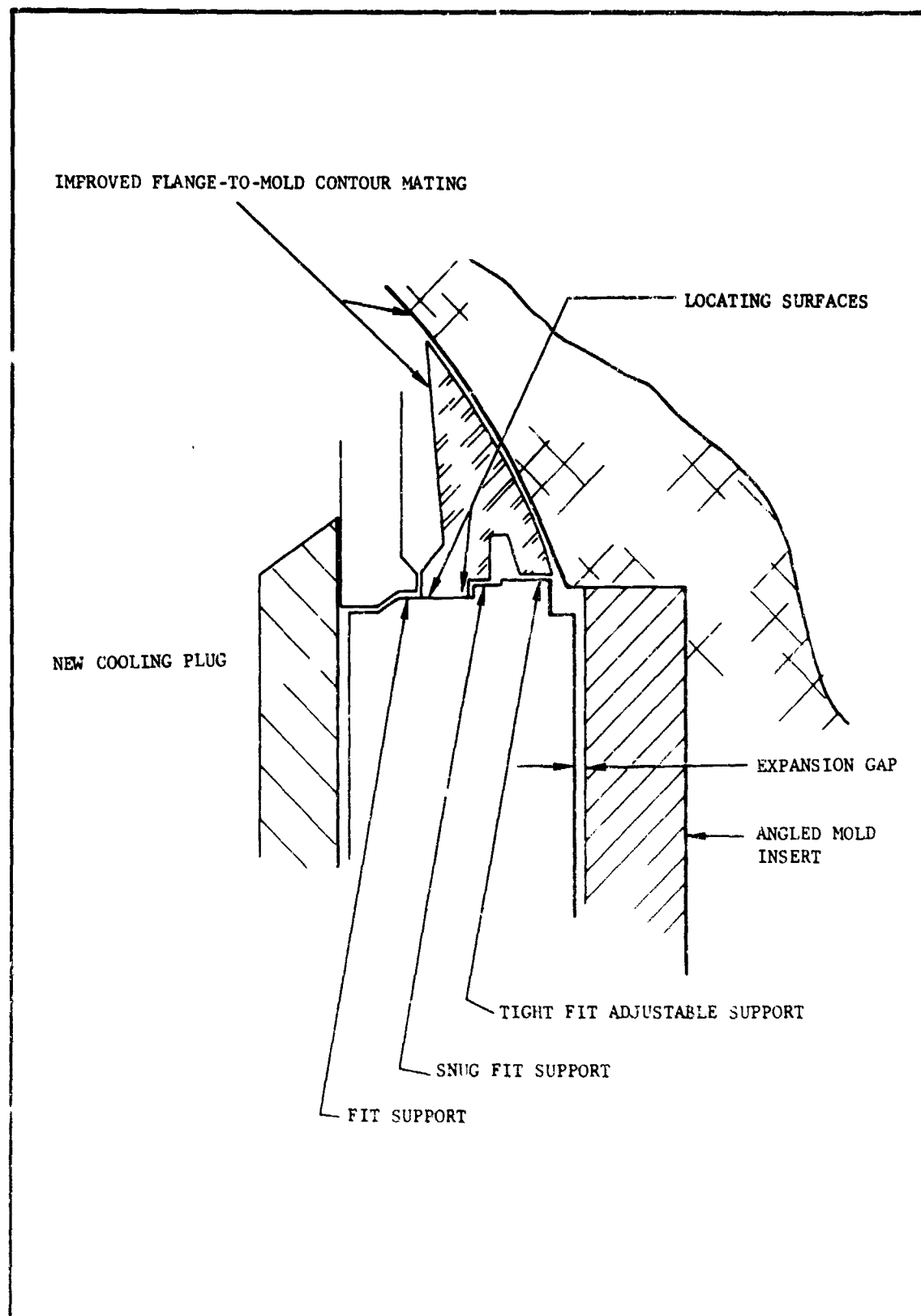


Figure 35. Flange-to-Mold Contour with Modified Cooling

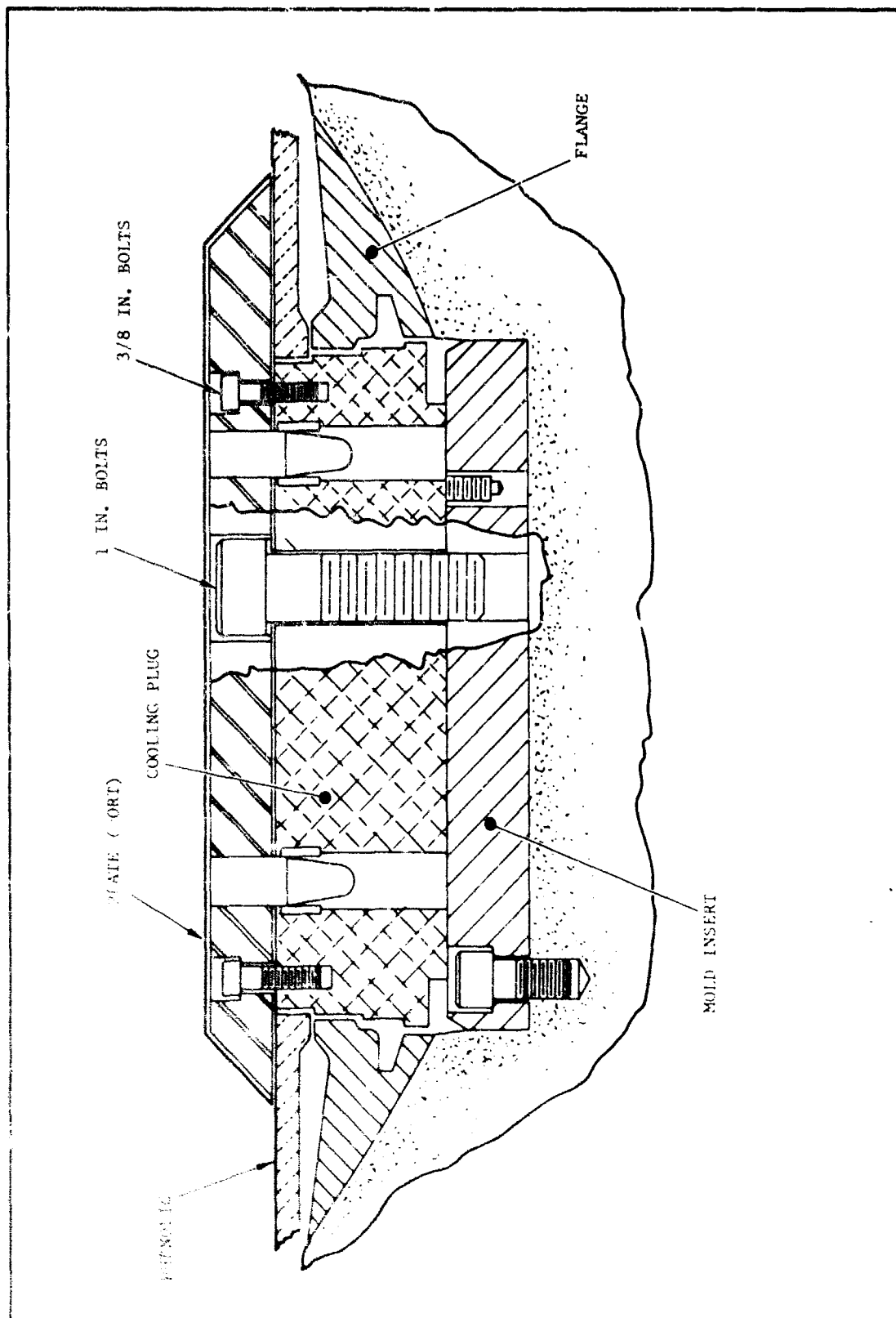


Figure 36. Aft-Dome Mold Nozzle Port Subassembly

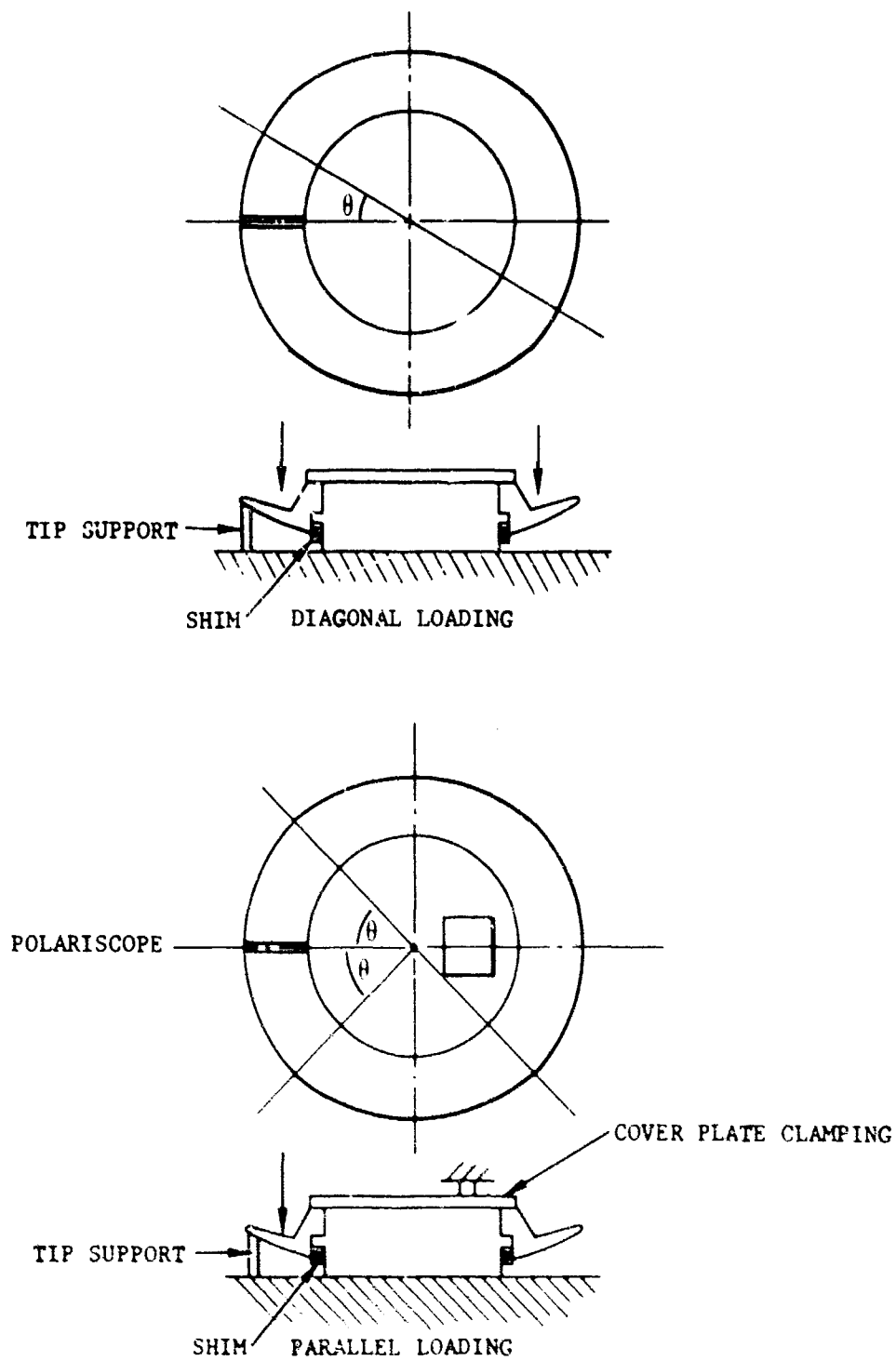


Figure 37. Shimming Support



Zyglo and metallurgical tests performed after molding indicated no cracks or stress corrosion in any of the flanges.

2. RP-6

Based on the results of RP-5, it was decided to repeat this test to see if the results could be duplicated. Aft dome RP-6 showed that modifications to the process and the mold were justified. The zyglo and metallurgical tests performed after molding indicated no cracks or stress corrosion in any of the flanges.

3. RP-7

Aft dome RP-7 was molded the same as RP-5 with the following exceptions:

- a. Instead of the 0.081 in. shim, each mold insert actually required a 0.092 in. shim on the outboard edge and a 0.112 in. shim on the inboard edge. This shimming, which changed the total taper of the mold insert from 0.026 in. to 0.046 in., was necessary to obtain minimum gapping between the flange and mold contours while maintaining contact between the cooling plugs and the mold inserts.
- b. A 0.010 in. pad of M-800 rubber, the same material as the dome is made of, was placed between the flange and the mold.

4. RP-5, RP-6, RP-7 Test Conclusions

Although there were no cracks in any flanges, the rubber pad did not meet expectations. In theory, the pad should have conformed to and filled all gaps between the flange and the mold. Use of the rubber pad was not justified by measurements of the pad thickness after molding.

The modifications to the tooling, as successfully demonstrated by moldings RP-5, RP-6, and RP-7, were concluded to be an effective solution for the cracking problem.

## SECTION V

### GOODYEAR REQUALIFICATION AND VERIFICATION

#### A. GOODYEAR REQUALIFICATION

Seven aft domes, designated RP-8, RP-8A through RP-13, were molded to requalify the Goodyear aft dome molding process. The process selected for requalification was that which was utilized in molding RP-5 except the mold inserts had the 0.046 in. taper instead of the 0.026 in. taper. From the seven production aft domes, four were selected to be wound in cases for hydroproof/hydroburst testing as part of the requalification program.

##### 1. Nozzle Port Flange Modification

Based on the results of the flange testing, the following changes to the nozzle-port flange, drawing 01A00480, were also incorporated at this point to further alleviate the cracking problem:

- a. The flanges were fabricated from die forgings instead of hand forgings.
- b. The radii of the inside corners of the snap ring groove were increased to  $0.040 \pm 0.010$  in. aft and  $0.025 \pm 0.005$  in. forward instead of the 0.005 in. maximum in both corners.
- c. The snap ring groove was chemical conversion coated instead of hard anodized.

##### 2. Testing of Domes

The first aft dome, RP-8, was molded to the initial RP-5 procedure and resulted in a separation between the aluminum and phenolic interface. While this was not a new occurrence and an approved repair procedure was available, this was not considered desirable. Therefore, the torquing requirements for the remaining six aft domes, RP-8A through RP-13, were modified to have the four one-inch bolts torqued to 500 in.-lbs to seat the flange, then loosened and retorqued to 400 in.-lbs. In addition, after assembling the flanges in the mold, each 3/8 in. bolt was loosened approximately one-fourth turn. This eliminated the phenolic separation problem experienced with RP-8.

- a. Three of the seven domes (RP-8, RP-8A, and RP-13) were subjected to the following investigation:
  - (1) The nozzle-port flanges were penetrant inspected with dyglo before and after molding.
  - (2) The nozzle port flanges were dissected and shipped to Hercules/Bacchus for metallurgical evaluation. (See Table XIII.)
- b. The other four aft domes, RP-9, RP-10, RP-11, and RP-12, were processed as follows:

TABLE XIII

## METALLURGICAL EVALUATION OF NOZZLE PORT FLANGES

Material	General Test	Test Conditions	Test Results
Kaiser Die Forging Test No. RP-8	Mold Aft Dome		No cracks apparent
	Metallurgical Analysis	Mercuric chloride treated	
	Port No. 1	Yes	Dye penetrant test negative. Surface attacked only.
	Port No. 2	Yes	Same as Port No. 1
	Port No. 3	Yes	Same as Port No. 1
	Port No. 4	Yes	Same as Port No. 1
Kaiser Die Forging Test No. RP-8A	Mold Aft Dome		No cracks apparent
	Metallurgical Analysis	Mercuric chloride treated	
	Port No. 1	Yes	Dye penetrant test negative. Surface corrosion only.
	Port No. 2	Yes	Same as Port No. 1
	Port No. 3	Yes	Same as Port No. 1
	Port No. 4	Yes	Same as Port No. 1
Kaiser Die Forging Test No. RP-13	Mold Aft Dome		No cracks apparent
	Metallurgical Analysis	Mercuric chloride treated	
	Port No. 1	Yes	Dye penetrant test negative. Surface corrosion only.
	Port No. 2	Yes	Same as Port No. 1
	Port No. 3	Yes	Same as Port No. 1
	Port No. 4	Yes	Same as Port No. 1

- (1) Two of the aft domes (RP-9 and RP-12) were used as replacement domes on insulator assemblies GY00549RX and GY00545RX, respectively. The removal and replacement of these aft domes was conducted per approved Repair Procedure MR-2. The insulators, GY00549RX and RH00545RX, were then wound into cases S/N RH00297 and RH00299.
- (2) Two of the aft domes, RP-10 and RP-11, were placed on new insulators, GY00557X and GY00558X.

### 3. Testing of Cases

The four cases were processed as follows:

#### a. Case S/N RH00298 (Insulator S/N GY00557X)

This case was dye-penetrant inspected then mercuric-chloride tested. It was then hydroproofed, dye-penetrant inspected again, hydroburst then metallurgical analyzed. No cracks were observed in the flanges after hydroproof, but the mercury had made intergranular penetration almost completely through the section of the flanges.

#### b. Case S/N RH00297 (Insulator S/N GY00549RX)

The test sequence of this case was planned to be exactly the same as RH00298; however, a crack in the number 2 nozzle port flange was observed after hydroproof and the case, therefore, was not hydroburst. Subsequent metallographic analysis of the flanges from both cases, S/N 297 and 298, showed that the mercury had made intergranular penetration almost completely through the sections of the flanges. Applications of mercuric chloride were found to be highly destructive in nature and; consequently, the cracking of the flange in RH297 during the 425-psi proof was not considered to be a valid test.

#### c. Case S/N RH00299 (Insulator S/N GY00545RX)

This case was dye-penetrant inspected, hydroproofed, dye-penetrant inspected after hydroproof, then metallurgically analyzed. No cracks or evidence of stress corrosion were found in any of the flanges. The grain flow lines were typical of the die forgings previously examined.

#### d. Case S/N RH00300 (Insulator S/N GY00558X)

This case was dye-penetrant inspected, hydroproofed, dye-penetrant inspected after hydroproof, then stored for 7 days. The case was dye-penetrant inspected after storage, mercuric-chloride tested, then metallurgically analyzed. No cracks were found in any of the flanges. The grain flow lines were good and typical of the previously analyzed die forgings. No evidence of stress corrosion was found.

4. Dome for Allied Research Associates, RP-15

One additional dome (RP-15) was molded to provide Allied Research Associates with the necessary data for evaluating the validity of the modifications initiated to correct the flange cracking problem at Goodyear. To allow direct comparison with RP-14, hand-forged flanges were used in ports number 1 and 3 and die-forged flanges were used in ports number 2 and 4. The uncured preforms and quadrant segments were instrumented with the pressure gages and shear-stress indicators in the same manner as RP-14.

Dye-penetrant and metallurgical examination by ARA revealed no cracks in any of the flanges. The measured mold pressure for the modified process was only 960 psi.

ARA's photoelastic testing with a full-size epoxy model showed the resultant stress at the base of the snap-ring groove produced by the 960 psi pressure would be 45,120 psi, which is not sufficient to cause flange failure during molding.

B. GOODYEAR VERIFICATION

In accordance with ECP's WS-133B-HP-B116-1R1 and 2R1, sampling plans and inspection procedures were initiated to establish and verify the reliability of requalified Goodyear insulator fabrication processes. The sampling plans were designed to provide checks at various production stages as follows:

1. Forgings

- a. Originally, the sample plan called for the dissection and testing of 21 forgings randomly selected from the existing supply, for flow line configuration and physical and chemical properties. However, subsequent data disclosed that the existing supply of die forgings consisted of 966 Hercules (H) owned forgings and 560 Goodyear (G) owned forgings. It was further determined that the H lot consisted of 580 forgings from Kaiser's heat lot FH-10 and 386 from heat lot FH-29. Therefore, the sampling plan was expanded to randomly select 30 forgings from the H lot (21 from heat lot FH-29 and nine from FH-10) and three forgings from the G lot.
- b. In addition, one out of each 20 forgings made subsequent to the existing supply was tested for flow-line configuration and physical and chemical properties.

2. Flanges

- a. Examine the first eight production flanges for conformance to physical-property requirements.

- b. Test and dissect the first eight flanges of item (1) for latent cracks using mercuric chloride.
- c. Test and dissect one out of each 20 flanges thereafter for latent cracks using mercuric chloride.
- d. Prior to anodizing, perform dye-penetrant inspection on all flanges.

3. Aft Domes

- a. Dissect and test for cracks all nozzle-port flanges in the first production dome fabricated, particularly at the keyway position and 180 degrees from the keyway.
- b. Dissect and test for latent cracks all nozzle-port flanges of one dome out of every 40 domes thereafter.
- c. Dye penetrant inspect all flanges in all domes for flange cracking.

4. Case Assemblies

- a. Dye penetrant inspect all nozzle-port flanges at case assembly level after hydroproofing.
- b. Dye penetrant inspect all nozzle-port flanges at case grain loaded level of assembly.

As of 10 May 1966, 92 consecutive units containing Goodyear insulators have successfully passed dye-penetrant inspection at the case assembly level establishing a 97.5 percent reliability demonstration at the 90 percent confidence level, or 99.3 percent reliability at the 50 percent confidence level.

## SECTION VI

### RELIABILITY ANALYSIS

A reliability evaluation was performed to determine the number of Stage III Minuteman motors with cracked nozzle-port flanges in the operational force and to establish the reliability of such motors compared to those having sound nozzle-port flanges.

#### A. EVALUATION OF ALL FIRED HARDWARE FOR CRACKING

All available nozzle-port flanges from fired QA motors were dye-penetrant inspected to determine how long the cracking problem had existed and to verify that the problem was confined exclusively to Goodyear hardware.

A total of 76 fired motors were dye-penetrant inspected. Of the 50 motors containing Goodyear insulators, 15 (14 Wing II and one Wing I) had one or more cracked nozzle-port flange. No cracked flanges were found in the 26 U. S. Rubber insulated motors.

From those findings, it was concluded that the nozzle-port flange cracking problem was confined exclusively to Goodyear insulators, and that the problem had existed since early Wing I.

#### B. CRACKED FLANGE MOTORS IN FIELD SERVICE

Based on the above information, the estimate of field force motors having cracked flanges was confined to those motors embodying Goodyear insulators. Since none of the -690 molded aft domes had been delivered to the operational forces, potentially cracked parts were narrowed down to Goodyear insulators with domes molded in the -243 tooling.

A sample of 57 motors was chosen as representative of the Goodyear -243 configuration motors in the operational force. This sample included five motors which had been recycled from the operational force plus one returned from the force for other purposes. All 228 flanges in this sample were dye-penetrant inspected.

Twenty of these motors were found to have at least one cracked nozzle port flange. On a total basis, 37 of the 228 flanges were cracked. Based on the results of this inspection, 36.1 percent of the motors having Goodyear insulators with aft domes molded in -243 tooling are predicted, with 50 percent confidence, to have at least one cracked nozzle port flange. On a 90 percent confidence basis, no more than 44.4 percent of these motors are predicted to have a cracked flange.

Therefore, with 50 percent confidence, Hercules predicted that 119 motors of the Wing II-V configuration existing in the field force on 11 February 1965 have at least one cracked flange. At 90 percent confidence, this figure increases to 147 motors.

The theoretical and experimental analyses applied in evaluating the ability of motors with cracked nozzle-port flanges to perform satisfactorily, were based on three requirements:

1. The motor must retain its ability to withstand the loads generated during static or flight firing.
2. The motor must have dome and nozzle deflection characteristics like those of uncracked nozzle-port flange motors so that interface, envelope, and guidance performance characteristics are not altered.
3. The cracked flanges must not alter the motor's capability to withstand transportation and handling loads and to ultimately perform properly as required under (1) and (2).

As an overriding rule, it was naturally required that the motor perform within Model Specification limits.

#### C. FULL SCALE STATIC FIRINGS

##### 1. Test Objectives

Three full-scale units were statically fired to evaluate the effect of a cracked nozzle-port flange. The specific test objectives are outlined in Hercules Test Plan MTO-162-228 and all applicable addenda. Briefly stated, these objectives were to evaluate:

- a. Overall ballistic performance.
- b. Distortion differences in nozzles installed in cracked nozzle-port flanges and nozzles installed in sound flanges.
- c. Possible localized case stresses created by cracked flanges.
- d. If existing cracks will propagate prior to or during an actual firing.

##### 2. Test Results

Descriptions of the test setup and results follow:

##### a. Ballistic Performance

The three motors, 5R0, 5T0, 5T3, contained prefiring cracks in eight of the twelve ports. Motors 5R0 and 5T3 had two cracked flanges each and 5T0 had cracks in all four flanges. Location and extent of each crack is listed in Table XIV.

Analysis of the firing data on these motors has shown that all ballistic parameters are within the established K-sigma limits. Of the minor variations which occurred, none was attributed to the presence of cracked nozzle flanges.



TABLE XIV  
FIRING EFFECTS DATA

NOZZLE PORT FLANGE CRACKING AND LOCATION  
AND MAXIMUM NOZZLE MOVEMENT DURING FIRING

Motor Number	Nozzle Port	Crack Location (Degrees of Angle)	Maximum Angular Distortion (Minutes of Angle)	Maximum Distortion at Exit Plane of Nozzle (Inches)
5R0	1	None	*	*
	2	290 to 80	43.8	0.34
	3	None	34.6	0.28
	4	110 to 250	38.9	0.30
5T0	1	135 to 240	*	*
	2	135 to 255	55.8	0.41
	3	135 to 240	49.0	0.37
	4	300 to 45	33.6	0.28
5T3	1	None	*	*
	2	145 to 240	47.2	0.38
	3	120 to 240	36.5	0.32
	4	None	46.6	0.36

- (1) The nozzle port keyway is zero position and angular measurements are clockwise from this position, viewing the motor case from the rear.
  - (2) Maximum angular distortion of the intake portion of the nozzle allowed by interface control requirements: 0° 57' 10.35"
  - (3) Maximum distortion at exit plane allowed by interface control requirements: 0.59 in. prior to 1.3 seconds action time and 1.00 in. after 1.3 seconds.
- \* Not instrumented

b. Nozzle Distortion

Nozzles 2, 3, and 4 of each test motor were individually instrumented with linear potentiometers to measure nozzle blast tube distortion at right angles to the nozzle vectoring motion. Of these nine nozzles, seven were in ports with cracked nozzle-port flanges; two were in ports with sound flanges.

Average angular distortion of the nozzle intake portion within a plane containing the nozzle and motor centerlines and exit plane distortion of the seven instrumented nozzles in cracked flanges was 43.5 minutes and 0.34 in., respectively. This compares to average values of 40.6 minutes and 0.32 in. for the two instrumented nozzles in ports with sound flanges. Individual determinations are present in Table XIV. When these figures are compared with maximum distortion allowed by interface and envelope control of 0 degrees 57 minutes 10.35 seconds and 0.59 in. prior to 1.3 seconds action time and 1.00 inch after 1.3 seconds, the measured deflections were not significantly different.

c. Theoretical Stress Analysis

In conducting this analysis, a pressure of 350 psi was assumed to be a representative level for evaluating the structural integrity of a flange as a device for resisting outward motion of the rocket nozzle during flight. It was further assumed that the tip region of the flange had been completely broken off at the forward radius of the nozzle snap-ring groove, leaving only the base region to resist the snap-ring force. (See Figure 38.)

The ARA analysis indicates a factor of safety of 1.25 for the cracked flange in field service.<sup>1</sup>

d. Localized Case Stresses

Strain gages were mounted on the aft domes of the three test motors to determine if cracked nozzle-port flanges create localized case stresses. These gages were mounted in accordance with Hercules drawing 12S00402. (See Figure 39.)

Resulting data were evaluated by comparing dome strains, according to geometric locations of the instrumentation, in the area of both cracked and uncracked flanges. The maximum average values are compared in Table XV.

These data show that cracked flanges do not create localized stresses on the case aft dome during firing.

---

<sup>1</sup> Becker, Hamilton and Kyle, "Photoelastic Investigation of the Stage III Minuteman Nozzle Port Flange", Documents No. ARA 289-1, ARA 289-2, and ARA 289-3

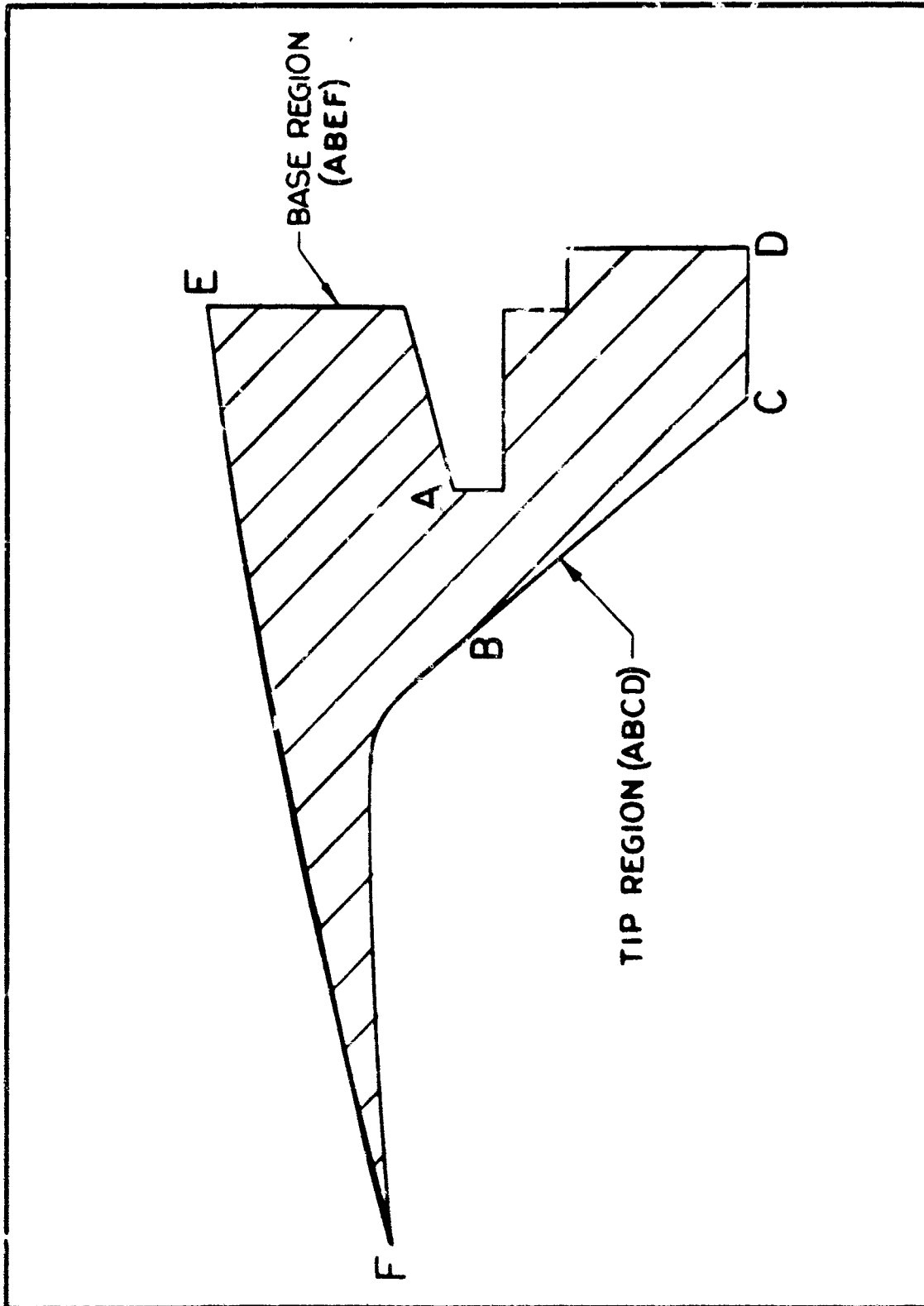
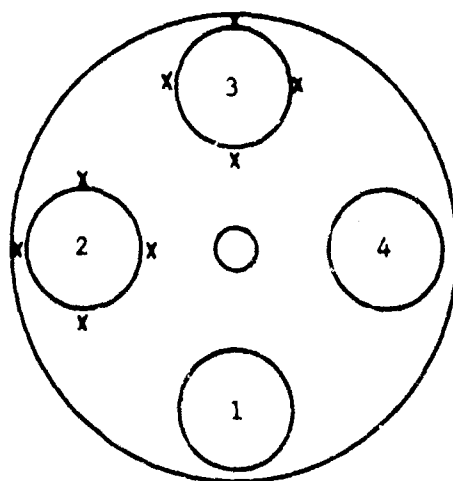


Figure 38. Geometry of Flange



LOCATION OF GAGES ON THE AFT  
DOMES OF MOTORS 5R0, 5T0 AND 5T3

Figure 39. Linear Potentiometer Location on Aft Domes  
of Motors 5R0, 5T0, and 5T3

TABLE XV

AFT DOME CASE STRAIN  
(Micro-Inches Per Inch)

Location	Flange Condition	
	Cracked	Uncracked
Inboard	3890	4600
Outboard	3160	3100
On case directly over cracked area*	7970	7820
On case directly opposite cracked area*	7700	7820
*Gages on cracked and uncracked flanges located in the same geometric position.		

e. Crack Propagation

In order to help determine the presence of unrelieved tensile stresses in cracked nozzle-port flanges, the port number 2 flanges of motors 5R0, 5T0, and 5T3 were treated with a stress detecting agent (mercuric chloride) prior to firing. If tensile stress were present, mercury would penetrate the aluminum flange intergranularly. If tensile stress were not present, only surface attack (pitting) would take place.

After a 24-hour treatment with mercuric chloride, no measurable change in the dimension of the cracks could be noted. Metallurgical examination of the flanges after firing showed surface attack only; no intergranular penetration had occurred.

From these findings, it was concluded that once a flange has cracked, the tensile stresses causing the failure are relieved and the crack will not propagate with age. Furthermore, these tests demonstrated that a crack will not propagate during firing.

f. Simulated Transportation and Handling Test

One of the test objectives of static test motor 4V1 was to evaluate cracked nozzle-port flange performance after being subjected to temperature shock, humidity, and motor vibration testing.

Prior to any conditioning tests, the cracked flanges in nozzle ports number 2 and 3 were dye-penetrant inspected to establish crack lengths. The cracks were located in the forward radius of the nozzle snap-ring groove and extended from 110 degrees to 230 degrees in port number 2 and from 180 degrees to 185 degrees in port number 3. Angular position was measured clockwise from the flange keyway.

The temperature shock test consisted of eight repeated cycles with each cycle consisting of one hour at 10°F followed by four hours at 80°F. After completion of the shock test, the motor remained in the conditioning box and began humidity conditioning at a minimum relative humidity of 85 percent at a  $90^{\circ} \pm 10^{\circ}\text{F}$ . The humidity cycle continued for 96 hours.

Vibration testing consisted of the following:

<u>Cycles</u>	<u>Frequency (cps)</u>	<u>Specified G Level</u>	<u>Actual G Level</u>
100	7-15	$2.5 \pm 0.00$ $- 0.25$	2.3
500	7-15	$2.0 \pm 0.25$	2.3
1000	7-15	$1.5 \pm 0.25$	1.7

A dye-penetrant inspection of the cracked flange in nozzle port number 2 was made following the temperature shock, humidity, and vibration tests. No measurable change occurred in the crack length. The cracked flange in port number 3 was not inspected after any of the above listed tests.

After firing, both cracked flanges were dye-penetrant inspected. Again, no measurable change had occurred in the crack lengths.

Ballistic results showed no anomalies that could be attributed to the cracked nozzle flanges or to the prefiring temperature shock, humidity, and vibration testing. See MTO-164-239 for complete ballistic results.

These tests provide good assurance that a crack will not propagate as a result of operational transportation and handling loads. Furthermore, they provided additional assurance that a cracked flange will not affect motor performance.

#### D. ADDITIONAL RELATED FIRINGS

In addition to the above, at the writing of this report, 14 additional motors with one or more known cracked nozzle-port flange have been test fired. (See Table XVI.) These 14 motors were not part of the original program plan.

Analysis of the firing data on these motors has shown that no performance degradation could be attributed to cracked nozzle port flanges.

Since the October 1964 initiation of the dye-penetrant inspection of nozzle port flanges, prior to nozzle installation, Hercules has established that no nozzle port found free of cracks before firing has ever exhibited cracks after firing. Therefore, it can be concluded that, prior to the dye-penetrant inspection initiated in October 1964, any flange found cracked after firing was also cracked before firing.

Based on this conclusion, the 15 Wing II motors previously discussed all fired successfully with one or more cracked nozzle-port flanges.

#### E. FLIGHT TEST PERFORMANCE

Wing II-IV flight tests conducted at AFWTR and AFEYR were reviewed in light of the cracked nozzle flange anomaly. A total of 41 flight motors utilizing the Goodyear insulator of -243 dome configuration have been flown as of this writing. Based on statistical data presented in Paragraph B, 18 of these motors should have had cracked nozzle-port flanges. There were no test anomalies associated with these flights which could be attributed to cracked nozzle-port flanges.

TABLE XVI

## FIRED MOTORS WITH KNOWN CRACKED FLANGE(S)

HPC Motor No.	Test No.	Environmental TSH *	Test Vibration	Ports Cracked
5R0	5-10-36			2,4
5T3	5-10-41			2,3
5T0	5-10-40			1,2,3,4
4V'	4-10-43	X	X	2,3
5S9	5-10-37			3,4
5F9	5-10-34			3
5P1	Recycle 1			3,
5L2	Recycle 3			4
5V4	6-10-7			2
9L8	6-4-12			
9L0	6-4-14		X	2
9M2	6-4-16		X	2
9L6	6-4-10	X		2
9M4	6-4-18	X		2
5X1	6-4-4	X	X	2,3,4
5W6	6-4-2	X	X	2,4
5X6	6-4-6			2,4
5X7	6-4-8	X	X	2,3

\* Temperature shock and humidity test



## F. RELIABILITY SUMMATION

For reliability purposes, three classifications of tests with Goodyear internal insulators will be used. The first group consists of the 18 motors that were known to have cracked nozzle-port flanges prior to firing. Group two consists of the 15 motors that were inspected after firing and found to have cracked flanges. The third group consists of the 18 flight test motors that were predicted to have cracked nozzle flanges.

The reliability of motors with cracked nozzle-port flanges, as established by the success of these three groups, is as follows:

	<u>90% Confidence Level</u>	<u>50% Confidence Level</u>
Group 1	88.0%	96.2%
Group 1 and 2	93.3%	97.9%
Group 1, 2, and 3	95.3%	98.6%

## G. CONCLUSIONS

Based on statistical analysis of the nozzle-port flange cracking problem, with 50 percent confidence, Hercules predicts that 119 motors of the Wing II-V configuration existing in the field as of 11 February 1965 have at least one cracked nozzle port flange. With 90 percent confidence, this figure increases to 147 motors.

Full-scale tests of at least 18 motors with known cracked flanges prior to firing has shown that:

1. A motor with cracked nozzle-port flanges still retains its ability to withstand loads generated during static and flight firing.
2. The aft-dome and nozzle-deflection characteristics were not significantly different from those of uncracked nozzle-port flange motors, and the interface envelope and guidance performance characteristics were not altered.
3. The cracked flange did not alter the motor's capability to withstand transportation and handling loads and to ultimately perform properly as required by (1) and (2).
4. The cracked nozzle-port flanges had no effect on the ballistic performance of the Stage III Minuteman motor.

The reliability of motors with cracked nozzle-port flanges based on static and flight tests, at 90 percent confidence level, is 95.4 percent.

## SECTION VII

### OVERALL CONCLUSIONS

The investigative efforts pinpointed the Goodyear molding operation as the major cause of the nozzle-port flange cracking problem. The problem was corrected by modifying the mold to relieve the excessive stresses imposed on the flanges during molding. Since the mold modification, no insulator has been rejected for cracks in the nozzle-port flanges. Several design and process improvements were also made to increase the strength of the nozzle port flange and its resistance to cracking.

Statistically, there are motors in the field force with cracked flanges. However, static and flight test data have demonstrated that the reliability of motors containing cracked nozzle-port flanges is not degraded.

# DISTRIBUTION LIST

## FINAL REPORT INVESTIGATION AND RECOVERY PROGRAM FOR NOZZLE PORT FLANGE SNAP RING GROOVE CRACKING PROBLEM OF THE MINUTEMAN STAGE III MOTOR

MTO-752-50

<u>Copy No.</u>	<u>Recipient</u>	<u>Mail Stop</u>
1	Hq. BSD (AFSC), Norton AFB; Attn: BSRPQ-3 - Capt. W. R. Cosgrove	
2	Hq. BSD (AFSC), Norton AFB; Attn: BSRKP-3 - Mr. D. W. Seagrave	
3-5	TRW, Norton AFB; Attn: Mr. J. R. McGibbeny/ Mr. J. E. Peterson	
6-9	TRW, Redondo Beach; Attn: Mr. D. E. Kennedy/ Mr. J. K. Beatty	
10-19	Defense Documentation Center, Cameron Station, Alexandria, Virginia	
20	OOAMA, Hill Air Force Base; Attn: OOYE	
21, 22	HI/CPD, Wilmington; Attn: Mr. D. H. Little/ Mr. J. B. Hathaway	
23	HI/SBDNO; Attn: Mr. K. E. Bricker	
24	HI/BC; Attn: Mr. J. S. Lampkin, Jr.	
25	HDO/AFFRO; Attn: Lt. Col. C. L. Houston, Chief	100-D
26	D. H. Black/J. C. Farber	816-1W13
27, 28	W. L. Covington	816-1W43
29	J. E. Haggard/J. L. Young	816-2W4
30	S. W. Harris/W. S. Collins	816-2E13
31, 32	R. J. Klare	100-E-U
33	M. W. Plunkett/D. E. Thompson	816-1W10
34	B. B. Purcell/K. A. Anderson	100-C
35	E. L. Talbot/A. L. Jackman	100-K2-2
36-38	Library	100-H-2
--	Plant 1 Central File (2 copies Distribution List only)	100-D